GASEOUS DIFFUSION THROUGH ZEOLITES

Thesis

Submitted for the Degree of

Doctor of Philosophy

at the

University of London

by

Lee Oleh DWORJANYN,

B.E., B.Sc. (Sydney).

Department of Chemical Engineering and Chemical Technology,

Imperial College of Science and Technology,

London, S.W.7

November, 1962

SUMMARY

Gas adsorption on molecular sieves and diffusion mechanisms for compact pellets have been investigated experimentally and theoretically.

A new experimental technique, using radioactive tracers, has been developed for measuring self exchange of gases in large pellets and in fine powders using a flow system under dynamic equilibrium. This method has been used to determine the pore-diffusion of carbon dioxide in packed beds of molecular sieve Type 4A and to determine the internal diffusion in the molecular sieve crystals. These results have been combined to interpret the adsorption behaviour of packed columns.

A stochastic approach was used to formulate special diffusion equations for molecular sieve Type A, and these equations were solved for cubic molecular sieve crystals.

Equations have been derived for the more complicated system of diffusion in one dimensional packed beds and pellets and explicit solutions, in the form of infinite integrals, were obtained for the one dimensional case and for spherical pellets.

One attempt has been made to compute the physical adsorption potentials of carbon dioxide on 4A and these

calculations were used to predict the initial equilibrium adsorption slopes. Existing theories were extended to show that the diffusion coefficient could be calculated from the above potentials.

ACKNOWLEDGEMENTS

It would be impossible to mention all those who have contributed during the last three years to make this research a success. I would like to extend to all of them my sincere thanks. However, I would like to record my special thanks to:-

My supervisor, Professor R.W.H. Sargent, for his constant help with technical and personal problems, and particularly for all the homework he did on the theoretical aspects of this thesis.

The glass blowers, for not only doing their job but for doing it at those times when it was most needed.

The laboratory assistant, R.Lewis, who always offered a helping hand, not just for my sake, but for the sake of scientific progress.

I would like to thank the Department of Scientific and Industrial Research for a grant to purchase the electronic equipment, and the Leverhulme Trust for their scholarship.

My sincere thanks go to my wife, Anne, for her initial encouragement and final patience and tolerance, and to my daughter, Tanya, whose welcoming smiles were such balm for tired eyes.

CONTENTS

I INTRODUCTION

This research forms part of an adsorption dynamics study investigating simultaneously the performance of a whole packed column and the adsorption by a single pellet.

The present thesis describes an experimental and a theoretical study of gas adsorption by a single pellet of synthetic molecular sieve 4A. Molecular sieve was chosen because of its useful industrial and scientific applications, such as its very high adsorptive capacity and the ability to remove minute traces of some gases, and because its pore structure has been accurately determined. Unlike conventional adsorbents, where adsorption takes place on surfaces inside variable capillaries and crevices, the molecular sieves have precise internal pores and cavities which are part of the crystal structure itself.

A considerable amount of data was available on adsorption equilibria for molecular sieves and zeolites in general; however, only very little could be found on diffusion through zeolites. It was therefore decided to concentrate on diffusion measurements. The initial intention was to use single crystals of known dimensions. As the synthetic molecular sieves could not be grown to sizes greater than 25 microns across[3], samples of large (5 to 10 mm) natural

chabasite were obtained from Dr. Hey of The British Museum of Natural History. Because of the structural similarity between chabasite and synthetic molecular sieves the understanding of diffusion mechanisms in one could easily be extended to the other.

Because only a few good chabasite crystals were available the initial test diffusion measurements were performed on molecular sieve pellets. The results obtained were so unusual and interesting that the whole research project was devoted to the interpretion of these results and all the work was done on synthetic molecular sieve 4A. This adsorbent was found also to be more convenient theoretically because it has a greater degree of symmetry than chabasite and thus requires considerably less computation time in calculating its properties.

The Structure of Molecular Sieves.

The synthetic molecular sieves were prepared first commercially by the Linde Division of Union Carbide in the United States. Their structure and properties have been worked out fully by Breck and his co-workers of the Linde Division.[3] The structure of the molecular sieves has been worked out also independently by Broussard and Shoemaker[5] and their results are in good agreement with those of Breck. A very clear description of the synthetic zeolites and the interpretion of their properties has been published by

Breck and Smith in the Scientific American[4] and a general review of the properties and applications has been made by Bering.[2]

The commercial molecular sieves are available in two basic structural forms A and X. These zeolites can also be prepared in the laboratory without any difficulty.[6] Both of these forms are made up of silica and alumina tetrahedra linked together to form a system of interconnected cages. To achieve a balance of charges in these crystals positive ions are incorporated in the structure. The chemical formulae of the sodium zeolites are given in Table 1.

Table 1. Chemical formulae of molecular sieves.

Type	Composition	Unit Cell Size, Å
4A	$Na_{12} \cdot (AlO_2)_{12}(SiO_2)_{12}$	12.30
13X	$Na_{88} \cdot (AlO_2)_{88}(SiO_2)_{104}$	24.95

The positive ions are essential for stability of the structure although they do not really form a part of it as can be shown by their migration in the presence of an electric field.[28] These ions can also be replaced easily by suspending the molecular sieve in a concentrated solution of a different ion.[18]

The cages of the molecular sieves are interconnected by windows through which adsorbed molecules have access to all

the internal cages. These windows are in fact rings of oxygen ions creating high negative potentials with high affinity for the attachment of positive ions which may partially block the windows. In type A the oxygen ring windows have an opening of 5 Å, but because of the blocking action of sodium ions the free diameter is only 4 Å - hence the nomenclature 4A in Table 1. By replacing the twelve sodium ions with six divalent calcium ions some of the windows are completely cleared allowing molecules up to 5 Å in diameter to enter the cages. Similarly by replacing the sodium ions with larger potassium ions the effective openings can be reduced to 3 Å.

Molecular Sieve 4A.

A section through a large cage of molecular sieve 4A is shown in Fig.1 from which it can be seen that the large cage, which has a volume of 775 $Å^3$, is connected to six similar cages in the directions of right angled axes. The interconnecting window is made up of a ring of eight co-planar oxygen atoms forming a free opening of 5 Å.

In the directions of the 3 - fold axes the large cages are also connected to eight smaller cages with a volume of about 157 $Å^3$. The interconnecting window can be seen in Fig.2 which is a view from the centre of a large cage in the direction (1,1,1). The six oxygen atoms forming the window lie in two slightly displaced planes and they have a free diameter of about 2 Å.

MOLECULAR SIEVE 4A

$Na_{12}(SiO_2)_{12}(AlO_2)_{12}$

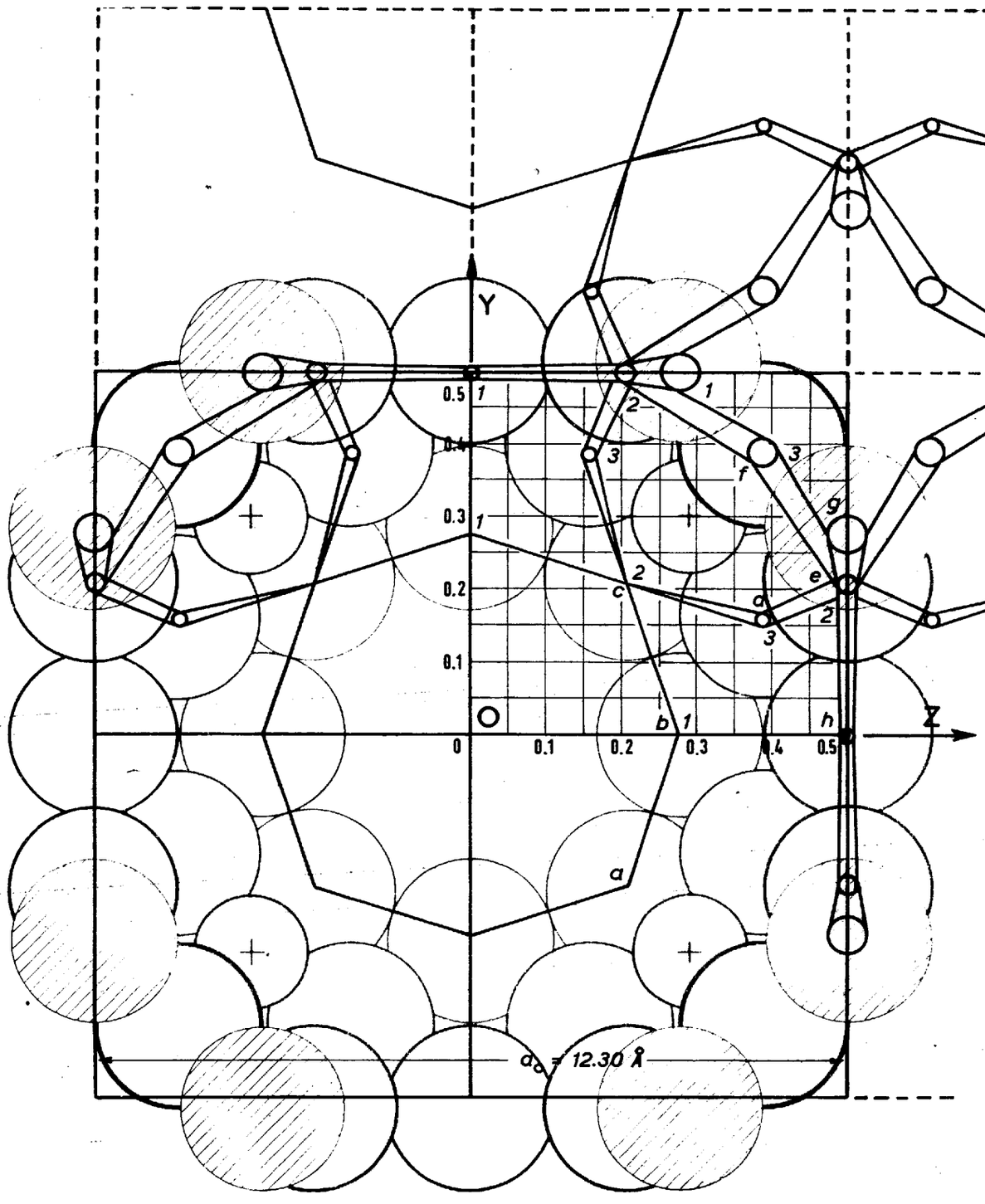

Cross-section through Large Cage

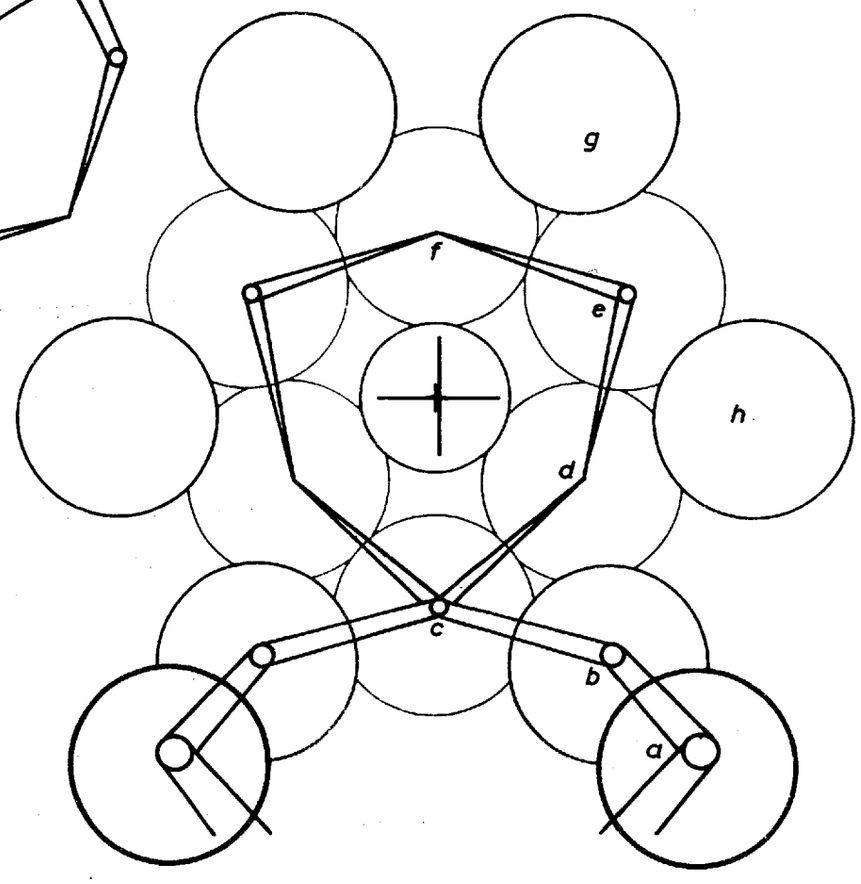

View in (1,1,1) Direction

Figs.1&2

Each unit cell of molecular sieve 4A consists of one complete large cell and one complete small cell and it has to accommodate 12 sodium cations. The most favourable positions for eight of these are in the eight small windows leading to the small cages (Fig.1), leaving the remaining four to be distributed in three large windows available per each unit cell. The result of this distribution is that all the small windows are blocked, two of the large interconnecting windows are fully blocked with two cations each, and the remaining four are partially blocked with one cation in each. However, because of the mobility of the cations and also because of thermal agitation it is possible for some molecules to penetrate even through the small windows.[4]

Crystal Shape and Size.

Because of the cubic crystal structure the external shape of the crystals is also cubic. Fig.3 shows an electron

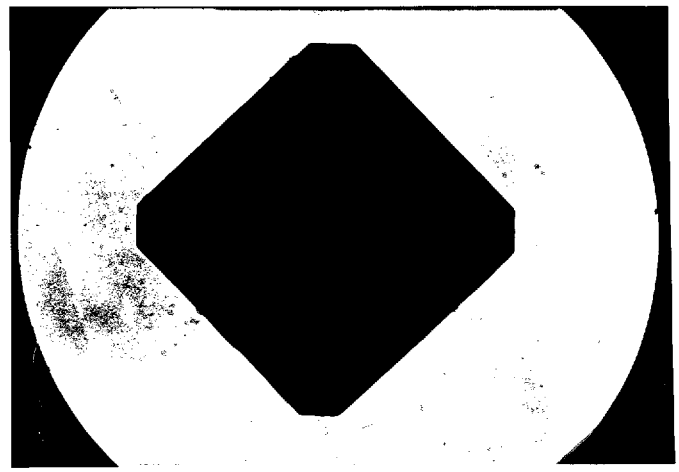

Molecular Sieve Crystal (4 microns). Fig.3

microscope enlargement of a typical molecular sieve crystal about 2 μ across. Most of the crystals are similarly shaped forming perfect cubes with their (1,1,0) edges removed. The crystal size of the commercial material varies between about 0.1 μ and 2 μ with an average size of about 1 μ. The particle size distribution is difficult to determine because the particles are just too large for an electron microscope and too small for the optical microscope. A distribution could be obtained using an electron microscope by taking a large number of pictures each containing only a few particles, but this would only be warranted if a satisfactory theory existed which could utilise the particle size distribution. No such theory could be found.

The usual methods of particle size determination which depend on a suspension in a liquid cannot be applied to molecular sieves because of the difficulty of achieving effective dispersion. This can be seen in Fig.4. The cubic shape of the particles means that they can attach themselves face to face to form large aggregates as shown in the figure. The best way found for dispersing the particles is to make a thick paste with water containing some dispersing agent and then gradually diluting the paste. Even then a particle size analysis performed on a Coulton Counter showed an average particle size of 10 to 20 μ which is quite false.

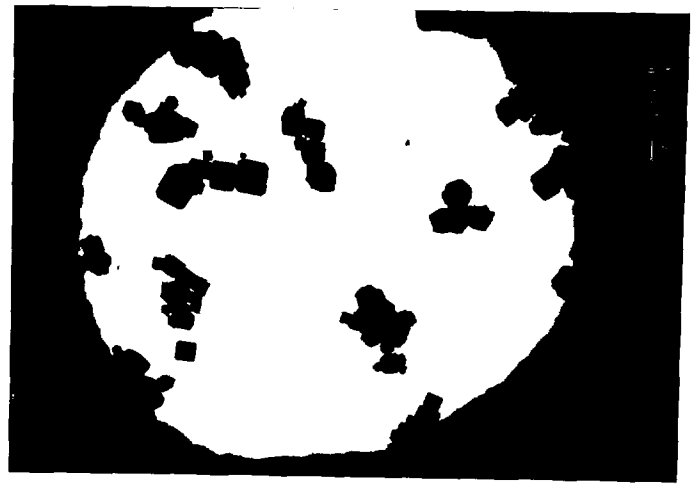

Agglomeration of Molecular Sieve Crystals. Fig.4

Molecular Sieve Pellets.

The molecular sieve crystals, which have the appearance of a white powder, have a very limited commercial application in the powder form. To make the powder useful as a conventional adsorbent it is compressed with the help of an inert clay binder to form spherical or cylindrical pellets.[9] The commercially available forms are 1/8 in. and 1/16 in. spheres and short cylinders whose length is about twice the diameter. Pellets of any desired shape can also be prepared in the laboratory.[8,12]

There is no published information on the binder and the mechanism with which it holds the crystals together. What is more important, there is no information on the distribution of the binder with respect to the crystals. This aspect is very important because a considerable fraction of the external

crystal surface could be blocked off by the binder thus slowing down the diffusion of adsorbed molecules. It is also possible that a substantial fraction of all the crystals could be completely encased by the binder creating pockets from which the diffusion might be negligibly small.

One way of studying the distribution of the binder would be by electron microscopic examination of pellet replicas. This is a rather specialised technique and it was not tried by the author.

The Complete Adsorption Column.

When the pellets described above are packed into a bed they form a complete adsorption system which can be subdivided into three types of voids and two types of solids as shown in Table 2. The binder density was assumed to be 2.59 g/cm^3.

Table 2. Void space of 1/8 in. pellets of M.S. 4A.

Hydrated crystal density	1.99 g/cm^3
Dehydrated crystal density	1.56 g/cm^3
Dry pellet density (20% binder)	1.09 g/cm^3
Bulk density	0.72 g/cm^3
Volume of solid	209 cm^3
Voids within solid (water)	164 cm^3
Volume of binder	56 cm^3
Free voids within pellets	234 cm^3
Free voids between pellets	337 cm^3
Total	1000 cm^3

Preliminary Diffusion Measurements.

The experimental methods and results will be described in Sections II and IV. To help in understanding the development of this research a brief description is given of the results of the first diffusion experiment.

A cylindrical pellet, 1/8 in. dia., was placed in a glass tube, evacuated while heating the tube, and then on cooling to room temperature saturated with radioactive carbon dioxide. When equilibrium was established non-radioactive carbon dioxide gas was passed at a uniform rate through the tube and over the pellet. The active gas adsorbed inside the pellet began to exchange (under equilibrium conditions) with the inactive gas outside the pellet. This exchange was followed by measuring the activity of the carrier gas leaving the tube. The results expressed as per cent exchanged against time are shown in Fig.5.

The probability - log time plot shows that within the time range of measurement the diffusion can be represented by asymptotic straight lines. No ordinary diffusion could give such behaviour. There would have to be either two or more different diffusion mechanisms, or possibly the simple diffusion equation itself (Fick's Law) may not apply. An experimental study was therefore undertaken to investigate the former, (Section IV) and a theoretical study to investigate the latter possibility (Section V).

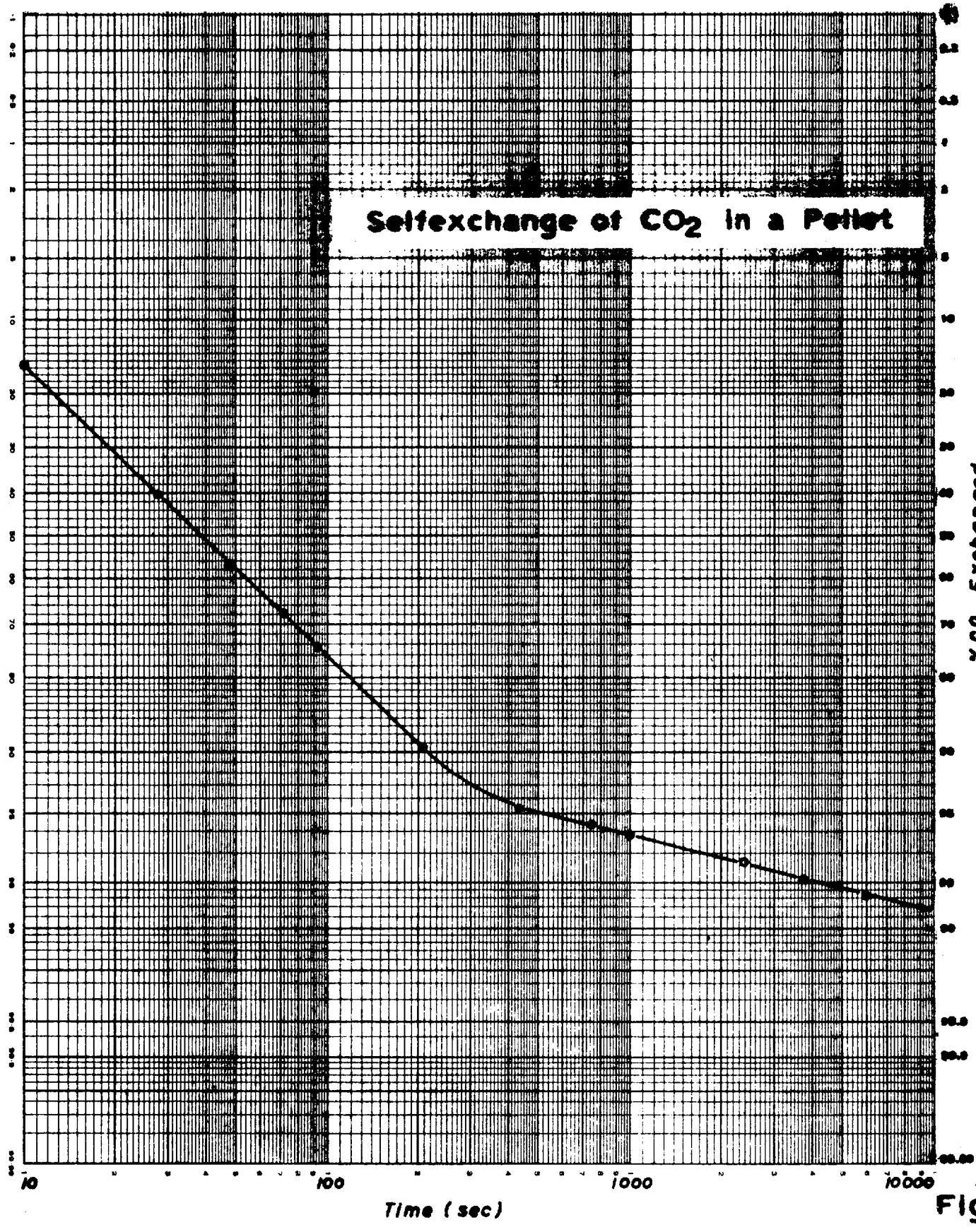
Selfexchange of CO_2 in a Pellet
$X CO_2$ Exchanged
10
100
1000
10000
Time (sec)

Fig.5

General Objectives of this Research.

The original intention of studying diffusion in single crystals of chabasite has been now transformed into the interpretation of the following systems presented in ascending dimension of complexity:

I The cages of the unit cell (Fig.1) ,

II A single crystal (Fig.3),

III A pellet made up of crystals and binder,

IV A packed column of pellets.

Ideally, we would like to be able to predict purely theoretically the adsorption equilibria and the break-through curves for packed columns.

A study of a packed column has been made already by Chandrasekharan[26], and the objectives of the other three systems were as follows:

I From known intermolecular potentials calculate the potential of an adsorbed atom inside the cages and use this to estimate heats of adsorption, equilibrium isotherms, and possibly cage to cage jump frequencies and hence diffusion coefficients.

II From the known types of cages inside the crystal formulate a diffusion equation and solve this equation for the known boundary conditions of the crystal. Determine experimentally the diffusion coefficient through the crystal.

III Formulate diffusion equations to represent a pellet and solve these for known boundary conditions. Compare the theoretical solution with experimental results.

Clearly, only a few of these objectives could be achieved. Unfortunately, because of various interconnections it was impossible to select just one or two of these and study them in detail. For example, equilibria have to be predicted before trying to predict jump frequencies which are more complicated, and before predicting these some experimental diffusion coefficients must be obtained for comparison. The author has therefore decided to examine each aspect theoretically and experimentally so as to clear the way for future work.

Experimental Approach.

There are no known reliable measurements of diffusion coefficients for synthetic molecular sieves. Breck et al.[3] have given a few rate of adsorption curves without calculating any diffusion coefficients and Habgood[29] has made a number of diffusion measurements on the adsorption of nitrogen and methane on 4A but his results are difficult to interpret.

Measurements of diffusion were therefore the main objectives of this research. From a theoretical point of view selfdiffusion coefficients would be more useful than

diffusion coefficients describing adsorption or desorption of a gas. This is because in measuring selfdiffusion all pressure and concentration differentials are eliminated, thus simplifying the mathematical model. A most useful corollary of this is that all the measurements are made at one constant value of the diffusion coefficient K. Another difficulty in making intrinsic diffusion measurements is the heat of adsorption which changes the internal temperature of the adsorbent thus complicating the diffusion even further. This effect is very noticable in adsorption equilibria studies (Section III) when, for example, in adsorbing carbon dioxide on 1 g of molecular sieve in a sample bulb the initial adsorption rate indicates that equilibrium should be reached in about 30 sec, while in fact it takes about 40 min for equilibrium to be established.

These considerations led to radio-tracer techniques which were specially developed for this purpose. These are described in general in Section II, and the analyses of the measurements are given in Section IV.

Selfdiffusion measurements were first made on a single pellet, as described earlier, and then on the molecular sieve powder by depositing a bed of powder on a special sintered glass plug and then passing the carrier gas through the powder bed. This method, at sufficiently high carrier gas velocity, should give a virtually inactive gas atmosphere around each crystal, and thus produce a diffusion coefficient

for the powder itself.

To measure the pore diffusion a glass tube sealed at one end was filled with molecular sieve powder and saturated with radioactive gas as before. By passing the nonactive gas over the free end of the tube pore diffusion could be obtained, provided the tube was long enough to make the particle diffusion negligible. This arrangement simplified the geometry to one dimension and eliminated the uncertain effect of the binder. Pore diffusion through the pellet can subsequently be simulated by pushing cylindrical pellets into slightly larger tubes and filling in the crevices with a crushed pellet.

All these techniques were specially developed for this project and they are fully described in Sections II and IV.

Equilibrium Measurements.

There is a substantial amount of data available on equilibrium adsorption isotherms for all the varieties of molecular sieves. The best collection is available in Union Carbide brochures[2] and in their publication by Breck et al.[3] Other references can be found in the Classified References section at the end of this thesis.

Despite the large amount of literature on adsorption equilibria there is no published information on the effects of desorption temperature on these equilibria although it has been often mentioned that the desorption temperature affects

the equilibria. The desorption temperature has a direct bearing on the diffusion measurements because it determines the amount of water remaining in the molecular sieve. The polar water molecules will attach themselves preferentially at the windows between the positive sodium ions and the negative oxygen ions (Fig.1) thereby affecting the diffusion very seriously.

Some unreproducibility was observed in the early diffusion measurements and a study of water desorption and carbon dioxide adsorption equilibria was made. Gravimetric and volumetric methods were used and the results are given in Section III.

An ideal way of studying the removal of the last traces of water is by using radio-tracer techniques. The molecular sieve is saturated first with tritiated water and then desorbed at the required temperature..It is then resaturated with inactive water and equilibrium is allowed to be established. This will distribute randomly the original undesorbed tritiated water. This water is now desorbed by heating and its activity determined.

Special equipment and gases for these measurements were obtained and the apparatus was arranged for the experiments. Unfortunately, permission could not be obtained for the use of tritium in the radiation laboratory and this experiment had to be abandoned.

Theoretical Approach.

The initial pellet selfdiffusion curve obtained (Fig.5) had one characteristic feature: a sudden change in rate at about 6% CO_2 remaining in the pellet, corresponding to about 20% present initially in the sample. This immediately suggested that the small cages of 4A, which have a volume of about 17% of the total cage volume, may have some effect on the diffusion.

The usual explanation of pore resistance causing the break in the curve could not be applied here because the initial high rate would mean that pore diffusion is high and crystal diffusion low - this is irreconcilable with the fact that about 90% comes out at the initial fast rate because only a fraction of one per cent is present in the gas pores.

The effect of cages on the diffusion equation and its solution is given in Section V. Attempts to represent the whole pellet will also be described in Section V.

A more basic approach to find the diffusion coefficients and to predict the adsorption isotherms was made by calculating the spatial potential function of a CO_2 probe molecule inside the molecular sieve cages. It should be noted at this stage that no useful theoretical predictions have been made, although the results look quite encouraging, if not in calculating the isotherms then in estimating intermolecular force constants from the isotherms.

II EXPERIMENTAL METHODS

1. GENERAL DESCRIPTION

The equipment was designed for the volumetric measurement of adsorption equilibria and for diffusion measurements using a dynamic radio-tracer technique. The apparatus can be subdivided into a vacuum system made mostly in pyrex glass, thermostats for temperature control, and electronic equipment for radioactivity measurement.

The glass equipment (Fig.6) consisted essentially of a high vacuum line connected to a diffusion manifold, volumetric adsorption burettes, and various bulbs for storage and preparation of active and inactive gases.

High Vacuum.

For obtaining the high vacuum a two stage backing pump was used, followed by a two stage oil diffusion pump. The backing pump was Edwards type 2SC50B provided with air ballast, the high capacity and the air ballast being necessary for the removal of large quantities of water vapour evolved from the molecular sieve on heating. An auxiliary smaller vacuum pump and an air blower were also provided for raising and lowering various mercury reservoirs.

The two stage glass diffusion pump was made to a standard design.[51] It was operated with silicon oil type 704

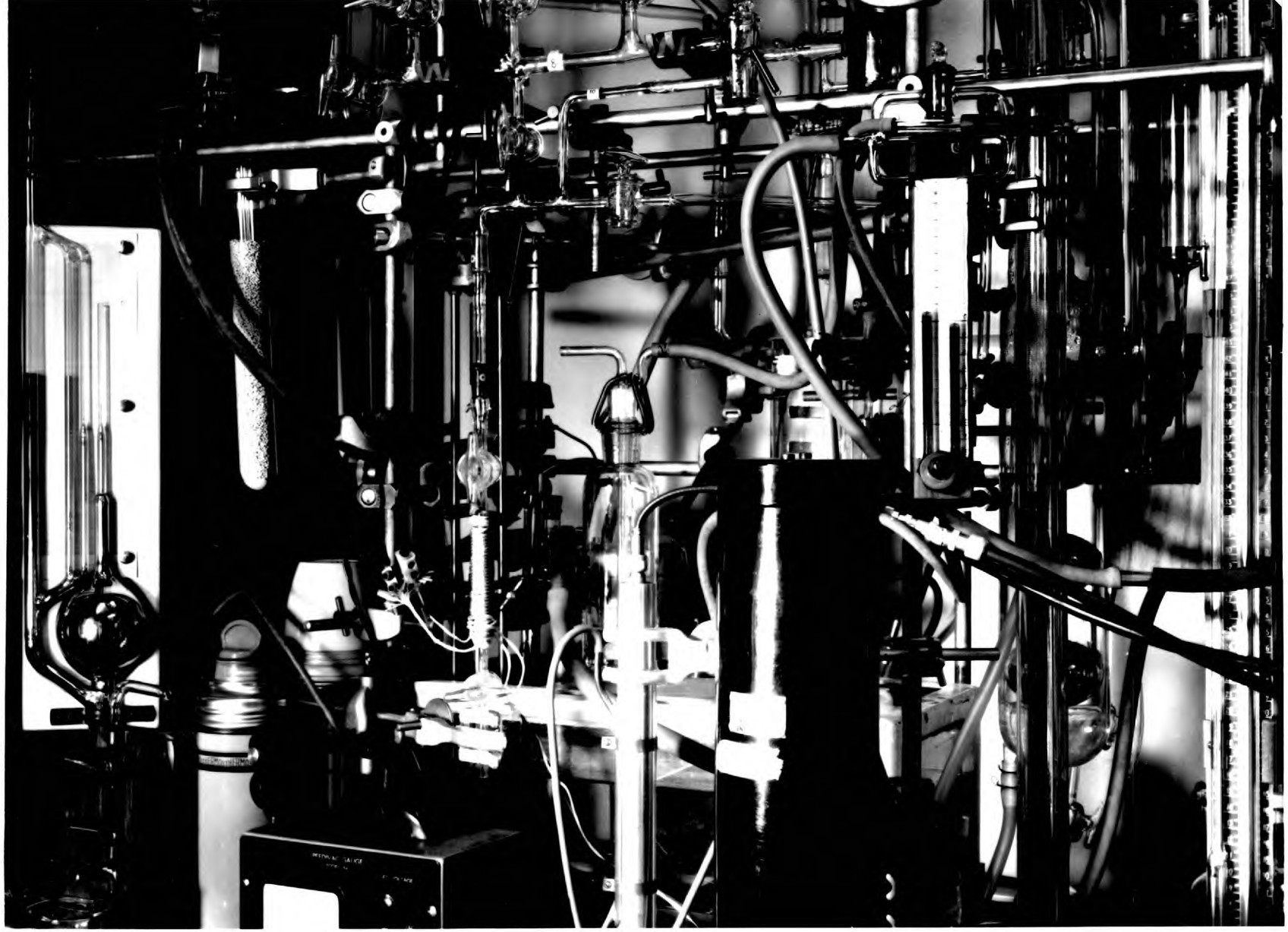

High Vacuum System

and an oil heater of 100 W capacity. The ultimate vacuum obtained was of the order of 10^{-6}mm Hg.

Measurement of Vacuum.

The vacuum was measured with a specially designed McLeod gauge, shown on the left hand side of Fig.6. It consisted of a bulb, 198.78 cm^3 capacity, from which the gas could be compressed into three different tubes of decreasing diameter. These were constructed from Veridia precision bore tubing, 9.98, 2.98, and 0.492 mm diameter and 6, 5.32, and 9.88 cm long respectively, matching tubes being used for comparison of mercury levels. Prior to assembly the tubes were accurately calibrated with mercury. Using this gauge it was possible to read accurately pressures from a few centimetres to 10^{-6}mm. To facilitate operation of the gauge a manifold consisting of three different capillaries was provided for controlled inlet and exhaust of air to and from the mercury reservoir. This not only made it easier to stop the rise of mercury in the capillaries, but made it much safer to lower the mercury from the capillaries as it is very easy to break the thread in the 0.5 mm capillary.

For continuous pressure indication a Pirani and a Philips gauge were used. These gave a continuous pressure reading in the range from 500 to 0.01 mm Hg.

The Diffusion Manifold.

The diffusion manifold (Fig.7) was designed for desorbing and saturating the diffusion cell and for conducting the diffusion experiments. With the double-oblique stopcock as shown the diffusion cell was evacuated through SC3 while measuring the pressure with a Pirani or a Philips gauge through SC2. The extent of desorption achieved could be easily determined by closing the stopcock to the vacuum line and noting the increase of pressure with either of the gauges.

When desorption was completed the double-oblique stopcock was turned to admit through SC6 the radioactive gas from its storage bulbs to the diffusion tube, its pressure being adjusted to a predetermined value and measured in a precision manometer. Prior to its use the activity of the gas was measured in a standard tube attached to the B10 joint. The completion of adsorption was determined by closing the main gas reservoir and observing the manometer.

In the meantime, with SC2, SC3, and SC5 closed, the flow of inactive gas was started through SC1 and SC4. The flow of the gas was controlled by maintaining constant pressure by means of a gas relief leg submerged in oil. At the exit of SC4 was attached an orifice with a pressure drop corresponding to that through the diffusion cell.

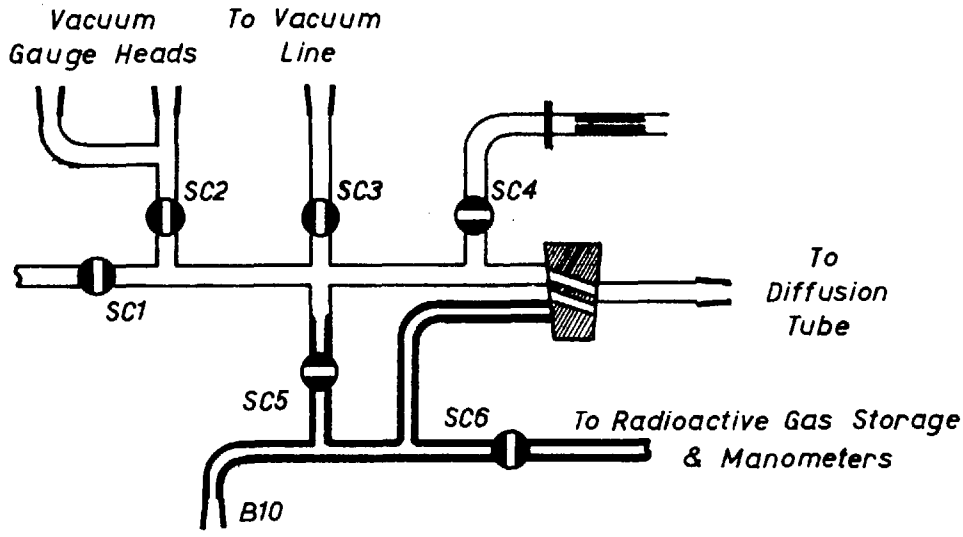

Diffusion Manifold

Fig.7

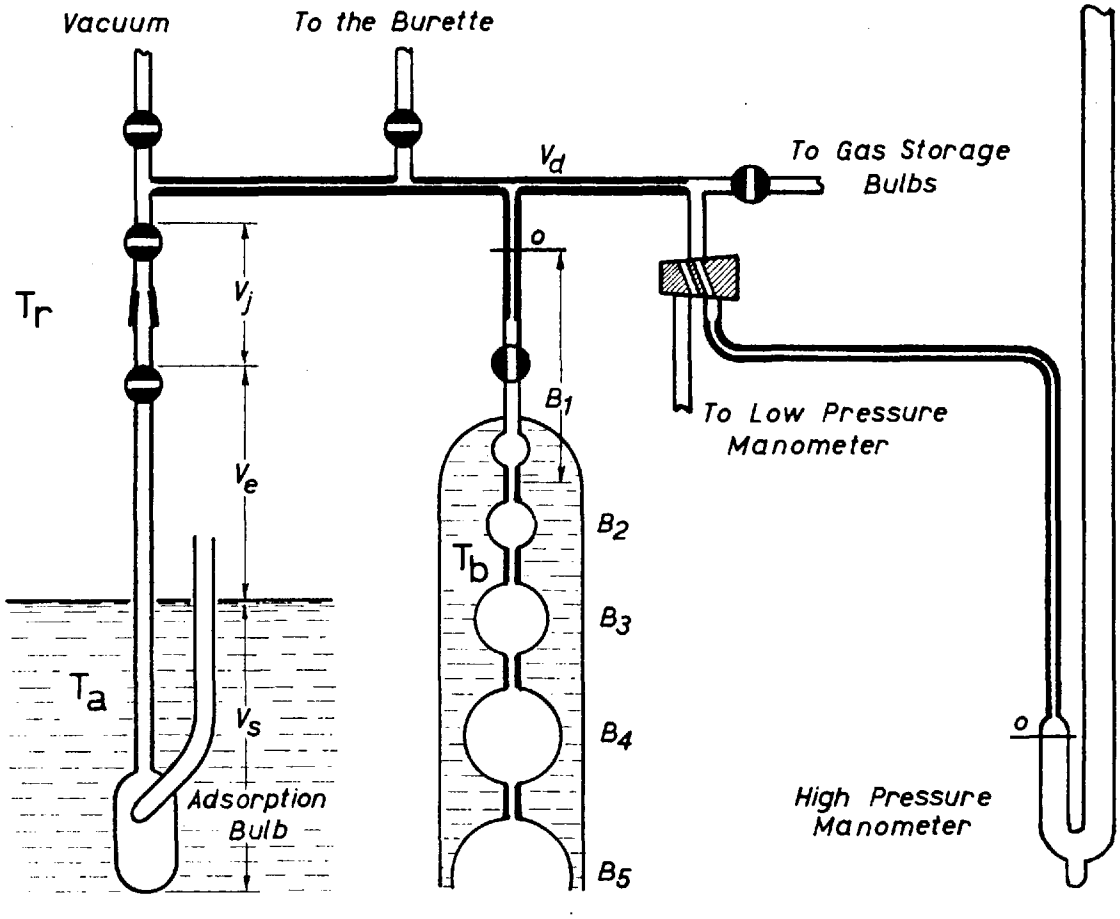

Volumetric Adsorption System

Fig.8

This enabled the gas pressure to be so adjusted as to give a regular bubbling rate through the relief leg. The gas was dried before entering the diffusion cell by passing it first through a bed of activated alumina and then through a bed of 1/16 in. pellets of molecular sieve 5A (left hand side of Fig.6). The latter was thoroughly activated under high vacuum and a temperature of 400°C.

On completion of adsorption of the active material SC4 was closed and the double-oblique stopcock turned to allow the flow of non-active gas through the diffusion cell. The gas flow rate was measured in a capillary flowmeter filled with dibutyl phthalate. The pressure drop across the capillary was read with a cathetometer, and the flowmeter was previously calibrated against a soap bubble flowmeter.

The Volumetric Adsorption Apparatus.

The apparatus for volumetric equilibrium measurement (Fig.8) consisted of calibrated displacement bulbs, a burette for filling the bulbs and for continuous volume variation, and two manometers, one for high pressure measurement and one for low pressure measurement. The gas bulbs (Volumes 5.768, 19.706, 49.060, 99.40, and 163.10 cm^3) were interconnected with capillary tubing of known bore (0.08 cm^3/cm) and calibrated with mercury so that volumes could be measured accurately to 0.01 cm^3. The bulbs were enclosed in a glass jacket through which water from the thermostat could be

circulated.

The burette had a capacity of 100 cm^3 and was calibrated uniformly. It was also jacketed for accurate temperature control. The main use of the burette was for filling the volumetric bulbs and for measuring with a reasonable accuracy the quantity of radioactive gas adsorbed in the diffusion cell.

Precision Manometers.

Two manometers were used. For measurement of pressures above 10 cm Hg absolute a 7 mm Veridia precision bore tube was used. This manometer (Fig.6) was backed with an engraved mirror scale. For reading the pressures a cathetometer was used. The cathetometer scale was used only for low pressure readings. For higher pressures only the cathetometer telescope was used. This enlarged the millimetre scale and eliminated parallax, and by means of a focused torch attached to the telescope enabled the mirror scale to be read very quickly and with an accuracy of ± 0.01 cm.

For low pressure measurements a 25 mm bore precision tube was used. This reduced mercury surface tension errors and enabled pressure to be read from 10 cm Hg down to about 0.1 cm by reading the cathetometer scale to 0.001 cm.

Because of the limited head room in the fume cupboard the burette and the high pressure manometer had to be specially mounted in perspex blocks with the mercury reservoirs placed

behind the tubes instead of below them. The flow of mercury into the burette and the manometer was controlled with a greaseless valve operating a neoprene gasket against a capillary orifice (made by Springhams of Harlow). The neoprene appeared to corrode with dirty mercury, thus contaminating it, but when triply distilled mercury was used no contamination was observed. This type of valve is essential for manometers because the mercury will inevitable carry through grease from a greased stopcock into the measuring arm. The valve is also much safer when it is necessary to elevate mercury to any height, as in the burette, when by compressing the gas even at one atmosphere the pressure at the base of the column can easily exceed two atmospheres.

The bulbs, the burette, and the manometers were connected by means of capillary tubing to the adsorption bulb which was attached to the system by means of a B10 ground glass joint. The arrangement was so chosen as to minimise the length of capillary tubing required, in order to reduce to a minimum the dead space between the bulbs, the burette, and manometers and the adsorption bulb. In this case the volume of the dead space was about 7 cm^3. This was determined accurately by utilising the previously calibrated volumes of the bulbs.

Radioactive Gas Preparation.

The radioactive gas was either purchased in its pure form, contained in glass ampoules, such as methane -C-14 and ethane -C-14, or else it was prepared from a solid as in the case of carbon dioxide. The glass ampoules were provided with break seals and they only had to be attached to the system and the seals broken when required.

Carbon dioxide was obtained in the form of active barium carbonate and it had to be generated by the action of an acid. This was done using a dropping funnel and a reaction tube attached to it by means of a ground glass joint. The reaction space was connected to the vacuum system and also to three coils in which moisture and carbon dioxide could be condensed using a solid carbon dioxide in alcohol bath, or a liquid nitrogen bath. The radioactive gas was prepared by placing a weighed quantity of barium carbonate -C-14 in the reaction tube, attaching it to the dropping funnel and evacuating the system. The stopcock to the vacuum line was then closed and carbonate covered with water via the funnel. Dilute acetic acid was then added through the funnel dropwise so as to maintain a controlled reaction with the carbonate. In this way the carbon dioxide could be prepared under vacuum, in the presence of water vapour only, without any risk of sudden reaction or excessive foaming. When the reaction was completed the carbon dioxide was condensed with

liquid nitrogen in one of the condensation coils, the stopcock to the reaction tube closed and the gas was freed from moisture by repeatedly passing it through a coil in a solid carbon dioxide in alcohol bath. The gas was then transferred to a storage bulb and diluted with non-active gas to the required concentration.

2. THERMOSTATS

Thermostats were required for maintaining the volumetric bulbs and burette at a constant temperature, slightly above ambient, and for maintaining the adsorption bulb and diffusion tube at a constant controlled temperature.

The ambient thermostat was an ordinary controlled water bath, heated with a bulb of low capacity so that the water temperature could be controlled easily within 0.01°C.

For adsorption and diffusion measurements a special low temperature thermostat was required for operation at temperatures down to -120°C. The function of the cryostat was to precool the inactive carrier gas and to maintain the diffusion tube at a constant selected temperature. It also had to be arranged in such a way that the diffusion tube could be easily withdrawn from the liquid bath without mechanically moving the tube which was attached to the vacuum glass system.

Mechanics of the Cryostat.

The assembled cryostat can be seen on the right hand side of Fig.10. The cryostat liquid (a carbon tetrachloride - chloroform mixture or petroleum ether for a lower temperature) was contained in a Dewar $7\frac{1}{2}$ in. diameter and 20in. deep. The Dewar was contained in a steel drum which could be raised and lowered inside another drum using pulleys and weights (Fig.10). All the components of the cryostat were attached to one half of a heavy wooden lid which rested on the rim of the outside drum as shown in Figs.9 and 10. The other half of the lid could be removed for observation.

With this arrangement the liquid level could be lowered six inches by lowering the inner drum containing the Dewar. By placing the diffusion tube close to the surface it was possible to submerge it for diffusion runs and have it above the liquid for heating the tube during desorption and during the final stages of the diffusion.

Cooling the Bath.

The subambient temperature was maintained by feeding liquid nitrogen into a heavy copper block immersed in the cryostat liquid. The cooling block was made from a 3/4 in. I.D. pipe, 1/8 in. thick. The pipe was sealed at the bottom and a thin copper tube, 1/8 in. diameter, was wound around it and soldered to it to act as a gas thermometer (Fig.9).

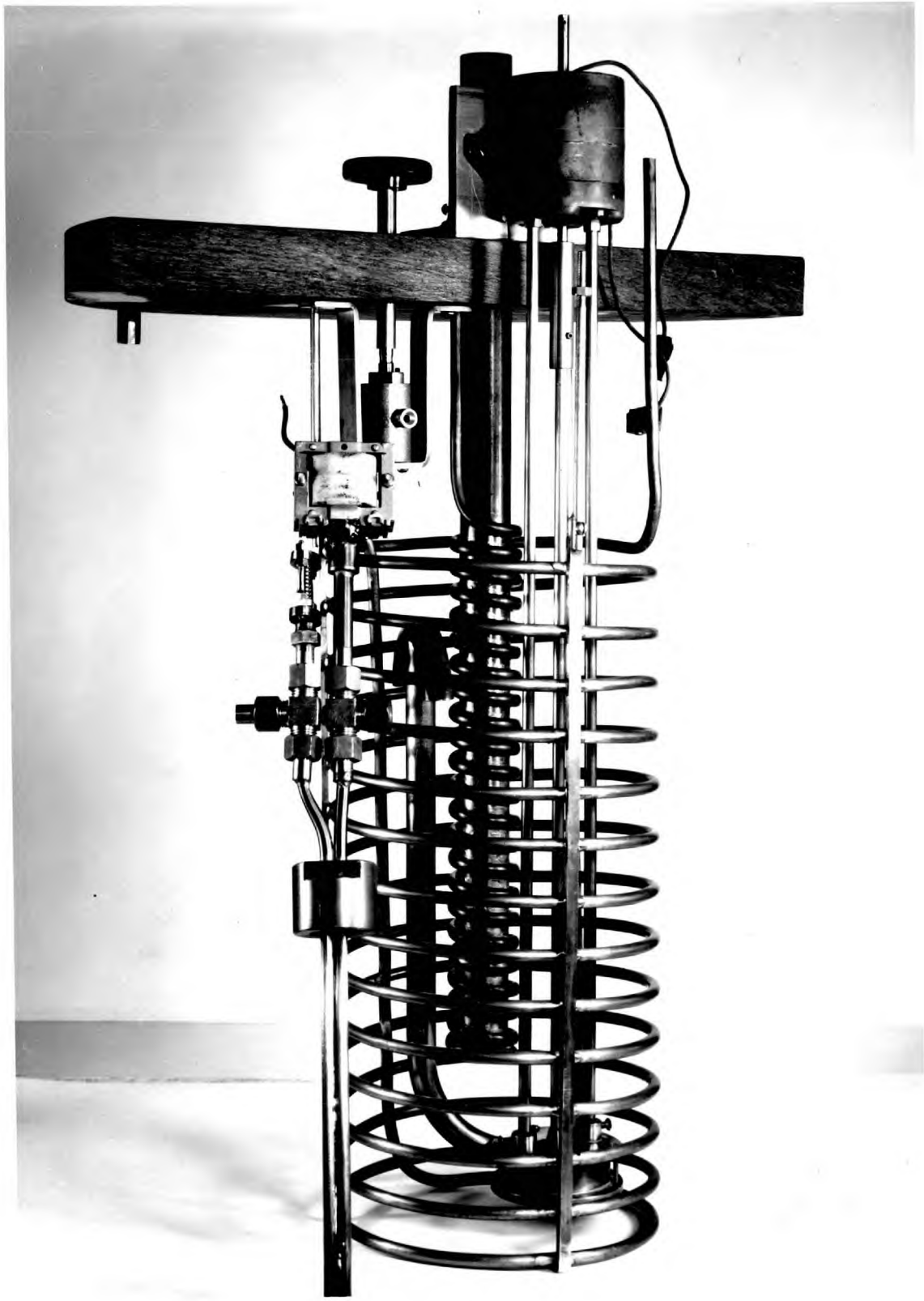

The liquid nitrogen was stored in a standard five gallon vacuum-insulated vessel and was fed to the copper cooling block, through a 1/8 in. copper line, by pressurising the vessel using compressed nitrogen from a cylinder. The liquid nitrogen flow rate was controlled by a solenoid operated on-off valve (leaning against the large coil in Fig.9), which consisted of a 1/8 in. ball bearing pressed by the weight of the solenoid plunger against a 1/16 in. orifice. An adjustable relief valve was provided for releasing excess nitrogen.

Controlling the Temperature.

The copper coil wound around the cooling block (the central coil in Fig.9) was filled with hydrogen and formed a sensitive gas thermometer. The coil was connected via nickel silver capillary tubing to a commercial manostat (K. D. G. Instruments) which acted as a switch for the solenoid valve. The manostat had a maximum pressure deviation of one inch of water, but because of its large volume it had to be immersed in a water thermostat at 25^{o}C in order to reduce the effects of atmospheric temperature variations.

The solenoid valve was operated at 240 V D.C. and a relay switch was used to connect it to the manostat which had a maximum current rating of 0.5 amp at 6 V.

This method of temperature control provides a very fast response to temperature changes in the cryostat and should produce a temperature stability within 0.02°C but this stability can be achieved only if the bath liquid is sufficiently agitated. For this reason a high speed circulating stirrer was provided which had the action of elevating the liquid from the bottom of the Dewar and throwing it on to the copper cooling block.

Diffusion Measurement.

The essential operations for diffusion measurements are to evacuate the cell while heating it, to saturate it at the required diffusion temperature with radioactive gas, and to pass precooled non-radioactive gas through it.

The nonactive gas was precooled by passing it through a 1/4 in. copper coil which just fitted inside the cryostat Dewar (outer coil in Fig.9). This coil was connected to one side of the diffusion cell through a specially made greaseless needle valve provided with metallic bellows which sealed the valve completely from the atmosphere. The other side of the cell was connected via a glass-to-metal seal to a glass vacuum stopcock positioned above the liquid level in the cryostat.

By evacuating the system from both sides of the needle valve high vacuum could be achieved in the diffusion cell and

there is, therefore, no need for the valve to be vacuum tight at the needle contact. The diffusion tube is saturated with radioactive gas by filling the precooling copper coil with non-active gas first and then filling the diffusion tube with the active gas. As the pressures on both sides of the needle valve are equal for each diffusion run there should be effectively no mixing of active and non-active gases when the valve is closed.

The valve and the diffusion tube were positioned very close to the liquid surface. By lowering the inner drum containing the Dewar the valve and the diffusion tube were exposed making it possible to heat the diffusion tube to achieve complete desorption in the final stages of each diffusion run.

3. RADIOACTIVITY MEASUREMENT

(a) Counting Equipment

Requirements.

It was necessary to select equipment which would be suitable for counting activity of radioactive gases over the whole range from very radioactive gases to those gases whose activity is only slightly above the background level. The most interesting gases to be investigated were those containing active sulphur ($H_2{}^{35}S$, $^{35}SO_2$), carbon ($^{14}CO_2$, $^{14}CH_4$, and other organic compounds), and hydrogen ($^3H_2$, ^3H_2O vapour). All these

gases are weak β-emitters and it is desirable to count these gases directly inside a counting tube rather than through a "window" of another counting tube, in which case the counting efficiency may be only 20% depending on the window thickness. Tritium cannot be counted at all through any window because its radiation is too weak (18 keV).

Radioactive gases inside a counting tube can be counted either in the proportional region or in the Geiger-Muller region. In the latter case the gases cannot be counted in their pure state and quench gases such as ethanol or carbon disulphide have to be added to slow down the positive ions on their way to the cathode. This is easily done for batch counting but is very hard to arrange in a flow system.

This means that for efficient counting in a flow system counting in the proportional region is to be prefered. There is, however, another substantial advantage of working in the proportional region. The maximum activity which can be counted in a counting tube depends on the resolving time of the tube. In the Geiger-Muller region this resolving time is about 200 μs but in the proportional region the resolving time is about 100 times shorter. This allows considerably higher initial activity which results in higher accuracy in the final stages of the diffusion experiments.

Equipment Selected.

With the above considerations the equipment was selected for Geiger-Muller and proportional counting in a gas stream of rapidly varying activity. All the electronic instruments were of commercial design and were selected individually on the basis of performance and cost from quotations submitted by all the British Manufacturers.

The equipment chosen consisted of the following:-

(i) Stabilised high voltage supply (General Radiological) - for supplying potential to the counting tubes.

(ii) Linear pulse amplifier (Ekco Type N568) - for amplifying the weak pulses from a proportional counting tube.

(iii) Scaler and Timer (Dynatron Scaler 1009 with Timer N108) - for batch counting, for counting of slowly varying activity and for count and time display (see Fig.10) for use with cine-photography during very rapidly varying count rates.

(iv) Ratemeter and Pulse Height Analyser (Ekco Type N600) - for general rate measurement and pulse bandwith selection for optimum activity to background ratio.

(v) High Speed Recorder (Philips) - for recording the count rate during diffusion experiments and for occasional thermocouple e.m.f. measurement.

All the units were arranged in a mobile rack as shown in Fig.10.

Operation of the Counting Equipment.

The instruments were connected as shown schematically in Fig.11. In proportional counting the output pulse from

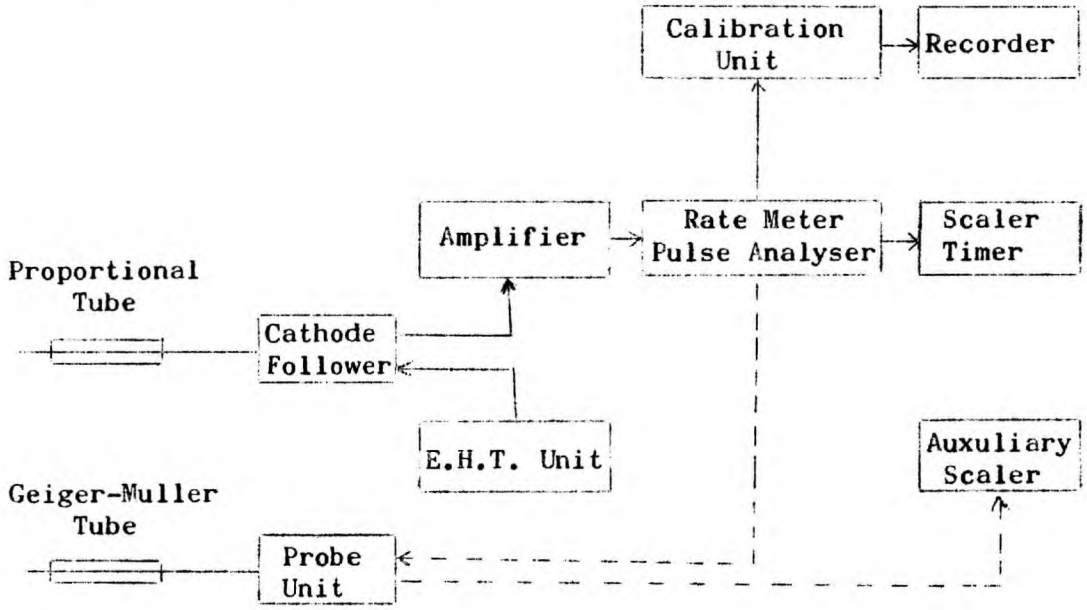

Counting Equipment Block Diagram. Fig.11

the amplifier was passed through the pulse height analyser of the ratemeter unit. Here two gates were adjusted so that only those pulses could be counted whose amplitude fell within a predetermined range. This range was selected around the mean pulse amplitude so as to get the highest count rate to background rate ratio.

The ratemeter output was fed through a calibration unit (at the bottom of the rack in Fig.10) to the recorder. The calibration unit consisted of a number of potential

dividers and was specially constructed for accurate adjustment of the pulse rates. A standard signal from a frequency generator was fed to the ratemeter and the potential dividers in the calibration unit were adjusted to give the exact reading on the recorder. The calibration unit also had a facility for converting half scale and two thirds scale on the ratemeter to full deflection on the recorder. These settings were also calibrated with a standard frequency source.

For diffusion measurements where the radioactive substance was exchanged slowly the recorder readings could be utilised directly: to give the count rate at any time, or by integrating the area under the curve to give the cumulative quantity of active material evolved. Alternatively, the scaler could be read by observation at regular intervals to give the cumulative count.

In some diffusion measurements the exchange took place so quickly that the count rate fell from, say 2000 c/s to 2 c/s in about 10 seconds. In this case the response of the ratemeter was much slower than the decay in the count rate and the ratemeter output could not be used for quantitative assay. Very accurate readings could be obtained, however, by photographing the dekatron tubes of the scaler and timer with a cine camera. This gave a permanent and accurate record of count versus time, the latter being shown to one tenth of a second. In cases of extremely rapidly varying count rate,

eg. in studying the resolution of a counting tube with a "square pulse", the cine camera was run at 50 frames per second so that the time was determined to two hundredths of a second.

In some cases it was desirable to pass the radioactive gas through two counting tubes and to measure the count in each one, the first one being accurate for early time and the second for late time. The first tube had a small volume with high resolution and the ability to register very high count rates, while the second had a large volume and a low background count. The second tube was usually a Geiger-Muller tube, shielded with two inches of lead. The output of this tube was recorded on an auxiliary scaler, the high voltage being supplied by a subunit of the ratemeter (Fig.11). The auxiliary scaler was photographed together with the scaler and timer giving a simultaneous record of the counting tubes.

(b) Detection Tubes

The radiation detection tubes used were either filled with a permanent gas mixture and provided with mica windows for radiation detection, or they were of the flow-through type with the flow gas carrying the activity and itself acting as a counting gas.

Side Window Counter.

For ordinary experiments where the maximum gas activity was about 1000 c/s registered in the counting tube it was more convenient to use a permanently filled Geiger-Muller tube as they are easier to operate than proportional counting tubes.

For detecting rapidly varying activity of strongly active gases a commercial side window counter was used (20th Century Electronics, Type SW12). The side window was made of mica (2 mg/cm^2) and had an area of about 1 x 12 cm. A special sheath was fitted around the window with an inlet and outlet at the two ends of the window (Fig. 12A). The volume between the sheath and the window was made very small (about 2 cm^3) which resulted in a very small gas delay time in the tube. Because of the linear flow there was also very little gas mixing, making this tube very suitable for initial diffusion measurements.

End Window Counter.

For measurement of low activity use was made of a standard end window counter (20th Century Electronics, Type EW3HA) to which a glass cell was attached for gas flow (Fig. 12B). This cell was most useful in measuring the final stages of diffusion when the activity is low and it changes very slowly. The background of this tube, operated inside a lead castle (1¼ in. wall thickness) was only 0.23 c/s.

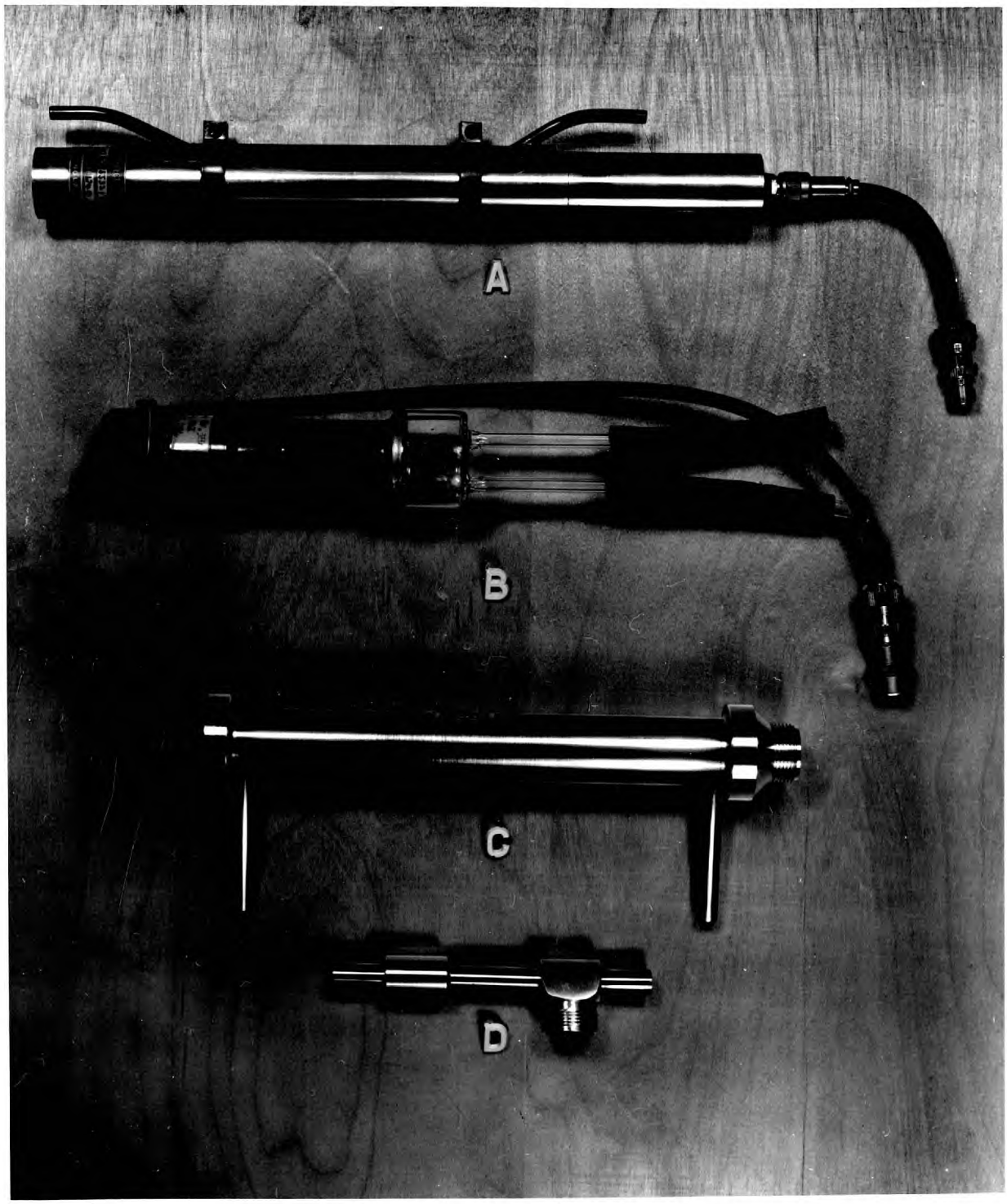

Radiation Detection Tubes

Fig. 15

Flow Counters.

For counting radioactive gases in the proportional region and in the Geiger-Muller region, where it is desirable to count the activity directly, flow-through counters had to be used. These were not available commercially nor could any references be found. Two such tubes were constructed and these are shown in Fig.12C and D.

The larger of these counting tubes has an internal diameter of 1 in. and a tungsten anode 0.1 mm diameter and it is very useful for the measurement of slowly varying low activity.

The smaller tube was used for the initial diffusion measurement when it is essential to have a small volume and streamline flow characteristics. It was made from 3/8 in. I.D. brass tubing with the two ends of the anode wire (0.1 mm dia.) suspended from two supports attached to insulators inside the tube wall.

(c) Pulse Resolution Corrections

In all random pulse measurements a correction has to be applied for the counting tube pulse width and for the resolution of the amplifying and scaling equipment. The correction is applied for the short dead period following each pulse. During this period the counting tube or the

counting equipment is inactive and any pulses arriving in that time are not registered. This correction becomes important for high count rates and for long resolution periods.

The overall or effective resolving time of the counting assembly is determined mainly by the greatest pulse width. If the resolving time of either the amplifier or the scaler is poorer than that of the detection tube then a small correction has to be applied to this resolving time for the resolving time of the tube.

Proportional Counting.

When gases are counted in the proportional region the pulses in the counting tube are very short (1 to 2 μs) and the effective resolving time is determined by the amplifier which shapes the pulses by adjusting the rise time and the decay time with the differentiating and integrating time constants. Calculation of the pulse shape and the resulting resolving time has been clearly described by Gillespie.[63]

For accurate pulse calculation the differentiating and integrating time constants of the N568 amplifier have been calibrated by measuring the resistances and the capacities on a potentiometer and a capacity bridge. The measurements and the calculated time constants are given in Table 3. For possible pulse height analysis the attenuator resistances of the amplifier have been measured also and the

corrected attenuations are given in Table 4.

Table 3.

Differentiating and integrating time constants of N568.
Differentiating resistance = 531.63 ohms.
Integrating resistance = 1815.5 ohms.

Nominal time constant μs	Differentiating constant			Integrating constant		
	Nominal capacity μμF	Measured capacity μμF	True time constant μs	Nominal capacity μμF	Measured capacity μμF	True time constant μs
0.08	120	118.3	0.0629	-	-	-
0.16	270	313.5	0.1667	100	87.0	0.1579
0.32	560	559.1	0.2972	180	193.4	0.3511
0.8	1200	1228	0.6528	470	467.8	0.8493
1.6	2700	2710	1.441	1000	1010	1.834
3.2	5600	5905	3.139	1800	1816	3.297
8	12700	13454	7.153	4700	4680	8.479
250	0.5μF	0.475μF	252.6	-	-	-

Table 4.

Attenuator calibration of N568.

Nom.att. dB	True att. dB	Nom.att. dB	True att. dB	Nom.att. dB	True att. dB
0	0	14	14.064	28	28.250
2	2.004	16	16.033	30	30.263
4	4.035	18	17.970	32	32.273
6	6.047	20	20.188	34	34.252
8	8.062	22	22.192	36	36.221
10	10.075	24	24.223	38	38.158
12	12.085	26	26.235	40	40.170

Geiger-Muller Counting.

The resolving time of a tube operated in the Geiger-Muller region is about one hundred times longer than for a proportional counter and may be as high as 800us in some halogen filled tubes. This severely limits the maximum permissable count rate and it has to be carefully studied if true count rates are to be obtained.

A typical pulse inside the end window counter described earlier is shown in Fig.13 where the pulse shape has been

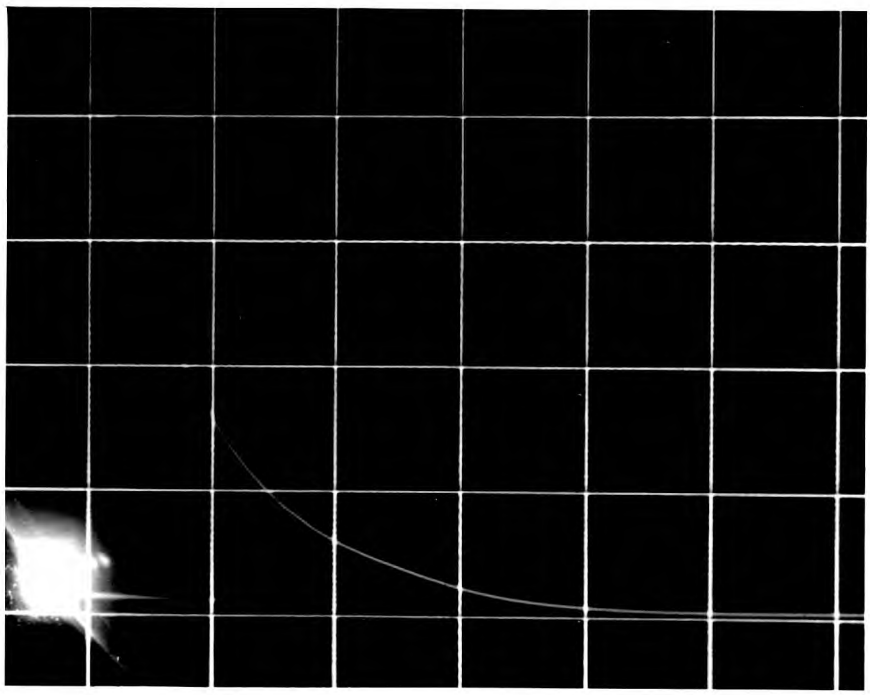

Geiger-Muller Pulse Decay. Fig.13

traced on an oscilloscope. The amplitude is in arbitrary units but one division of the horizontal time base represents 200 µs. The pulse thus consists of a very rapid rise followed by exponential decay. This curve gives a qualitative idea for the time during which the tube is inactive, say 500 µs, but no accurate measure of the recovery time can be obtained from the curve itself.

The true recovery time can be obtained by the method shown in Fig.14. Here a high count rate has been used resulting in a set of superimposed decay curves obtained by triggering the time base with the pulse itself. The spread

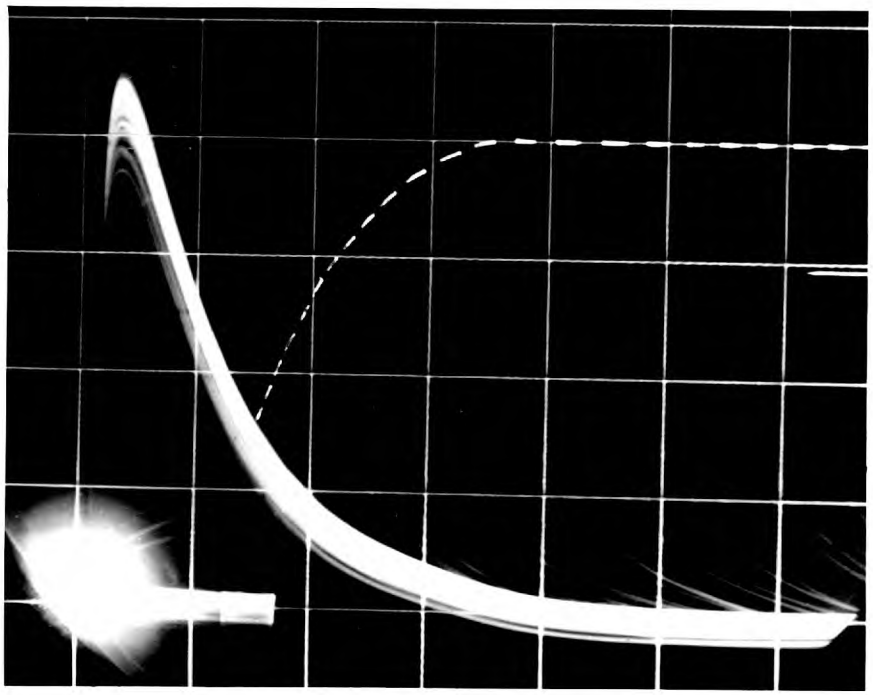

Pulse Recovery Envelope. Fig.14

in the decay curves is due to a slight variation of pulse amplitude as well as to a drop in the applied high potential after each pulse.

Following each initial pulse any other pulse arriving within the scan time of the oscilloscope should also be shown. It can be seen from Fig. 14 that there is a minimum time below which no pulses are recorded. Beyond that minimum the pulses arrive with increasing amplitude until they are fully recovered, as shown by the dotted envelope line. The recovery time of this tube (end window counter) is therefore about 300 μs. The exact time depends on the amplifier sensitivity and the scaler threshold level as only pulses of a certain minimum amplitude can be recorded.

The three or four pulses outside the envelope in Fig. 14 should be disregarded. They are due to a faulty oscilloscope which sometimes started a scan without being triggered by a pulse from the counting tube.

Resolving Time of Sidewindow Counter - Scaler.

The sidewindow counter was used at very high count rates and it was necessary to determine the total resolving time of the counter amplifier and scaler very accurately.

The recovery time of the tube was determined by constructing from oscilloscope traces the decay curve (1) and the pulse recovery envelope as shown in Fig. 16. To

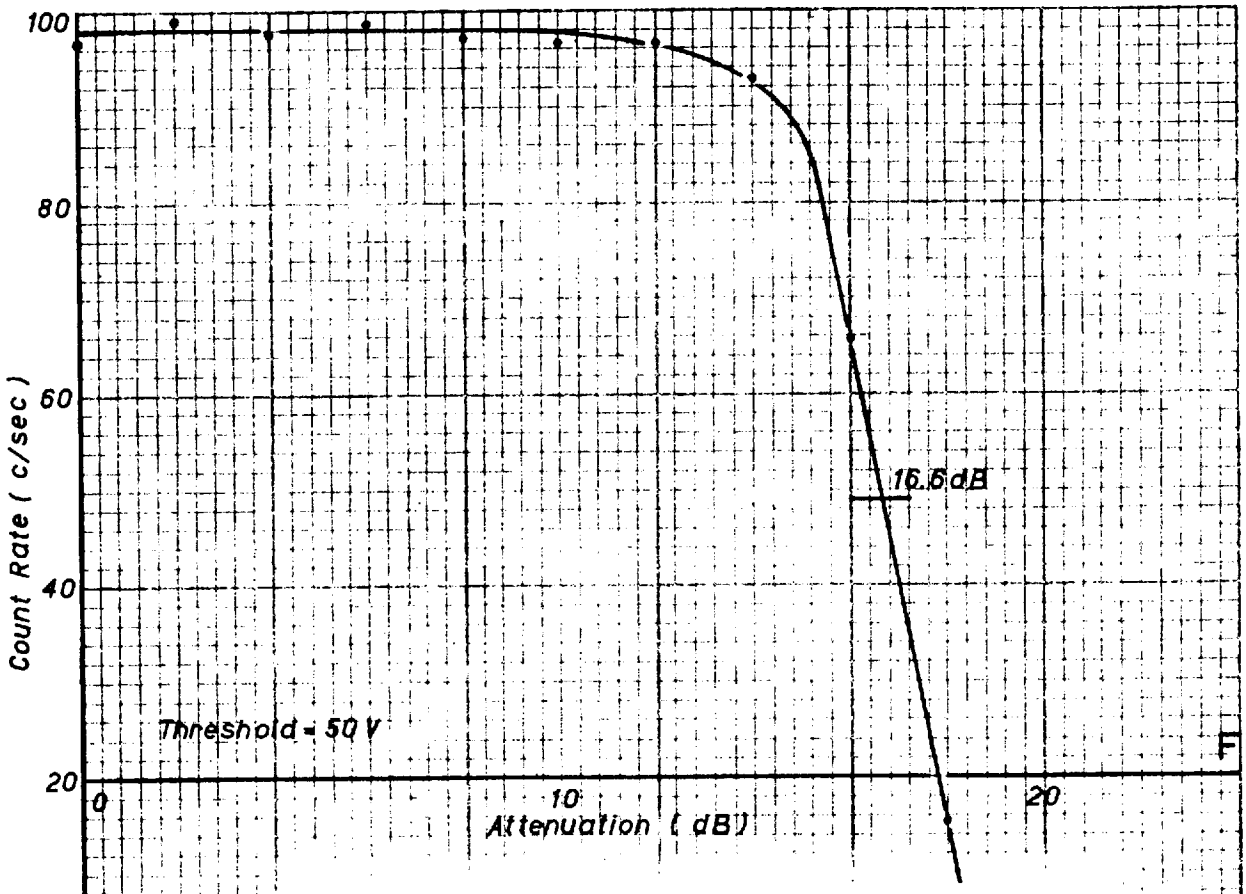

Fig.15

Determination of Resolving Time

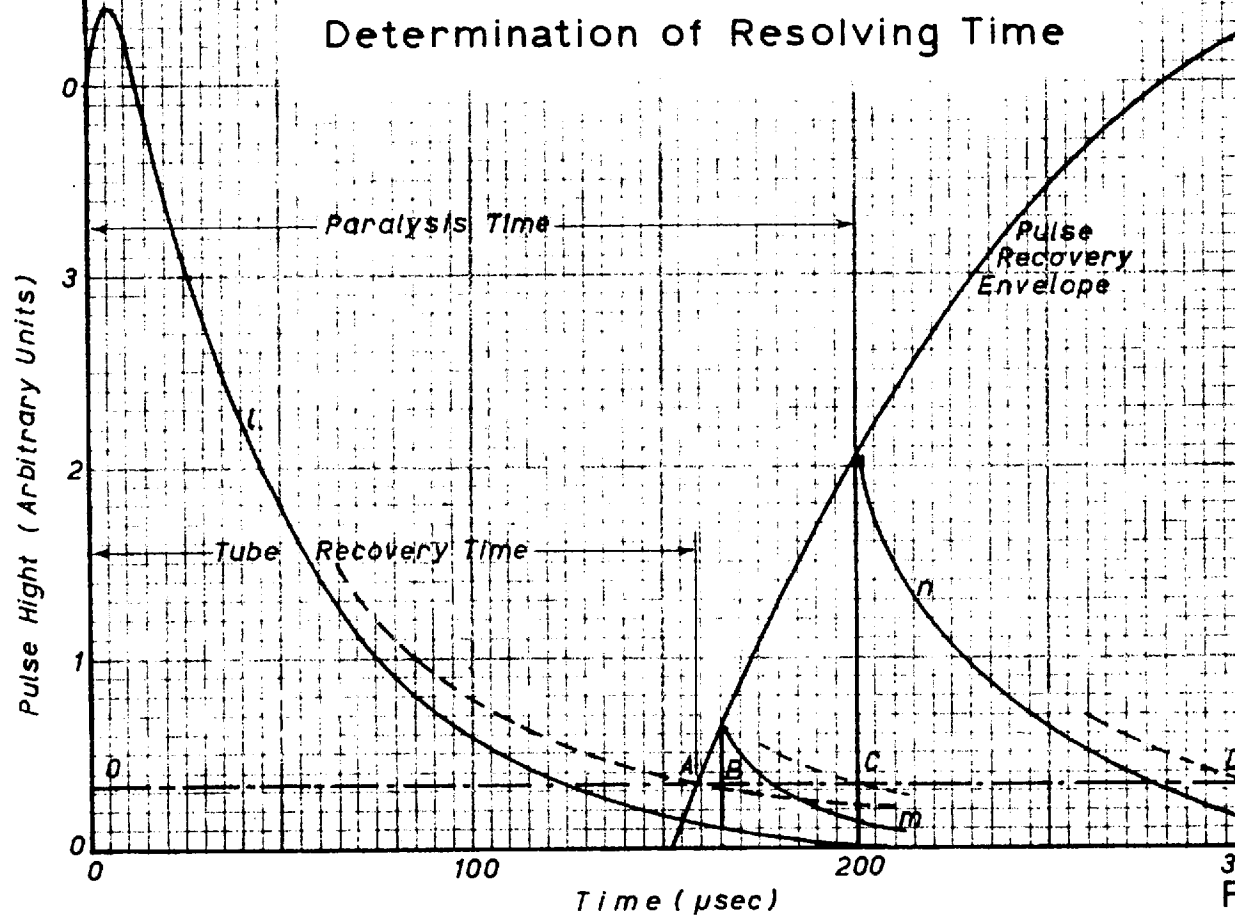

Fig.16

determine the minimum amplitude recorded an arbitrary pulse rate was recorded against amplifier attenuation (Fig.15) with the scaler threshold at 50 V. From this curve it was found that at 16.6 dB the mean pulse height was 50 V. Thus at normal operation (10 dB and 5 V threshold) the mean pulse height was calculated to be 107 V, and the minimum pulse detected is given by 4.4 x 5/107 = 0.205 arbitrary divisions in the units of Fig. 16. The intersection of the dotted line, 0.205 divisions higher than the decay curve 1, with the pulse recovery envelope determines the tube recovery time (159 μs).

Because this recovery time is unstable and varies with the age of the tube and to some extent with the count rate, a paralysis time of 200 μs was imposed by the scaler after each pulse. For this type of arrangement the ordinary corrections for pulse resolution[67] do not apply, and a special correction was derived as follows.

In the notation of Fig.16 the two curves m and n are critical, for any pulse arriving between O and B would not be recorded and the dead time would remain at 200 μs. Any pulse arriving between B and C would not be recorded either, but it would extend the dead time by up to 100 μs.

Let N = observed count rate (c/s)
No= true count rate (c/s)
T = paralysis time (s)
s = BC (s), Fig.16
t = CD (s), Fig.16

Then, after each recorded pulse the instrument is dead for NTs/s. Also for each pulse arriving within s the instrument is dead for an extra $N_o st/2$ seconds on the average.

$$\text{Therefore total dead time} = NT + NN_o st/2$$

$$\text{and actual counting time} = 1 - NT - NN_o st/2$$

$$\text{But } N_o \simeq N/(1 - NT)$$

$$\text{Therefore } N_o = \frac{N}{1 - NT - \frac{N^2 st}{2(1-NT)}}$$

Using this formula and the values of s and t from Fig.16 a correction curve ($N_o - N$ against N) was constructed and used for correcting the side window counter results.

When no paralysis time was applied (when using the ratemeter and the recorder) then the usual resolving time correction was used.[67]

$$N_o = \frac{N}{1 - NT_r}$$

where T_r is the recovery time of the tube as defined in Fig.16.

III EQUILIBRIUM MEASUREMENTS

The main purpose of the equilibrium measurements was to determine the optimum desorption temperature for diffusion measurements by observing the effect of desorption temperature on equilibria. It was also necessary to obtain accurate equilibrium measurements on powders, as such equilibria were not available, and to check the accuracy of the commercial equilibrium adsorption curves[42] for pellets.

The general apparatus has been described in the last section and a schematic diagram of the essential parts of the volumetric apparatus was given in Fig.8, p.28.

The molecular sieve powder or pellet sample (1 to 5 g) was held in detachable sample bulbs of the type shown in Fig.17A. The bulbs were provided with a 2 mm stopcock and a B10 ground glass joint so that they could be detached easily from the system and weighed while under vacuum. A small thermocouple well was attached to the bulbs for temperature measurement. A directly sealed-in platinum and platinum/rhodium thermocouple would have been more sensitive but it was found impossible to achieve a permanent vacuum tight joint between the platinum wire and Pyrex glass.

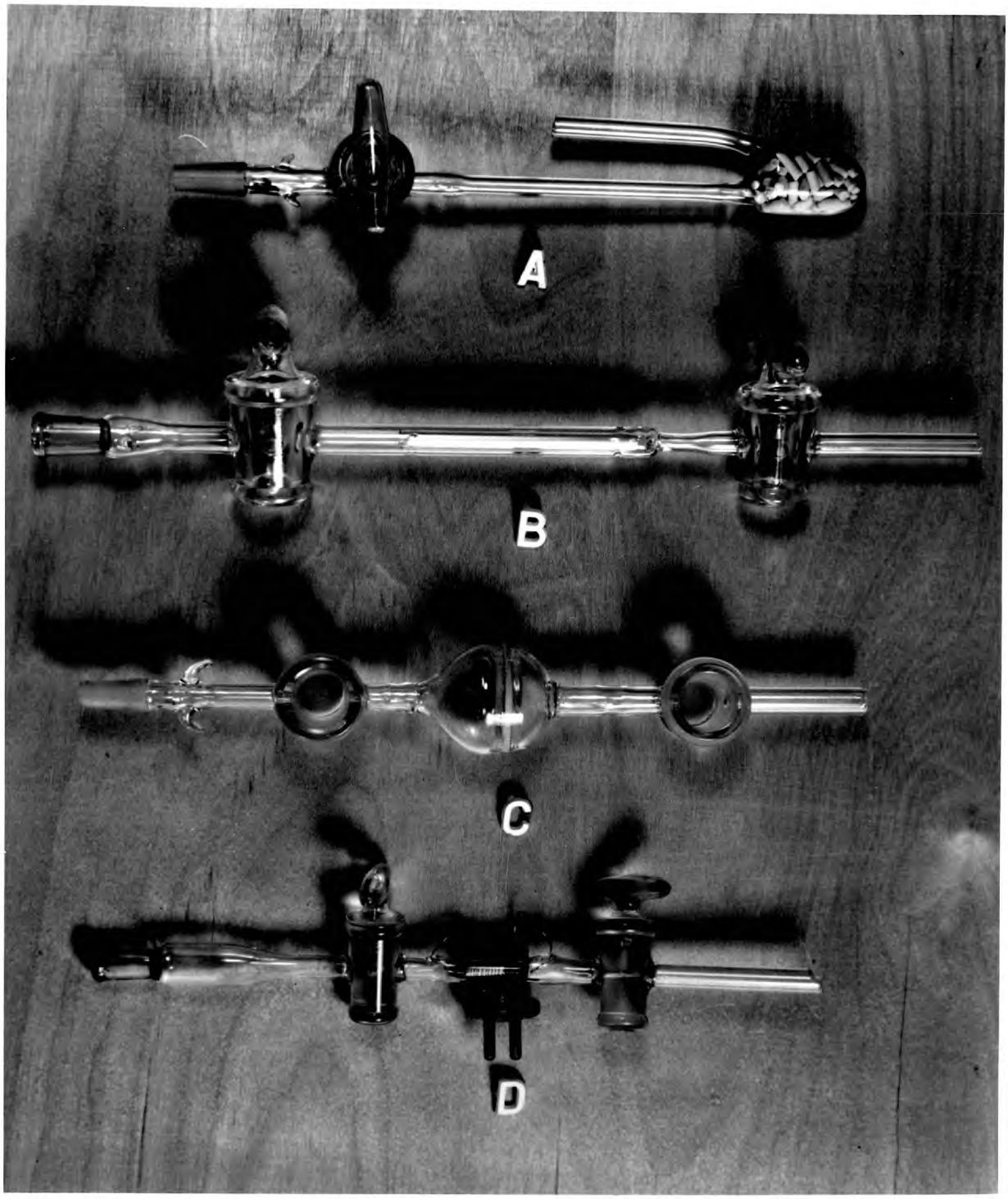

Equilibrium Bulb and Diffusion Tubes Fig. 17

Desorption Furnace.

To remove the moisture adsorbed on the molecular sieve the sample has to be evacuated while heating it at temperatures up to 500°C. To obtain a uniform desorption temperature a small furnace was built by winding nichrome wire around a thick walled silica tube (1¼ in. I.D.). More resistance wire was wound around the ends of the tube to improve the uniformity of temperature distribution, one end of the tube was sealed to reduce convection, and the whole was well insulated with vermiculite. During desorption measurements of the temperatures inside the furnace and inside the sample bulb thermocouple were well within 2°C of each other.

Desorption Measurements.

The simplest way to study the freedom from adsorbed gases (water in particular) is by weight loss under evacuation and heating. This was done for pellets and powder by weighing a sample of the molecular sieve in the sample bulb described earlier (Fig.17A).

The pellets originally saturated with atmosphere moisture were desorbed at 25, 300, 400, and 500°C while evacuating with the full capacity of the backing and diffusion pumps. The desorption - time curves are shown in Fig.18. The 25°C curve is not shown because the desorption of moisture was so slow that after 30 hr only about one fifth of the adsorbed moisture was removed.

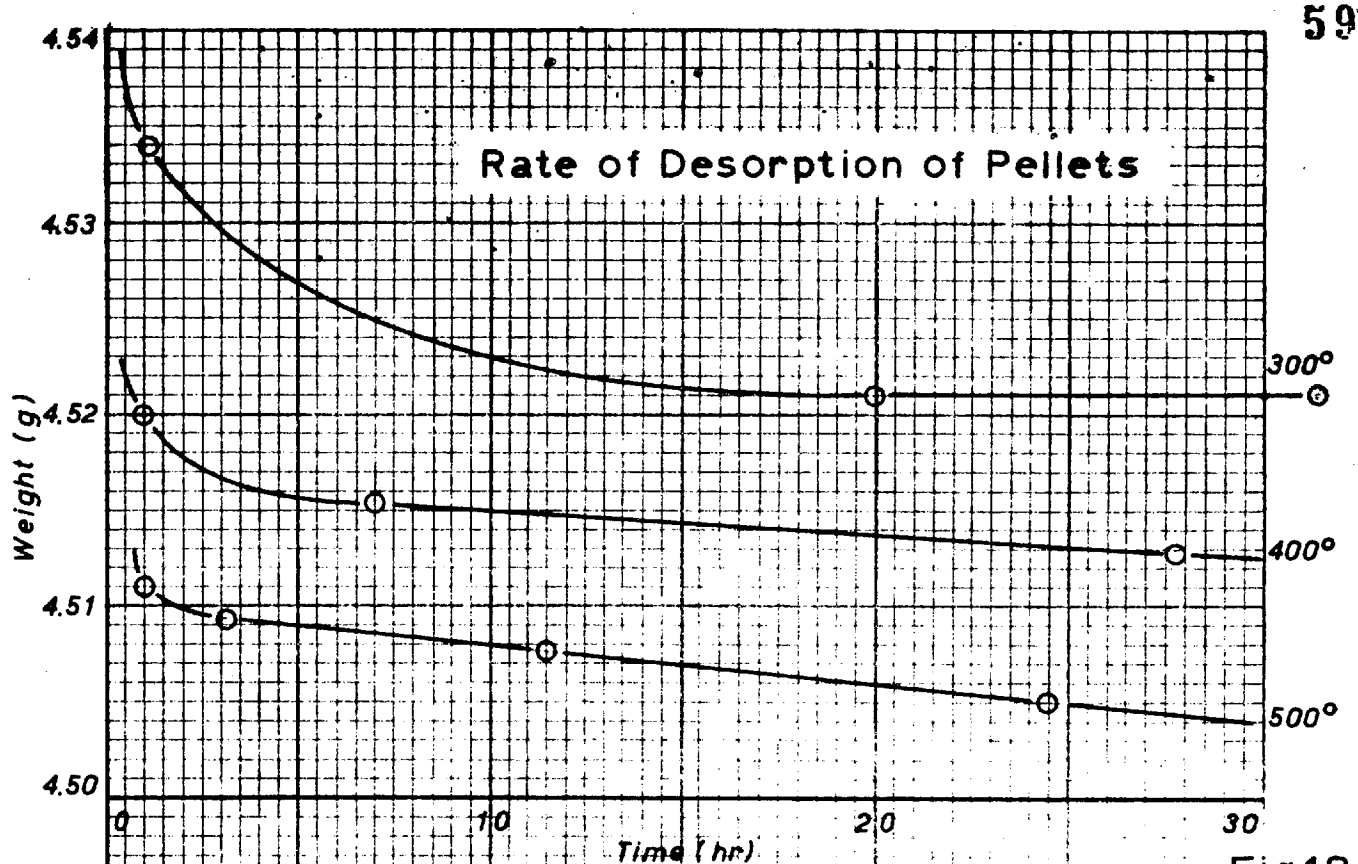
Rate of Desorption of Pellets
4.54
4.53
4.52
4.51
4.50
Weight (g)
300°
400°
500°
0
10
20
30
Time (hr)

Fig.18

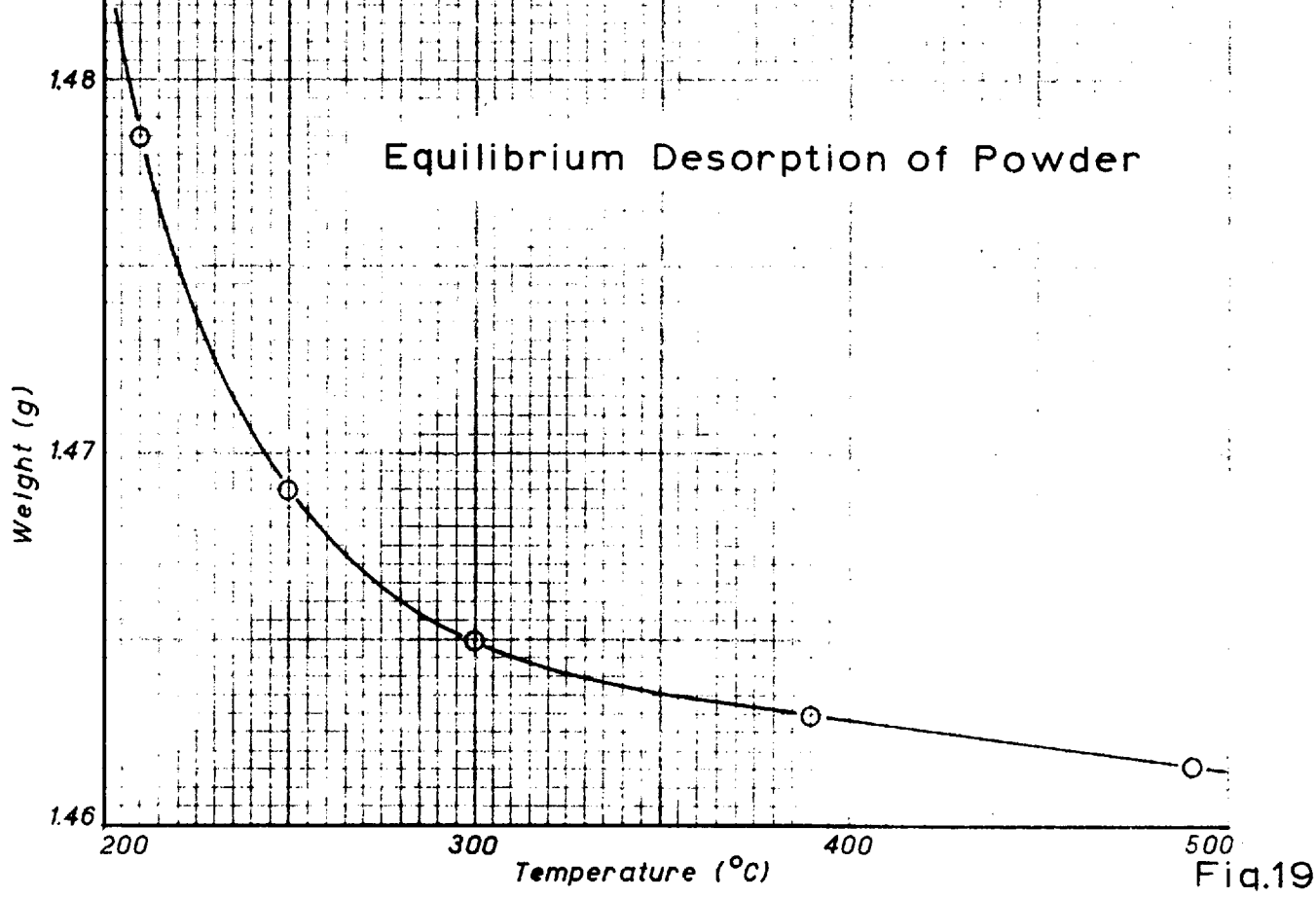
Equilibrium Desorption of Powder
1.48
1.47
1.46
Weight (g)
200
300
400
500
Temperature (°C)

Fig.19

The curves are only semiquantitative because the time shown is the cumulative total heating time and equilibration had occurred while the weighings were made. However, two features are clearly shown; the approach to apparent equilibrium was faster at higher temperatures and no true equilibrium could be reached at 400 and 500°C. This means that we cannot really determine how much dry molecular sieve we have. The reason for this is not very clear but is probably associated with the binder present in the pellets. Part of the binder may begin to dissociate at the higher temperatures or alternatively some of the molecular sieve powder may be fully encased by the binder resulting in a very slow escape of adsorbed gases by diffusion through the binder.

The above assumptions were substantiated by carrying out a similar desorption study on a powder sample. Unfortunately rate of desorption curves, similar to those in Fig.18, could not be obtained because the initial desorption had to be carried out very slowly to prevent carryover of the powder. However, unlike the measurements with the pellets, a steady weight was reached at each temperature, for example at the desorption temperature of 490°C three weighings after 2, 16, and 32 hours were all within 0.2 mg of the mean, well within the experimental weighing errors.

The results of this powder desorption study are given in Fig.19. It can be seen that even at 500°C steady weight has

not been reached although the weight loss is fairly small in the range 300 to 500°C. It should be noted that this desorption was done under full vacuum (better than 10^{-5} mm Hg.) and it is hard to see why at each temperature there is different equilibrium value. The water adsorption isotherm must be somewhat non-reversible. Certainly there must be some very strong bonding between the polar water molecule and the positive and negative ions forming the walls of the cages, but the exact nature of those is not known.

Carbon Dioxide Adsorption Isotherms.

Adsorption isotherms were obtained partially volumetrically and partially gravimetrically with the arrangement shown in Fig.8. The gravimetric method consisted of detaching the sample bulb and weighing it. This gave the direct weight of gas adsorbed, but because this method is very slow, necessitating cleaning and regreasing of the high vacuum joint and waiting for equilibrium to be re-established, it was used only at high pressures where the volumetric errors are large because of the cumulative errors of each point and because of the inherent inaccuracy in the dead space.

The volumetric method consisted of displacing a known volume gas from the volumetric bulbs into the adsorption bulb and measuring the pressure before and after adsorption. This is best illustrated by a sample calculation.

Calculation of an Isotherm Point.

Referring to Fig.8, p.28, $(V_e + V_s)$ is the total sample bulb volume, including the stopcock, from which the sample volume (Table 2, p.15) has been substracted. V_e is the volume at room temperature, T_r and V_s the volume at the adsorption temperature, T_a. The dead space, $(V_j + V_d)$, represents the volume occupied between the stopcocks and the zero marks of the volumetric bulbs capillary and the manometer. The volume of the bulbs is as shown in the figure, while B_l can be split further into its part at room temperature B_{lr} and at bulb temperature B_{lb}.

Using the notation $W = PV/T$ we have before adsorption, with the adsorption bulb stopcock closed,
relative weight of free gas in the sample bulb,

$$W_s = (V_s + V_e T_s/T_r)P_s/T_s,$$

and the relative weight of gas in the dead space and the volumetric bulbs,

$$W_b = [(V_j + V_d + B_{lr} + \sigma' + \rho')T_b/T_r + (\Sigma B_i + \sigma'')]P_b/T_b$$

where σ' and σ'' are the mercury level corrections to be applied if the mercury has not been set exactly at the zero mark and the calibration marks between the capillaries respectively, and ρ' is a similar correction for the manometer.

After adsorption, by opening the sample bulb stopcock and displacing the gas from all or some of the volumetric bulbs, similar equations apply and, designating these by W_s^* and W_b^*, we

have the weight of gas adsorbed,

$$W_{ads} = (W_s - W_s^*) + (W_b - W_b^*)$$

and the isotherm point is obtained by summation of lower isotherm points, thus the total amount adsorbed,

$$q = \Sigma W_{ads}.$$

Example:

Adsorption bulb volume	$= 8.990\ cm^3$
Dry weight of M.S. pellets	$= 4.5120\ g$
Volume of M.S. and binder	$= 2.660\ cm^3$
Free volume of adsorption bulb	$= 6.330\ cm^3$

$V_e = 0.830\ cm^3$	$V_d + V_j = 10.670$
$V_s = 5.500\ cm^3$	$B_{lr} = 2.000$

Before adsorption all the bulbs were occupied with carbon dioxide and we had

$P_b = 35.114$ cm Hg	$\Sigma B_s = 161.10\ cm^3$
$\sigma'' = 0$	$T_r = 296.93^\circ$ K
$\rho' = 0$	$T_b = 298.15^\circ$ K

and $W_b = (12.67 \times 298.15/296.93 + 161.10)35.114/298.15$

$= 20.489$

From the previous adsorption point we had $W_s = 0.114$.

After adsorption all the gas was displaced from the volumetric bulbs and we had

$P_s = 36.217$ cm Hg	$T_s = 298.15^\circ$ K
$P_e = 36.217$ cm Hg	$T_r = 296.91^\circ$ K
$\sigma' = 0$	$\rho' = 1.580\ cm^3$

thus $W_s^* = (5.500 + 0.830 \times 298.15/296.91)36.217/298.15$

$= 0.769$

and $W_b^* = (10.670 + 1.580)36.217/296.91$

$= 1.494$

Therefore $W_{ads} = (0.769 - 0.114) + (20.489 - 1.494)$

$= 18.340$ relative weight units

$= 18.340/0.1417$ mg

$= 18.340/(0.1417 \times 4.512)$

$= 2.868$ wt.%

Total gas adsorbed at previous isotherm points = 11.738 wt.%

Therefore $q = 2.868 + 11.738$

$= 14.61$ wt.% at 36.22 cm Hg and 25.0°C.

Pellet Isotherm.

Adsorption measurements were made on the pellets after desorption at 300 and 400°C. Taking the desorbed weight at 400°C for the dry weight of molecular sieve no difference could be detected between the 300° and 400° isotherms. The experimental points obtained are plotted in Fig.20 against the commercial isotherms from Union Carbide.[22]

It can be seen that the agreement is excellent over the entire range and the commercial curves can be used with a high degree of confidence.

Powder Isotherm.

There is no available accurate data on carbon dioxide adsorption on molecular sieve 4A. A 25°C isotherm was therefore

ISOTHERM DATA SHEET NO. 21
ADSORBATE: Carbon Dioxide
TEMPERATURE: −75°C to 350°C

TITLE: Carbon Dioxide Adsorption
ADSORBENT: Molecular Sieve Type 4A Pellets

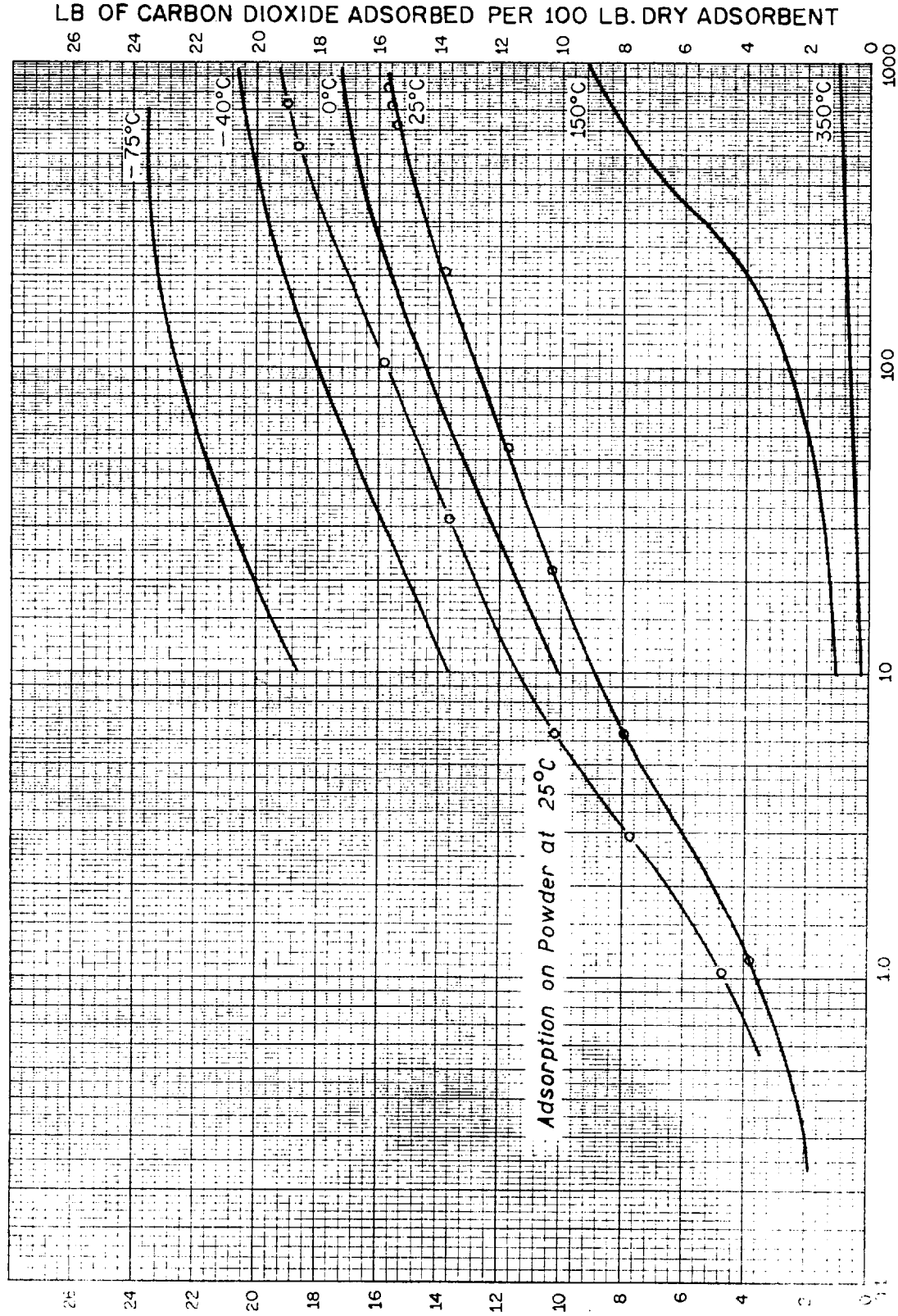

Fig 20

determined and this is shown also in Fig.20. The powder isotherm has a similar shape to that of the pellet and assuming that the binder does not adsorb any carbon dioxide the apparent powder content of the pellet is 78% as determined by adsorption at 0.1 cm Hg rising to nearly 82% of powder at atmospheric pressure. This can be reconciled by assuming that the binder (probable particle size 0.01 to 0.1 μ) has also adsorptive capacity and as its characteristic adsorption curve need not be the same as that of the powder this can account for the variation in apparent percentage composition.

Conclusions.

From the isotherm determinations it is apparent that the desorption temperature has little effect on the quantity of carbon dioxide adsorbed, provided that it is at least 300°C and that full desorption has been reached. There is however a definite equilibrium loss at all desorption temperatures up to 500°C for powders. With pellets no equilibrium weight could be reached at the higher temperatures, probably because of some action associated with the binder.

It is hard to tell from this what the effect would be on diffusion measurements, particularly on the slow desorption rate shown in Fig.5, p.17. It is quite possible that this slow rate may be entirely due to the action of the binder, in which case the desorption temperature may have a significant effect on this rate.

IV DIFFUSION MEASUREMENT

1. GENERAL PRINCIPLES

The experimental equipment and techniques have been described earlier. Although the methods used do not involve any new principles not one published reference could be found either on the interpretation of the flow system or on the measurement of rapidly varying radioactivity.

Special tubes were developed for activity measurement. These were described in Section II 3(b) and recommendations will be made later for improving them.

Because this is a new method full details will be given on the interpretation of the system and a sample calculation will be given also for diffusion through powders.

An ideal behaviour of the system is shown by the solid lines in Fig.21. Fig.21A represents the variation of gas activity (c, counts per second) as measured by a counting tube situated at the exit of a diffusion tube (Fig.17), while Fig.21B represents the cumulative count ($\int c$, counts). The count rate, c, is obtained from the ratemeter or, by differentiation, from the cumulative count, $\int c$, registered on the scaler.

The instruments are switched on before the flow is started and the ratemeter shows a constant background rate which is slowly integrated by the scaler as shown in Fig.21B.

Ideal Diffusion Measurement

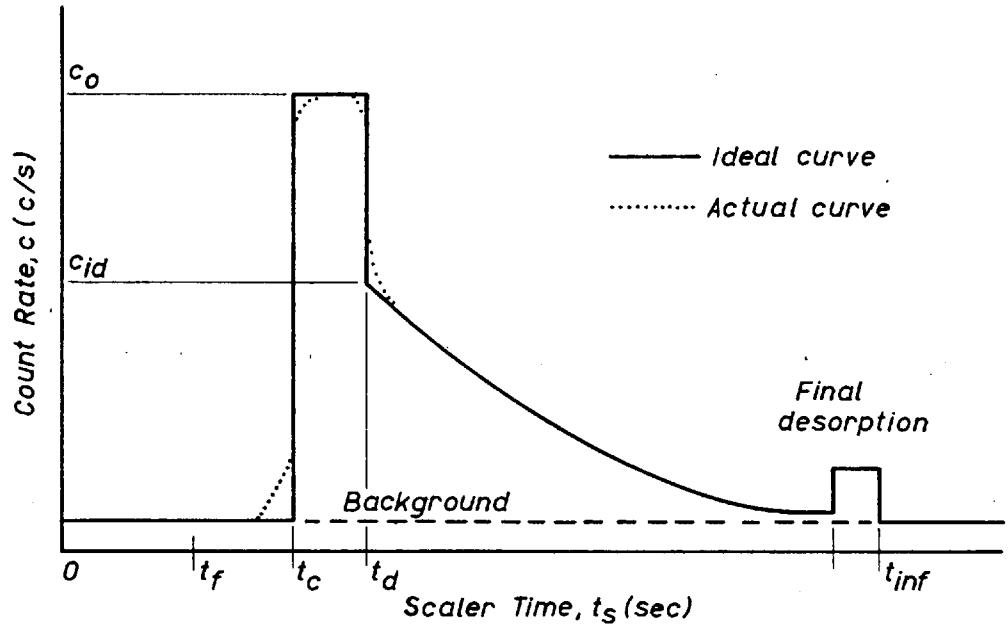

A.

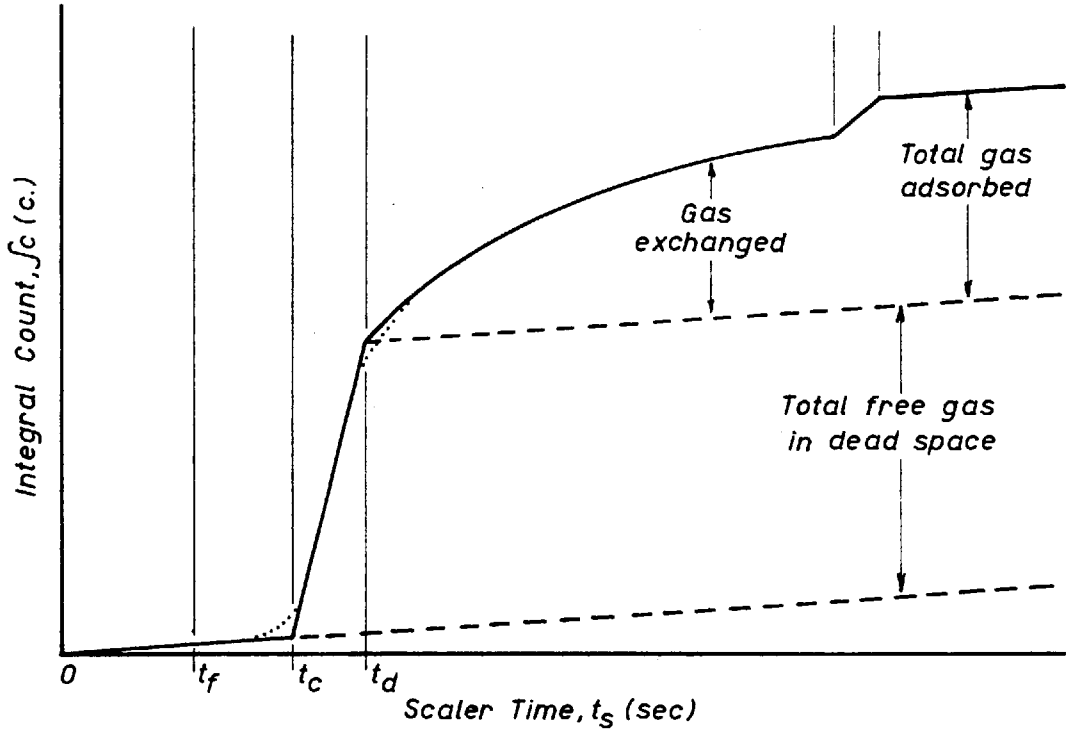

B.

Fig.21

t_f Seconds later gas flow is commenced through the diffusion tube beginning the displacement of radioactive gas from the diffusion tube. No increase in activity is observed by the counting tube until the radioactive gas reaches it at t_c, when suddenly the count rate increases to c_o, the activity of the radioactive adsorption gas.

As soon as the active gas has been displaced from around the adsorbent the activity drops suddenly to C_{id} representing the initial diffusion rate. Thereafter the count rate keeps decreasing as more and more of the adsorbed radioactive gas is exchanged, until the count rate reaches the background value of the counting tube.

The behaviour of the integral count is shown in Fig.21B. Between t_c and t_d there is a constant gradient, corresponding to the constant rate in the counting tube. At t_d the gradient changes suddenly and then decreases gradually until it reaches the background gradient.

In practice all the sharp corners shown by the solid line in Fig.21 are rounded because of gas diffusion and mixing, and because of finite volume of the counting tube.

Gas diffusion cannot be prevented, but it is minimised by placing the counting tube as close as possible to the diffusion tube. Mixing is reduced by streamlining the flow path. In general these two cannot be predicted, but correction

can be made for these by calibration.

In the absence of any mixing the correction for counting tube resolution can be estimated quite accurately if the volume is known. For example, the initial foot at t_c in Fig.21A, when plotted from accurate scaler data, gives an excellent straight line representing uniform increase in activity as the initial sharp wavefront moves through the counting tube.

In ordinary adsorption - desorption rate measurements it is very difficult to decide when equilibrium has been reached and the final point is quite arbitrary. In the present method, however, the final point can be determined precisely by heating the sample and thus rapidly displacing the final traces of adsorbed gases. This is illustrated in Fig.21B. The last points have, therefore, a high absolute accuracy because they are obtained directly and not by the difference method as in ordinary adsorption.

2. DIFFUSION IN A PELLET

The exchange of carbon dioxide in a pellet has been shown in Fig.5, p.17. Diffusion measurements can be made by simply suspending a pellet inside a tube fitted with two stopcocks. However during desorption the pellet must be heated to at least 400°C by winding a heater on the outside of the diffusion tube. This requires that the high vacuum stopcocks be far apart to prevent the grease from melting (during heating the system must maintain a vacuum of 10^{-5} mm Hg). As a result

there is a very large dead space inside the counting tube which considerably reduces the accuracy of the diffusion measurements.

A substantial reduction in the dead space can be made by using an internal heater as shown in Fig.17D. This utilises the hot wire microscope principle in which a noble metal junction is used simultaneously for heating and temperature measurement by using an oscillator switch which allows the passage of a heating current in one half of the mains cycle and during the other half permits the e.m.f. of the junction to be measured with a potentiometer.

This principle has been fully described by Welch[96] who gives circuits and the method of operation. The complete oscillator is shown in Fig.10 standing on top of the potentiometer. As suggested by Welch the instrument was adjusted with an oscilloscope to make sure that the switching took place at zero potential of the current cycle, otherwise the switch would be rapidly eroded under heavy current.

The thermocouple, made of 5% rhodium/platinum and 20% rhodium/platinum, was used as shown in Fig.17D. Thin wire (0.03 mm dia.) was wound around the pellet so that the thermocouple junction came in the centre of the pellet. The thin wire was then joined to the thicker similar wire (0.5 mm dia.) and taken out through the walls of the tube to be connected to the oscillator. The diffusion tube was made from soda glass which gives a better seal with the platinum wire

than pyrex glass, particularly for sealing in a thick wire. Soda glass is the main limitation of this method as the desorption temperature must be limited to 400°C maximum.

This particular combination of the thermocouple wire was used because it has a flat temperature response at room temperature eliminating the need for a cold junction. This would not only be inconvenient but would also require a large length of thick and expensive platinum wire.

To reduce heat losses from the diffusion tube to the atmosphere a small heating coil was wound around the tube, but this was much smaller than would be required in the absence of the thermocouple coil so that the length of the tube and its internal volume could be kept down to a minimum.

3. DIFFUSION IN MOLECULAR SIEVE CRYSTALS

(a) The Diffusion Tube

The selfdiffusion coefficient for molecular sieve crystals has been found by using a diffusion tube of the type shown in Fig.17C. The molecular sieve powder was suspended in water and allowed to settle by gravity onto the sintered glass disc in the centre of the tube. The slow settling from a water suspension has the advantage that the larger particles, consisting mostly of coagulated lumps of powder, will settle first thus forming an impervious bed on which finally even the smallest crystals (about 0.1 u) can be effectively suspended.

Three porosities for the sintered glass disc were tried (2x, 3x, and 4x), but only 3x (about 20 μ pore size) was found to be satisfactory. With the larger porosity it was too difficult to form a bed and even with the tube initially filled with water, some of the particles would fall through the disc under gravity. The smaller porosity formed a good support but it gave a high pressure drop which is a disadvantage in diffusion measurements with high diffusion coefficients. An ideal combination would be to have a compound disc formed of a very thin layer of 4x on 2x for support.

With this type of diffusion tube it was hoped that at sufficiently high gas velocities through the bed, an inert atmosphere could be obtained around each powder crystal thus allowing the measurement of carbon dioxide exchange in the crystal itself.

(b) Calculation of Diffusion Curves

Experimentally we have a record of the integral count, registered by a scaler, as a function of time. From this we would like to calculate two types of curves, one giving the percent of the active gas exchanged in the molecular sieve as a function of time, as already shown in Fig.5, p.17, and the other giving the percentage gas count rate, or carrier gas activity (C/C_o) as a function of time.

Table 5.

Carbon dioxide exchange in molecular sieve crystals.

1	21	2	3	4	18	19	20
Scaler time, t_s sec	Diff. time, t_d sec	Integ. count, $\int c$ c.	Dead space, $\int r$ c.	$\int c - \int r$ c.	$\int c' - \int r'$ c.	$\int C$ c.	CO_2 Exch. %
57.20	-	96	96	0	0	-	-
79.40	-	258	258	0	0	-	-
79.78	-	800	800	0	0	-	-
80.10	-	1300	1300	0	0	-	-
80.50	-	1900	1900	0	0	-	-
81.20	-	2900	2820	80	170	(0)	-
81.90	(0.40)	3900	3540	360	470	(480)	(2.25)
82.82	(1.32)	5110	4210	900	810	(1510)	(8.65)
83.68	(2.18)	6110	4670	1440	1090	(2500)	(14.3)
84.44	2.94	7010	5000	2010	1330	3340	19.1
85.24	3.74	7900	5210	2690	1550	4240	24.3
86.16	4.66	8800	5400	3390	1770	5160	29.6
87.08	5.58	9705	5530	4175	1975	6150	35.2
88.00	6.50	10500	5620	4880	2150	7030	40.2
. . . . .							
. . . . .							
133.20	51.7	19906	5940	13966	13000	16966	97.28
150.8	69.3	20104	5990	14114	3000	17114	98.13
206.4	124.9	20278	6090	14190	3000	17190	98.57
	*180						98.70
	*230						98.74
	*332						98.80
	*805						98.82
	Inf.					17440	100.00

* These points were obtained from the end window counter.

Table 6.

Activity decay in carrier gas.

5	12	6	7	8	9	10	11
Count time, t_c sec	Diff. time, t'_d sec	Gradient, m deg	Count rate, c c/s	D.T. corr. c' c/s	Corr. for D.T. c+c' c/s	Corr. for B.G. C c/s	C/C_o %
0	-	55.8	1470	610	2080	2078	100.0
2.5	-	55.8	1470	610	2080	2078	100.0
3	0.2	54.1	1381	529	1910	1908	91.8
3.5	0.7	51.9	1275	440	1715	1713	82.4
4	1.2	50.1	1196	378	1574	1572	75.7
4.5	1.7	49.0	1150	350	1500	1498	72.1
5	2.2	47.8	1103	317	1420	1418	68.2
. . . . .							
47.3	44.5	-	28.2	0.1	28.3	26.6	1.28
58.4	55.6	-	15.0	0	15.0	13.3	0.64
81.4	78.6	-	4.6	0	4.6	2.9	0.14
109.2	106.4	-	2.3	0	2.3	0.6	0.03

Table 7.

Corrections for diffusion tube dead space.

5	13	14	15	16	17
t_c sec	grad. deg	r c/s	r' c/s	c'-r' c/s	$\int c' - \int r'$ c.
0	55.8	1470	610	0	0
0.5	55.8	1470	610	0	0
1.0	55.8	1470	610	0	0
1.5	52.2	1303	467	143	71
2.0	47.8	1103	320	290	226
2.5	42.9	929	213	397	425
3.0	35.3	708	118	411	640
. . . . .					
28.0	-	-	-	-	2998
30.0	-	-	-	-	3000
Inf.	-	-	-	-	3000

The most convenient way to show how these curves were obtained is by the following sample calculation for experimental run E36.

The diffusion run was performed at atmospheric pressure and temperature (the precise pressure and temperature are immaterial). The powder sample was desorbed under high vacuum and a temperature of 400°C, and then saturated at room temperature with radioactive carbon dioxide. Non-active carbon dioxide, at the same pressure as during saturation, was passed through the tube and the sample bed, and the resultant activity, detected with the side window counter described earlier, was measured on a scaler and is shown in columns 1 and 2 of Table 5.

The empty diffusion tube, free of molecular sieve powder, was calibrated earlier by filling it with similar radioactive gas and displacing it with non-active gas at the same velocity as during the diffusion run. The activity detected by the side window counter in this test is shown in Fig.23.

The calculations which were performed on this experimental data are shown in Fig.22 and Tables 5,6, and 7. The columns of all these three tables are numbered in the order in which they were derived from the experimental results. The following notation is used:

$\int c$ - integral count (total cumulative count) as actually registered on the scaler during the diffusion run,

$\int r$ - actual integral count during the calibration run, under similar conditions of gas concentration, pressure, and flow,

c,r - count rates obtained by differentiation of $\int c$ and $\int r$; these count rates could have been obtained alternatively directly from the ratemeter and recorder,

c',r' - count rate corrections for counting tube pulse resolutions,

C - fully corrected count rate,

C_o - initial corrected count rate,

$\int C$ - fully corrected integral count,

t_s - scaler time,

t_c - time from start of count,

t_d - time from start of diffusion.

In terms of these symbols the gas exchanged in the solid is given by $\int C = \int(c + c') - \int(r + r')$ while the activity of the gas is given by C. These two quantities were obtained in the following sequence of calculations.

The experimental diffusion results consisting of a cine film record of scaler time, t_s, and integral count, $\int c$, were plotted on a large scale graph, Fig.22. Some of the initial and final points are shown in columns 1 and 2 of Table 5. A similar plot of the calibration run was made in Fig.23.

These two runs were adjusted to the same time scale by measuring time from the commencement of count in each run. This

starting time, t_c, was obtained from the intersection point of the initial steady count rate and the background line as shown in the figures. Using adjustable time scales values of the integral dead time correction, $\int r$, were read off from Fig.23, corresponding to the experimental points of the diffusion run given in columns 1 and 2, and these are given in column 3. The correction points for times higher than those shown in Fig.23 were obtained by numerical extrapolation using an accurate value of background rate determined previously.

The integral count, corrected for the dead space, $\int(c - r)$, was obtained by subtracting column 3 from column 2 and is given in column 4. Before the true integral count can be obtained column 4 has to be corrected for the pulse resolution of the radiation detection tube and the counting assembly used.

First, the count rate, c, was obtained from the integral curve in Fig.22 by measuring the slope, m, and converting this to the rate. Initial measurements were taken at uniform intervals of count time, t_c, while later measurements, which were off the graph, were obtained numerically from adjacent points. Typical initial and final results are given in columns 5, 6, and 7 of Table 6.

The corrections for the resolving time of the counting assembly were worked out for the rates of column 7 using the method described in Section II, 3.(c). These corrections (column 8) were added to the count rate to give column 9 from

which only the background rate (1.7 c/s) had to be subtracted to obtain the true gas count rate, C, given in column 10. The relative activity, C/C_o, is given as percentage of the initial activity in column 11.

The corresponding diffusion times, t'_d, given in column 12, were measured from the beginning of the break-through curve, as shown in Inset A of Fig.22.

A similar method was applied to the calibration curve (Fig.23) to obtain the resolution correction, r'. These corrections, calculated at intervals t_c, similar to those of column 5, Table 6, are given in column 15 of Table 7.

The differential correction c' - r', given in column 16, was obtained by subtracting column 15 from column 8 and this was integrated by simple addition, column 17, and plotted in Fig.22. This plot was used for reading the corrections at the desired time intervals of column 1, as shown in column 18 of Table 5.

The quantity of activity exchanged between solid and gas, $\int C$, was obtained by adding columns 4 and 18 to give column 19. To determine the approach to equilibrium the remaining amount of radioactivity still present in the solid was driven off by heating the diffusion tube (200°C). The carrier gas flow was stopped during the heating and restarted when steady temperature had been reached. This was necessary because the system was working under a constant pressure and any change in pressure drop resulted in a change in carrier gas flow velocity.

Heating the diffusion tube increases the gas viscosity and thus reduces the gas flow rate. To avoid complicated integration under variable flow conditions the flow was stopped during heating and restarted when a steady temperature was reached. This gave a reduced but steady flow rate which was then used to adjust the desorbed activity to a rate corresponding to the main diffusion run. This adjusted value was added to the last diffusion point in column 19 to give the total activity desorbed at infinity. Using this figure the percent of active gas exchanged was calculated and this is given in column 20.

When $\int C$ was plotted against time, Inset B, Fig.22, it was found that the start of the diffusion, t_d^*, did not correspond to the value, t_d, determined from C in Inset B. In the absence of any a priori reason for the initial shape of the $\int C$ curve the average value, at $t_d = 0$, was taken as shown in the inset. This in fact corresponded to a straight line from which the initial $\int C$ points were read off (enclosed in brackets in Table 5).

The sequence of operations just described may appear rather long and thus introduce a lot of cumulative errors. This sequence, however, preserves the most important experimental points $\int c$ (column 2) and the cumulative errors apply only to the corrections and not to the main diffusion measurement. In an improved system of small dead space and low counting tube resolution correction (proportional counting) these corrections would be small and the resultant absolute accuracy quite high.

Analysis of Powder Diffusion Experiment E36

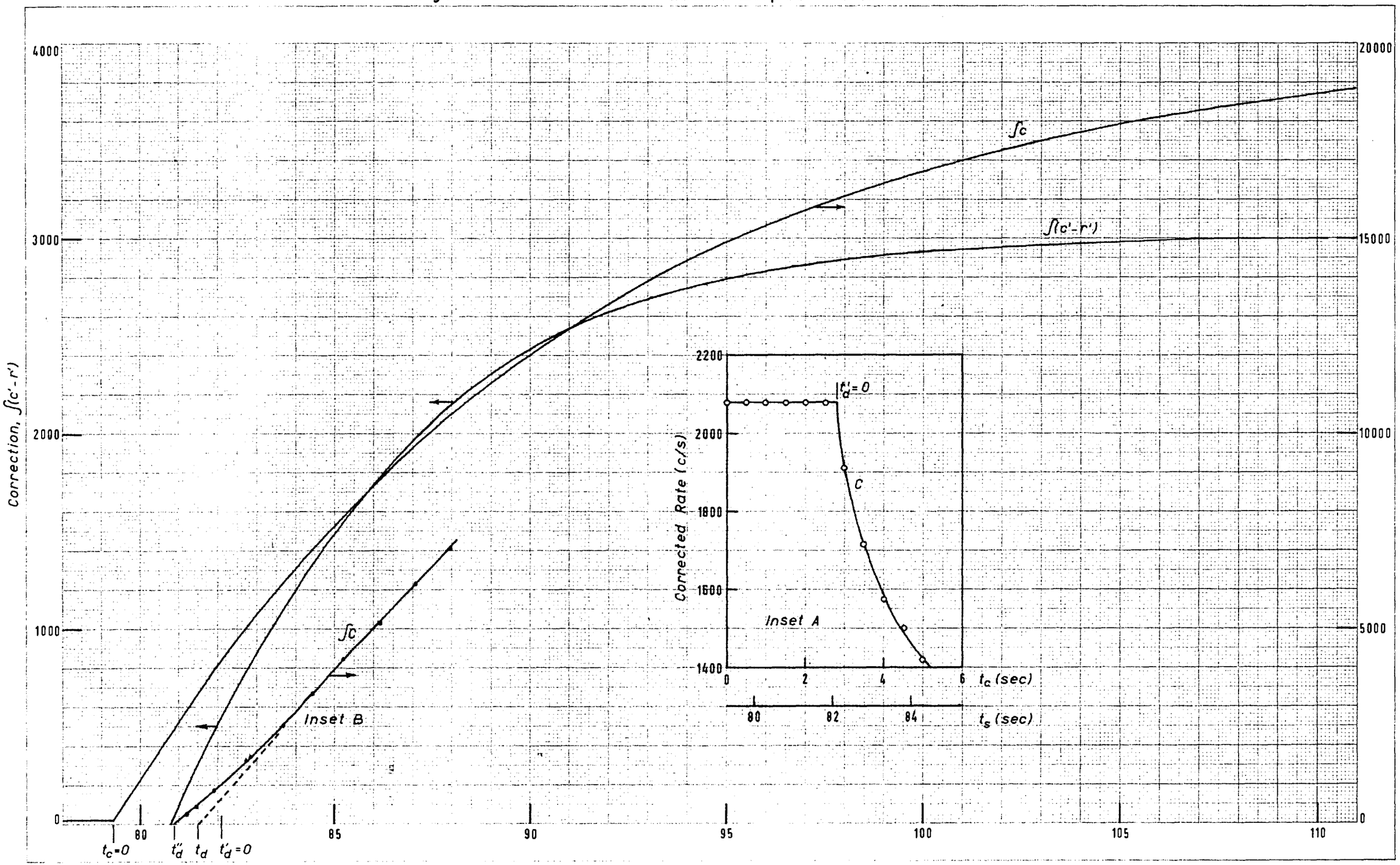

Fig.22

Calibration Run for E36

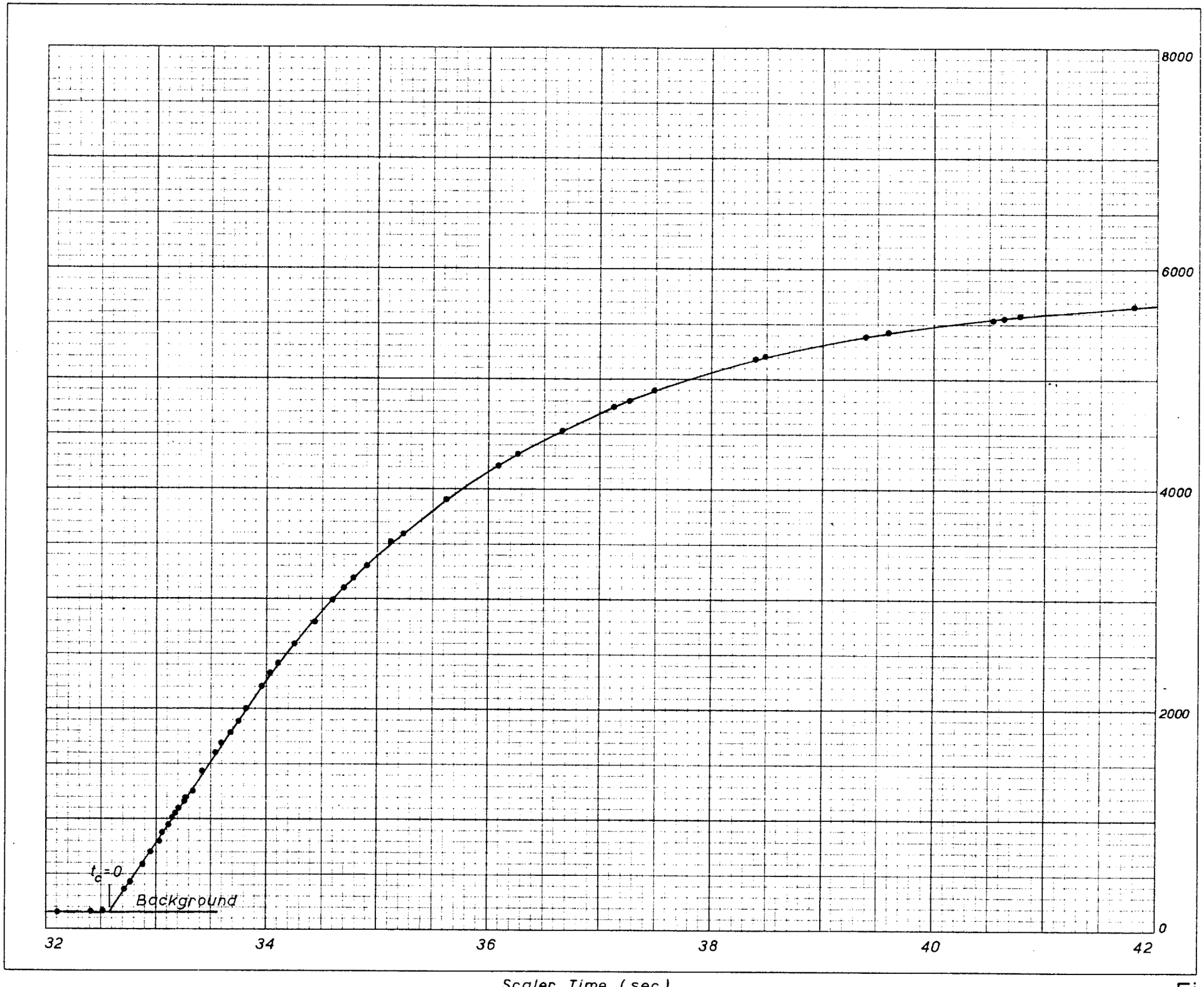

Fig.23

(c) Interpretation of Results

Probability Plot.

The first examination of the powder diffusion results was made by comparison with the pellet measurements made earlier. Two typical powder diffusion curves were therefore superimposed on Fig.5 to give the curves in Fig.24.

It is immediately apparent that carbon dioxide exchange in the powder is much faster than in the pellet which implies that the intercrystalline pore resistance is very significant, and that the two rate process still exists.

However the two powder diffusion curves, obtained by varying bed thickness, show that they do not represent directly the diffusion of carbon dioxide in the crystals. The same shift in the curves was also observed by varying the gas flow velocity, and no limit to these curves could be obtained even at the maximum velocity possible with the equipment. Clearly the desired condition of surrounding each crystal of the powder with virtually pure inactive gas has not been reached, so that the curves represent a dynamic adsorption and are similar to break-through curves in packed columns.

It should be noted that the inability to get a direct measure of the diffusion coefficient is a consequence of the very high selfdiffusion of carbon dioxide in molecular sieve. It will be shown in the next subsection that an accurate and

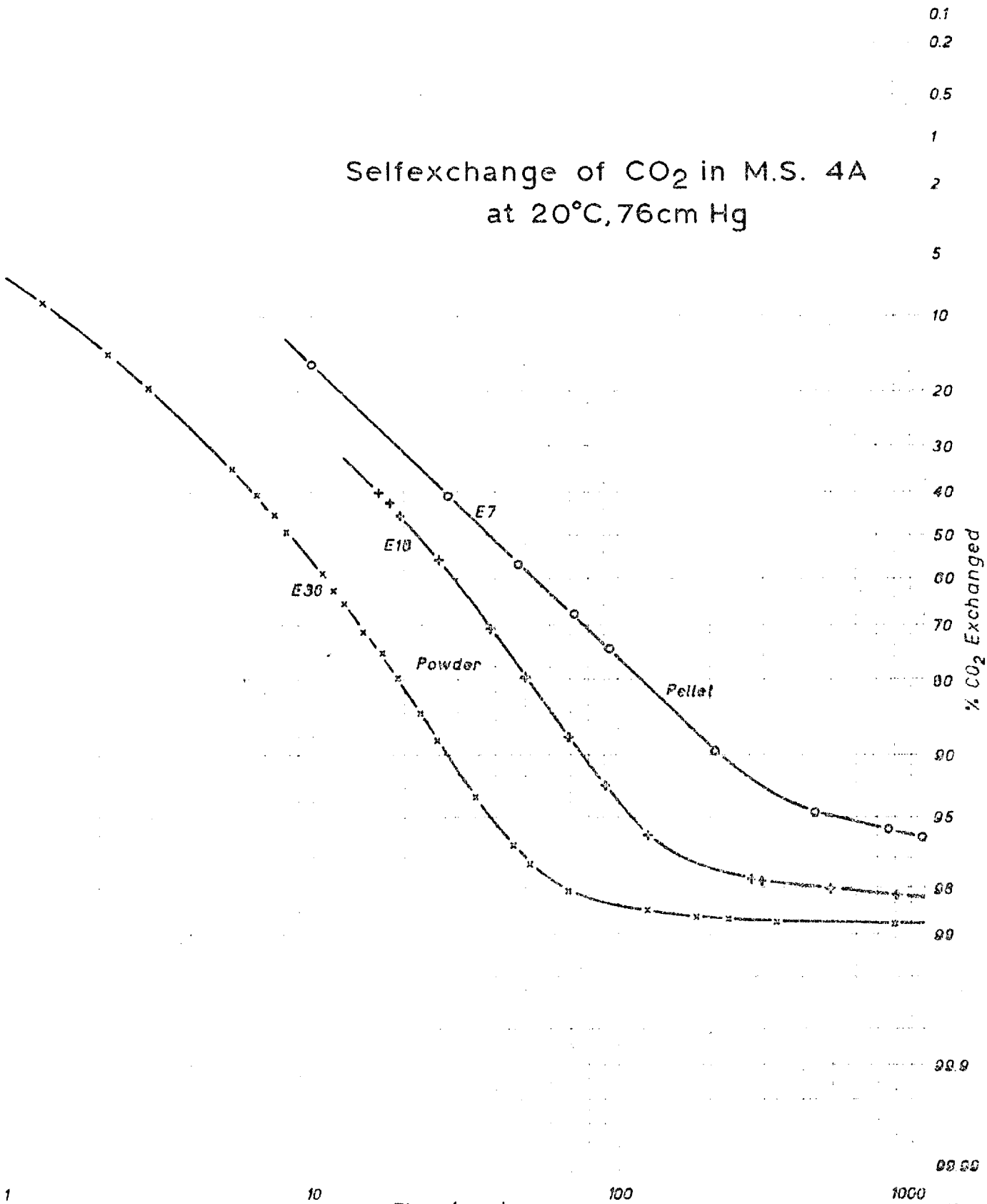
Selfexchange of CO_2 in M.S. 4A
at 20°C, 76cm Hg
0.1
0.2
0.5
1
2
5
10
20
30
40
50
60
70
80
90
95
98
99
99.9
99.99
% CO_2 Exchanged
E7
E10
E30
Powder
Pellet
1
10
100
1000
Time (sec)

Fig.24

direct determination of the diffusion curve should be possible for systems which give a slower rate of exchange.

Exponential Decay.

It often happens in practical systems that an attempt to achieve a sudden change in surface concentration results in an exponential change. This type of exponential decay was in fact observed in this case as shown in Fig.22, Inset A.

A solution for this type of problem is already available for the simple case of diffusion into a sphere.[87] Assuming the crystal surface activity to decay in the form

$$C = C_o e^{-\beta t}$$

the diffusion from a sphere is given by,

fraction exchanged

$$= 1 - \frac{3D}{\beta a^2} e^{-\beta t}\left[1 - \left(\frac{\beta a^2}{D}\right)^{\frac{1}{2}} \cot\left(\frac{\beta a^2}{D}\right)^{\frac{1}{2}}\right]$$

$$+ \frac{6\beta a^2}{\pi^2 D} \sum_{n=1}^{\infty} \frac{e^{-Dn^2\pi^2 t/a^2}}{n^2(n^2\pi^2 - \beta a^2/D)}$$

where β is the decay coefficient, D the diffusion coefficient, and a the particle radius. The solution is also available in graphical form where the fraction exchanged is plotted against $(Dt/a^2)^{\frac{1}{2}}$ for different values of $\beta a^2/D$.

The experimental run E36, calculated earlier, has been fitted to the solution given in Crank.[87] The accuracy of the fit is shown in Fig.25, where the circles represent two theoretical points corresponding to two adjacent decay coefficients.

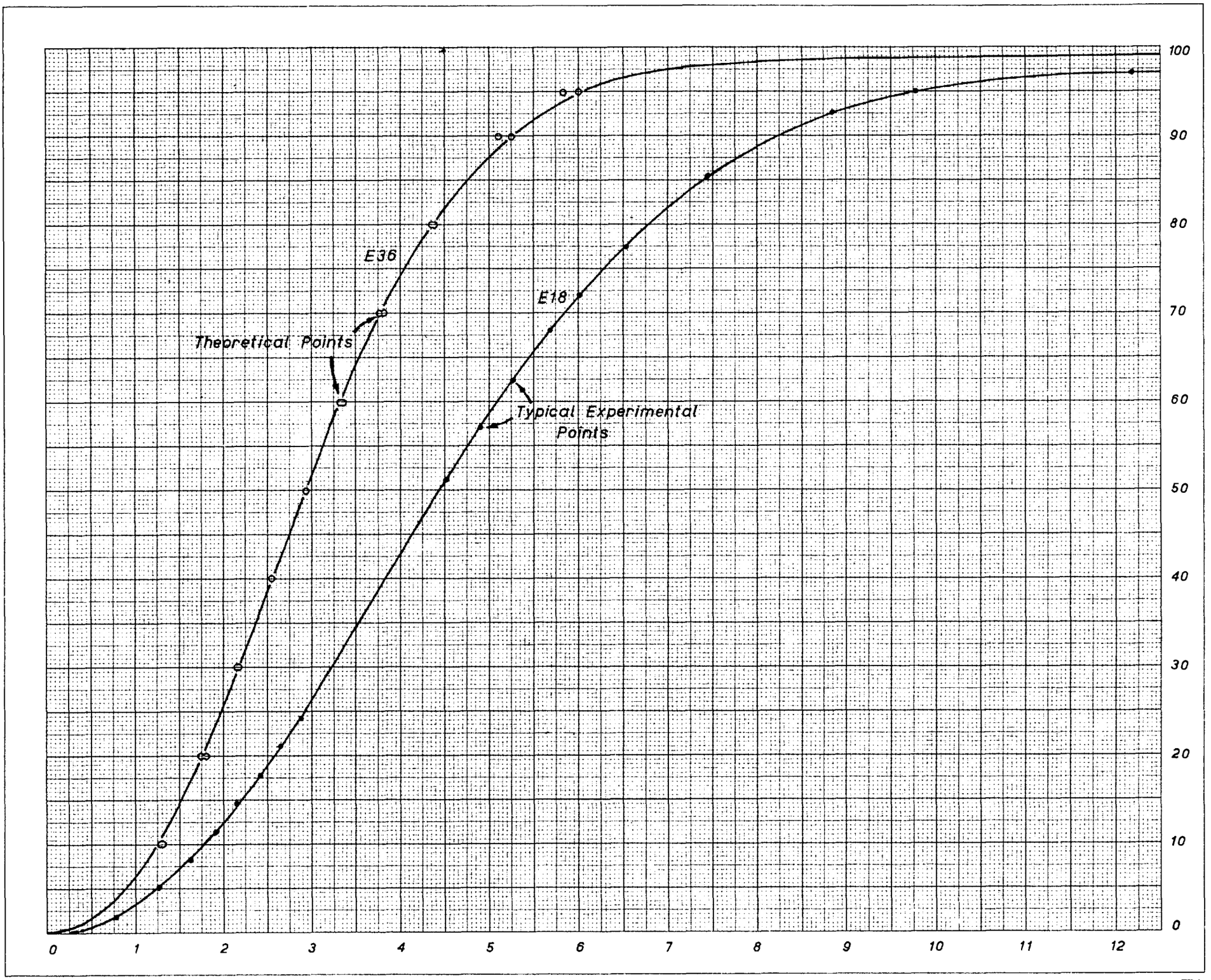
Powder Diffusion under Exponential Decay
E36
E18
Theoretical Points
Typical Experimental Points
100
90
80
70
60
50
40
30
20
10
0
% CO_2 Exchanged
0
1
2
3
4
5
6
7
8
9
10
11
12
Square Root of Time ($sec^{1/2}$)

Fig.25

The experimental curve therefore lies between two theoretical curves with $D/a^2 = 0.092$ sec^{-1} and $D/a^2 = 0.171$ sec^{-1}, where a is the particle radius. By interpolation the best fit is obtained with $D/a^2 = 0.13$ sec^{-1}.

Disregarding the initial values, where there are inaccuracies because of uncertainty in zero time (cf. Fig.22, Inset B) and final values, where there is a complicating mechanism, the fit of experiment with the above theory is excellent over the range 20 to 80% carbon dioxide exchanged. However the absolute measure of D/a^2 is poor because altering the diffusion coefficient does not alter the curve very much. This is an intrinsic difficulty with the system because an increase in the diffusion coefficient has a similar effect to an increase in the exponential decay coefficient. In the absence of an a priori knowledge of one, the other has to be determined not from the position of the diffusion curve (known accurately) but from its precise shape. To this should be added the fact that we have cubes instead of spheres, a particle size distribution instead of a single size, a bed depth with a resultant surface concentration distribution, and finally, as will be shown later, a complicated diffusion equation rather than the simpler Fick's law.

Run E18, shown in Fig.24, was similarly fitted to the curves given by Crank to give $D/a^2 = 0.15$ sec^{-1}

Packed Column Approach.

The most logical approach to interpret the powder measurements is to consider the crystal bed as a packed column with the rate decay curve C/C_o representing a break-through curve of inactive gas by plotting $(1 - C/C_o)$ against time. The run E36, and others, are shown plotted in this way in Fig.26.

Of all the available theories for the dynamics of fixed beds [85,91,93] the most appropriate one to the present problem is due to Rosen [91] who has obtained complete mathematical and numerical solutions for a packed adsorption column with solid diffusion with the following basic assumptions:

(i) Spherical particles, radius a, with a solid diffusion coefficient D.

(ii) Gas film resistance around each particle.

(iii) Linear adsorption equilibrium relation.

(iv) Constant flow velocity of the gas stream with a step input of adsorbate.

All except the first of those assumptions are valid for the present problem and an attempt was made to fit this theory to the powder diffusion measurements.

The comparison with theory was made by superimposing the experimental curves over the theoretical curves and choosing the one with the best overall fit. The solid diffusion coefficient and the film resistance were obtained then from the

Break-through Curves for Selfexchange of CO_2 in M.S. Powder Beds

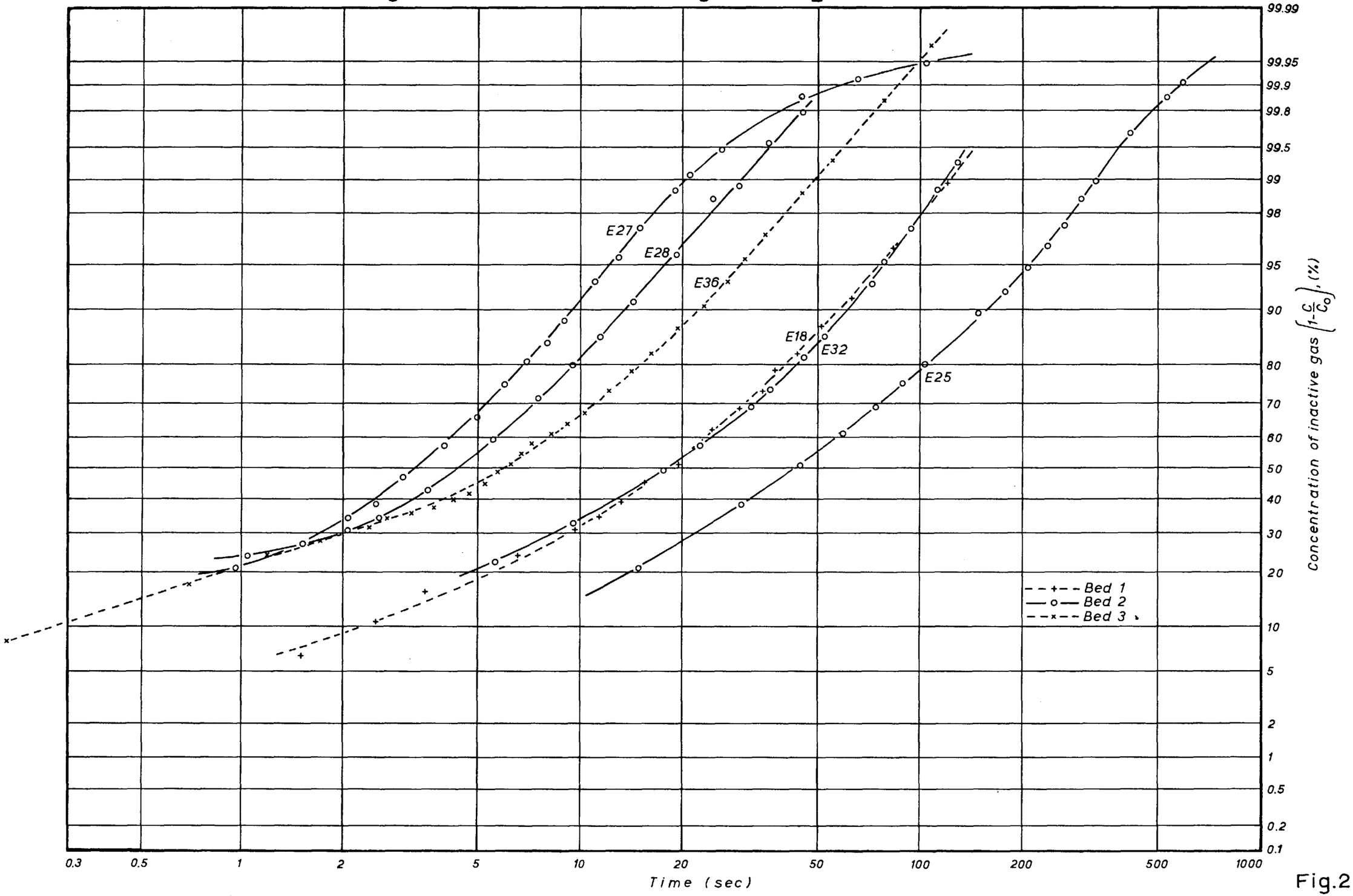

Fig.26

parameters describing the curves.

Rosen curves are given as plots of $(1 - C/C_o)$ against y/x for the two parameters x and σ/x

where $x = 3DKz/mva$, bed depth parameter

$y = 2D(t - z/v)/a^2$, constant time parameter

$\sigma = 3DKR/a^2$, film resistance parameter

and D = diffusion coefficient

K = equilibrium constant

z = bed depth

a = particle radius

m = void volume per unit solid volume

v = linear carrier gas velocity

t = time from start of process

R = effective surface film resistance.

Matching of the experimental curves with the theory was done by comparing the experimental curve with a set of curves with different σ/x values at a chosen level of x. This is shown in Fig.27 where E36, calculated earlier as an example, was shifted across the time scale as shown.

From the degree of horizontal shift we get

$$\frac{y}{x} = \frac{2mv}{3Kz}\left(t - \frac{z}{v}\right)$$

$$= \frac{2mv}{3Kz}t \text{ for thin beds}$$

$$= 0.084t,$$

hence $\frac{2mv}{3Kz} = 0.084 \text{ sec}^{-1}$

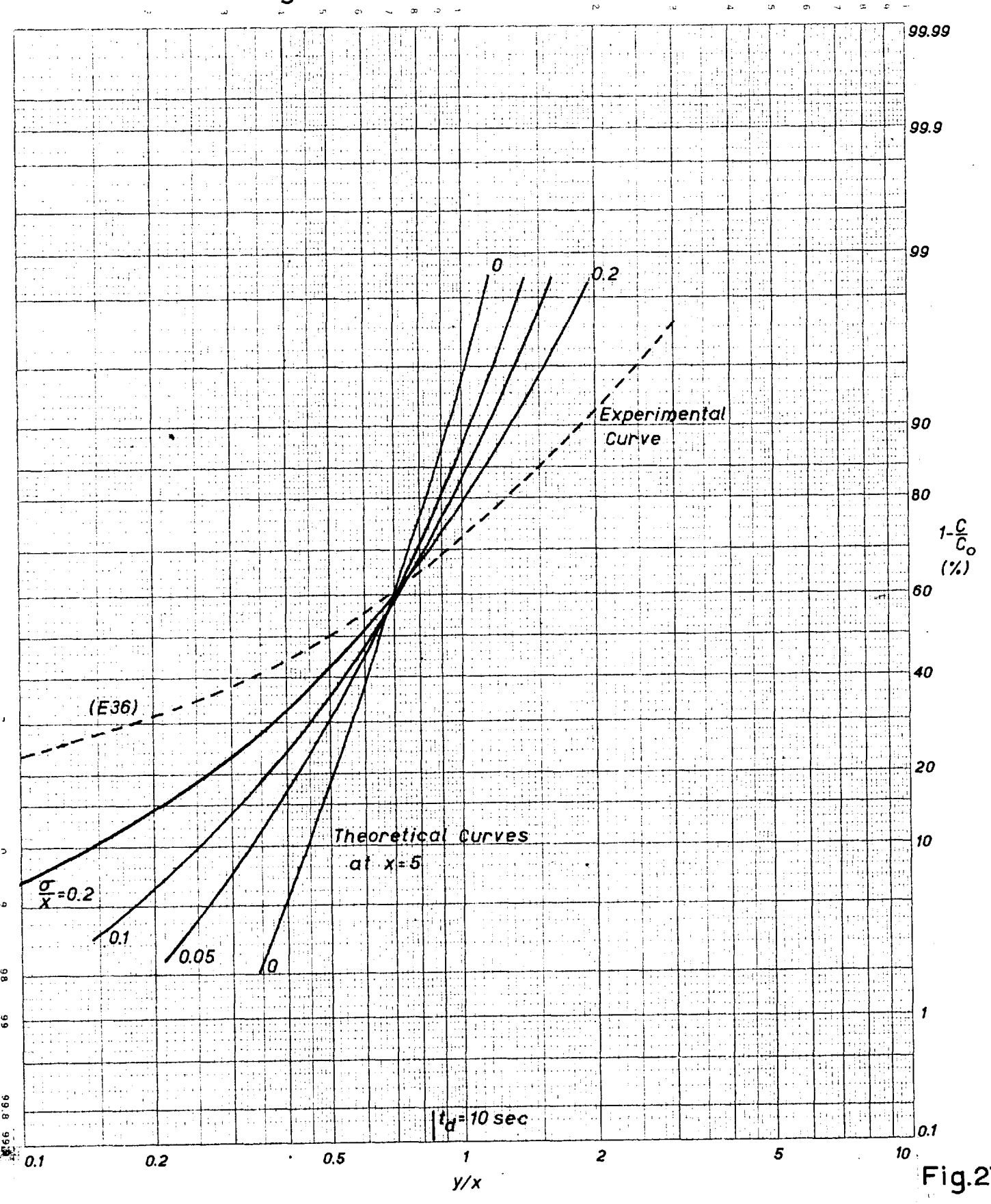
99.99
99.9
99
90
80
60
40
20
10
1
0.1
1-C/Co (%)
0
0.2
Experimental Curve
(E36)
Theoretical Curves at x=5
σ/x=0.2
0.1
0.05
0
td=10 sec
0.1
0.2
0.5
1
2
5
10
y/x

Fig.27

From the chosen set of curves (for best fit) we have $x = 5$ and by extrapolating the σ/x curves we estimate σ/x to be about 0.5

$$\text{But} \quad x = \frac{3Kz}{2mv} \frac{2D}{a^2}$$

$$\text{therefore} \quad D/a^2 = 5 \times 0.084/2$$

$$= 0.21 \text{ sec}^{-1}.$$

The gas film resistance is given by

$$R = \frac{\sigma a^2}{3DK}$$

hence under experimental conditions when $K = 175$ we have

$$R = \frac{5 \times 0.5}{3 \times 0.21 \times 175} = 0.023 \text{ sec}^{-1}$$

The experimental curves shown in Fig.26 have been analysed similarly and the results are summarised in Table 8.

Table 8.

Rosen parameters from experimental diffusion curves.

Exp.	x	$\frac{\sigma}{x}$	$\frac{2mv}{3Kz}$	$\frac{D}{a^2}$	R	v	$\frac{2m}{3Kz}$
	-	-	sec^{-1}	sec^{-1}	sec^{-1}	cm/sec	cm^{-1}
E18	10	0.5	0.030	0.15	0.065	1.20	0.025
E25	20	0.5	0.012_3	0.12	0.159	0.122	0.101
E27	2	0.3	0.160	0.16	0.007	1.58	0.101
E28	2	0.4	0.120	0.12	0.013	1.17	0.103
E32	10	0.6	0.029_5	0.13	0.094	0.289	0.102
E36	5	0.5	0.034	0.21	0.023	1.18	0.071

The maximum value of σ/x calculated by Rosen is 0.2 and it is immediately apparent from Table 8 that most of the experimental curves were badly out of range of the theoretical curves. There is no method of extrapolating these and the two parameters x and σ/x in Table 8 are only estimates used to obtain the order of magnitude of the diffusion coefficient. The fairly constant value of diffusion coefficient shown in Table 8 cannot be taken as a measure of accuracy because the curves were fitted on the assumption that there must be one single value of D/a^2. A reasonable fit was obtained for all the curves by taking D/a^2 to be about 0.14 sec^{-1}. If a different average value were chosen then some of the curves might fit better, while others would not fit at all. For example in Fig.27 an equally good fit of E36 with theory would have been obtained by taking $x = 2$ and $2mv/(3Kz) = 0.086$ which would give $D/a^2 = 0.086$.

The main difficulty is that curves are not available for high surface resistance (σ/x larger than 0.2) and also that there are deviations from the theoretical shape (cf. Rosen's first assumption). The particles are cubic, there is a particle size distribution (0.1 to 2 μ), with possibly some coalescence forming little granules of powder, and finally the simple diffusion equation is probably not obeyed in molecular sieve 4A. The last of these difficulties would cause deviations at large times (cf. Fig.25) and the others would result in deviations at early times.

The only way in which a reasonable estimate of the diffusion coefficient can be made, using Rosen's solution, is to make a large number of runs on the same bed at different velocities and then work back by trial and error to find the most satisfactory diffusion coefficient.

The results of Table 8 cannot be used in this way because they represent three different beds in three sizes of tubes. The last column, obtained from columns 4 and 7 is a reciprocal measure of bed thickness, and it can be seen that only four experiments were done on the same bed. The relative gas film resistance, R_g, has been plotted against the experimental gas flow velocity, v, in Fig.28 which shows the expected behaviour of decrease in gas film resistance with increasing gas flow rate.

In large packed columns one would expect the gas film resistance to be a function of velocity only. However for a thin bed of powder this is certainly not the case as can be seen from E18 and E36 in Fig.28. This variation is probably due to variation in porosity of the packed powder bed. In a packed column containing 1/8 in. pellets, say, the stagnant gas film might be about 0.1mm thick, and this would not vary much with the packing, but in a powder bed consisting of 0.01 mm particles the degree of packing would be expected to have a considerable effect on the gas film. No published correlation could be found for predicting the mass transfer coefficient at the experimental Reynolds number of about 0.001.

Powder Bed Film Resistance

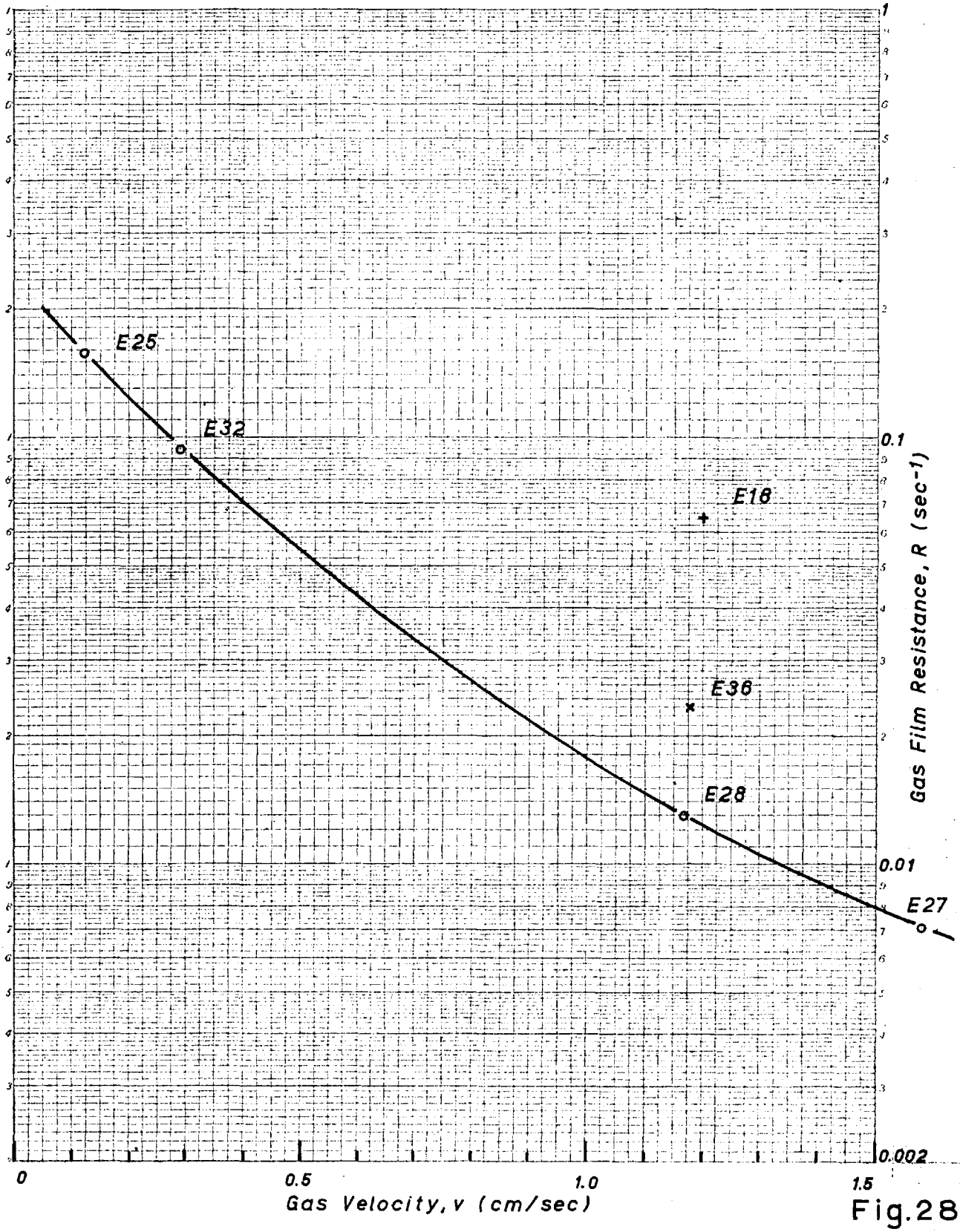

Fig.28

Conclusion.

The diffusion measurements in powder have been interpreted in terms of assumed exponential decay at the surface of the crystals, and in terms of Rosen's solution of an adsorption column with solid diffusion, to give $D/a^2 = 0.14$ sec^{-1}. Taking the average a = 0.5 μ the selfdiffusion coefficient for carbon dioxide in molecular sieve 4A at 20°C was found to be 3.5×10^{-10} cm^2/sec.

An accurate measure of the diffusion coefficient could not be made because there is no appropriate theory, and also because of the inherent difficulty of measuring the diffusion coefficient in a solid which is surrounded by a large stagnant gas film. This means that assuming a thinner film produces a similar effect to assuming a higher diffusion coefficient, and the distinction between these two has to be made on the basis of precise break-through curve shape rather than break-through position.

4. DIFFUSION IN ONE DIMENSIONAL POWDER BED

Measurements on a powder bed have produced an estimate of the crystal diffusion coefficient in solid molecular sieve. To help interpret the original pellet results of Fig.5 an experiment was designed in which the intercrystalline pore diffusion could be measured by making it the controlling factor.

This was done very simply by packing molecular sieve powder into a tube (6.80 cm long) sealed at one end.

Diffusion measurements could then be conducted by saturating the adsorbent with radioactive gas and passing inactive gas over the open end of the tube.

A diffusion cell of this type is shown in Fig.17B, p.57. The inlet stopcock was made large enough so that with the stopcock removed the powder tube could be dropped into the diffusion cell. The tube was supported with three point contacts inside the cell to keep the gas flow uniform. As usual a heater element was wound around the cell for desorption which had to be applied extremely slowly to prevent expelling the lightly packed powder at the surface of the tube.

This one dimensional cell experiment was designed mainly for the following two reasons. Firstly, it soon became apparent that the mathematics of the pellet is very complicated and it seemed unlikely that a useful solution, or any solution at all would be found. Dealing with a one dimensional case simplifies the mathematics and moreover the prescribed boundary conditions would be satisfied precisely because the geometry and the porosity are known exactly and the unknown effect of the binder is eliminated. Secondly, making the diffusion flow path much larger than in the pellet (0.16 cm radius) must either lead to a direct measure of the pore diffusion, or else imply that pore diffusion in the pellet is completely negligible.

Experimental Results.

Two measurements were made on the one dimensional powder

cell and one of these is shown in Fig.29. Measurements were made as before by recording the integral count, $\int c$, and a calibration run was also made by conducting the experiment with a sealed dummy glass ampoule in the diffusion cell. During these experiments the exit carrier was was passed first through the side window counter and then through the end window counter and both of these were recorded simultaneously with the same time scale (Fig.11, p.42).

The earliest parts of the integral curves for the two counters are shown in Fig.29. It can be seen that the side window count shows an "ideal" behaviour. The initial rate, due to pure radioactive gas drops from about 1300 c/s (corrected for pulse resolution) to about 10 c/s within two seconds. The end window counter, with its larger volume, takes about 20 seconds to get adjusted. The apparently lower initial rate in the end window counter is due to the fact that there is insufficient concentrated radioactive gas to fill the whole tube.

The start of diffusion was determined by extrapolation of the side window counter curve as shown in Fig.29, and after about 40 seconds readings from the end window counter were used. The readings from the two counters were adjusted for time difference and for count so as to give a continuous line in the integral count curve. This is equivalent to assuming a constant count rate ratio between the two counters.

Selfexchange of CO_2 in a Onedimensional Pellet

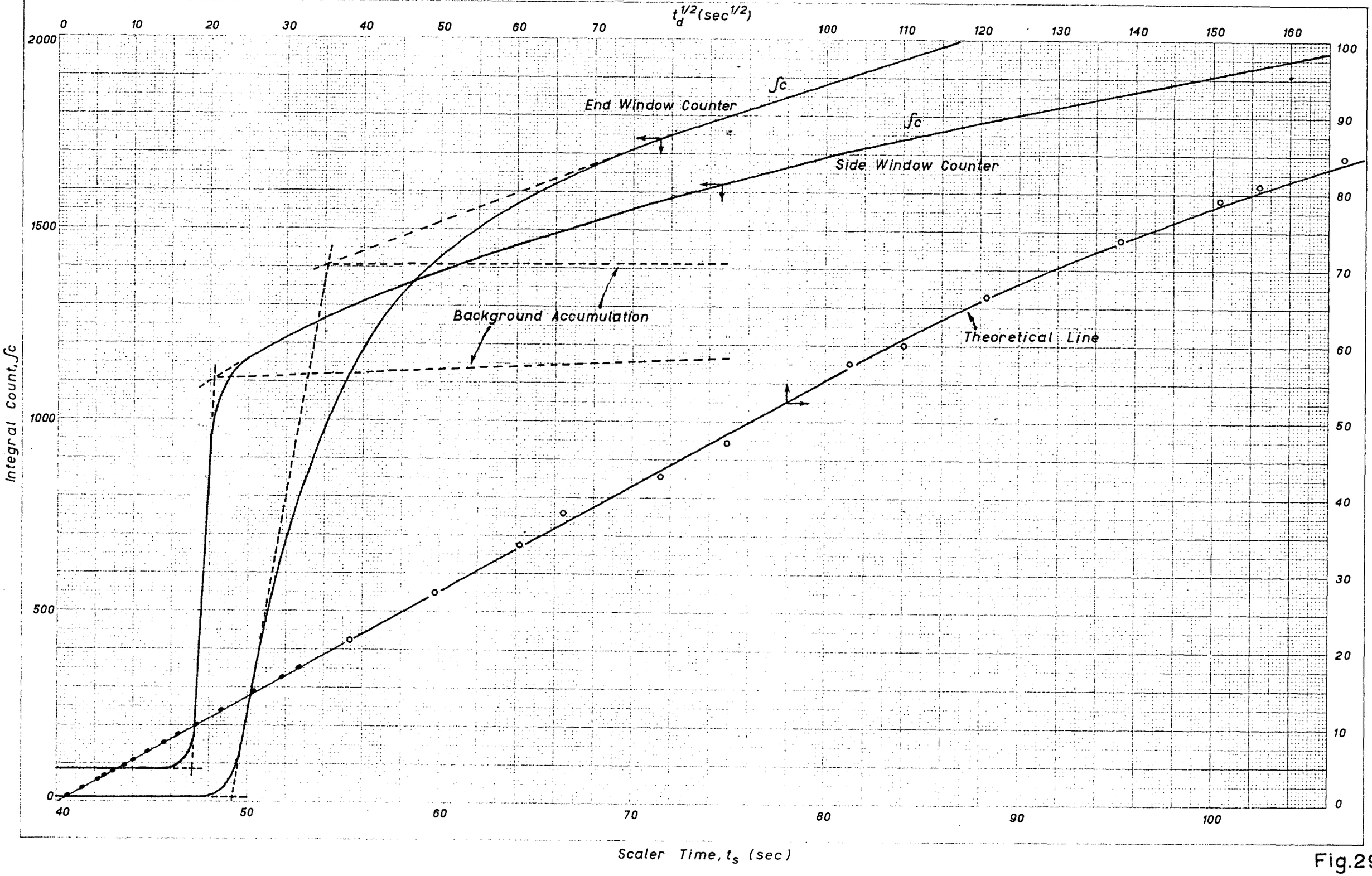

Fig.29

The final diffusion point was determined as before by desorption on heating. The effectiveness of this whole method of diffusion measurement can be appreciated by observing that the initial diffusion integral curves in Fig.29 cover the range from about 1000 to 2000 counts, but the final integral point lies at 56,000 counts and 28,000 seconds.

The resultant selfdiffusion points are also shown in Fig.29, plotted against $t^{-\frac{1}{2}}$.

Interpretation of Results.

Clearly the straight line plot of Fig.29 indicates that a simple diffusion mechanism must be controlling. An attempt to solve the complete equations will be given in the next section, but for this problem the appropriate solution is obtained by completely neglecting crystal diffusion.

We can therefore write down for the one dimensional cell

$$D_p \frac{\partial^2 C}{\partial x^2} = \frac{\partial C}{\partial t} + \frac{\partial Q}{\partial t} \frac{1}{m}$$

$$\text{and } Q = KC$$

where D_p is the pore gas diffusion coefficient, C the gas concentration, Q the solid concentration, m the volume ratio of voids to solid, and K the equilibrium constant. In this case K stands for the ratio of radioactive isotope in the solid to the same isotope in the gas and is constant throughout the experiment, because instantaneous local equilibrium is assumed.

The above two equations reduce to the simple diffusion equation

$$D_e \frac{\partial^2 C}{\partial x^2} = \frac{\partial C}{\partial t}$$

by the substitution $D_e = D_p(1 + K/m)^{-1}$

where D_e is an effective diffusion coefficient.

The solution of this simple equation is well known[86,87] and the solid line in the $t^{\frac{1}{2}}$ plot in Fig. 28 is the theoretical solution for $D_e/l^2 = 2.36 \times 10^{-5}$ sec^{-1}. But $l = 6.80$ cm, hence the effective pore diffusion coefficient is $D_e = 1.09 \times 10^{-3}$ cm^2/sec.

From the predetermined volume of the diffusion tube and the weight of dry molecular sieve in the tube ($\rho = 1.36$ g/cm^3) m was found to be 2.46 cm^3 voids/cm^3 M.S., and from the equilibrium isotherms K was found to be 180 at 23.5°C and 76.8 cm Hg. Hence the pore diffusion coefficient is given by

$$\begin{aligned} D_p &= D_e(1 + K/m) \\ &= 0.00109(1 + 180/2.46) \\ &= 0.0797 \text{ cm}^2/\text{sec}. \end{aligned}$$

This can be compared with the selfdiffusion coefficient for free gas D_g, which is 0.107 cm^2/sec at the same temperature and pressure.[79]

V THEORETICAL ANALYSIS

1. INTRODUCTION

The general objectives of this research have been described in the Introduction on p.18. The practical aim was to devise experimental methods to measure all the components of a complex diffusion system, while the theoretical aim was not only to interpret these results but to take every possible approach to the whole problem so as to examine where useful results could be obtained.

Three distinct methods were used for examining the present problem. Firstly, statistical mechanics was used to study the physical adsorption potentials and to show how these could be used to predict adsorption equilibria, heats of adsorption, and jump frequencies or diffusion coefficients. Secondly, a stochastic approach was used to show the diffusion behaviour through molecular sieves and to derive the crystal diffusion equations. Thirdly, macroscopic equations were constructed and solved in certain cases for diffusion through powder compacts.

An alternative approach may have been to select one certain aspect of this work and pursue it more fully; however, since no theoretical work has been done previously on any of the aspects treated in this thesis it was not only

difficult to decide which specific problem to examine, but it would have been very hard to succeed in a single problem because of various interconnections and the lack of physical data on the system.

2. ADSORPTION

(a) Intermolecular Potentials

Various forces which exist between uncharged, charged and polarised atoms and molecules have been fully discussed by Hirschfelder, Curtiss and Bird.[79] In calculating the adsorption potential of carbon dioxide molecules in molecular sieve cages it was assumed that all the zeolite atoms are in a fully ionised form. This assumption had to be made because there is no knowledge of the state of ionisation of the individual atoms.

The adsorption potential consists of the following three contributions[79]:

$$\text{Dispersion, } \phi_D = -\frac{\alpha_1\alpha_2}{\alpha_1/\chi_1 + \alpha_2/\chi_2} \cdot \frac{6mc^2}{r^6}$$

$$= -A/r^6$$

$$\text{Polarisation, } \phi_P = -\frac{1}{2}\alpha f^2$$

$$\text{Repulsion, } \phi_R = \frac{A\sigma_e^6}{2} \cdot \frac{1}{r^{12}}$$

Where α - polarisability,

χ - diamagnetic susceptibility,

m - mass of electron,

c - velocity of light,

f - electrostatic field, e/r^2,

σ_e - equilibrium separation.

The total adsorption potential is the sum of all these contributions and it has to be calculated with respect to every atom of the zeolite crystal.

The carbon dioxide molecule has also a small quadrupole moment which makes a contribution to the total potential[78], but this had to be neglected in order to simplify the problem.

(b) Potential Constants

To calculate the intermolecular potentials we have to know the potential constants A, σ_e, and the polarisability α. For gas - gas interactions these constants are available, having been calculated from compressibility or viscosity data. Here we are concerned, however, with the interaction between a neutral gas molecule and ions of the zeolite for which there is no direct experimental data available. The constant A was therefore estimated, as shown above, from the polarisabilities and magnetic susceptibilities of the interacting molecule and ion.

A further difficulty arises from the lack of experimental data on α and χ, particularly for the ionised atom. For aluminium and silicon these had to be estimated from the screening constants of the electron shells. These calculations, which depend on the known electronic structure of the ions are fully explained by Hirschfelder, Curtiss, and

Bird[79] and they will not be shown here.

For ease of computation instead of considering the potentials due to individual Al^{3} and Si^{4+} ions an average ion $AS^{3\frac{1}{2}+}$ was used, its properties being calculated from the geometric mean polarisability and arithmetric mean diamagnetic susceptibility and equilibrium radius.

The theoretical and experimental constants are all summarised in Table 9. The experimental constants were

Table 9.

Intermolecular potential constants.

Quantity	CO_2	O^{2-}	$AS^{3\frac{1}{2}+}$	Na^{+}	Units
α	26.5	38.9	0.66	1.80	x $10^{-25}cm^3$
χ	34.5	20.9	3.76	6.95	x $10^{-30}cm^3$
A	225	193	9.09	22.9	x 10^{-60}erg cm^6
r_e	2.26	1.40	0.48	0.98	x 10^{-8}cm
σ_e	4.52	3.66	2.74	3.24	x 10^{-8}cm
$A\sigma_e^6/2$	96.0	23.1	0.192	1.32	x 10^{-104}erg cm^{12}
$\alpha e^2/2$	30.5	-	-	-	x 10^{-44}erg cm^4

obtained from Gmelin's Handbook of Inorganic Chemistry, Landolt-Boernstein Tables[98], and Hirschfelder, Curtiss, and Bird.[79]

(c) Calculation of Adsorption Potentials

Crystal Structure.

The crystal structure of molecular sieve 4A has a space group O'-Pm3m and the coordinates of the atoms are given in Table 10.[3]

Table 10.

Atomic positions in the aluminosilicate framework.
Unit cell, a_o = 12.30Å

No./ Unit cell	Atom	From the centre of small cage	From the centre of large cage
12	O_1	0 ,0.2229,0.5000	0 ,0.2771,0.5000
12	O_2	0 ,0.2937,0.2937	0.2063,0.2063,0.5000
24	O_3	0.1117,0.1117,0.3407	0.1593,0.3883,0.3883
24	Si,Al	0 ,0.1822,0.3713	0.1287,0.3178,0.5000
8	Na_1	0.2082,0.2082,0.2082	0.2918,0.2918,0.2918
4	Na_2	Indeterminate	Indeterminate

A cross-section through a large cage, constructed from the positions given in Table 10, is shown in Fig.1,p.11. Only the oxygen and known sodium atoms are shown, the silicon and aluminium atoms being hidden inside tetrahedra formed from the oxygen atoms. The superimposed tracing identifies the three types of structural oxygen atoms and shows more clearly the positions of the six membered and eight membered interconnecting windows characteristic of the structure. It should be noted that all the oxygen atoms of one type are at the

same distance from the centre of the cage, making this a convenient point for manual check calculation of the adsorption potential.

The shape of the six membered window is shown in Fig.2 which is a view along the three-fold axis from the centre of the cage. The coordinates of the atoms in Fig.2 were obtained by transforming the coordinates given in Table 10. Thus, for example, for atoms c and d in Fig.1 we have

$$(X,Y,Z)_c = (0.5000, 0.2063, 0.2063)$$

$$(X,Y,Z)_d = (0.3883, 0.1593, 0.3883)$$

and in Fig.2 these have been transformed to

$$(x,y,z)_c = (0.5264, -0.2300, 0)$$

$$(x,y,z)_d = (0.5401, -0.0934, 0.1618).$$

For the coordinates of the sodium atom in Fig.2 we have, of course, $(0.2918\sqrt{3}, 0, 0)$.

By averaging the contributions of silicon and aluminium atoms, as described earlier, full advantage can be taken of the resultant symmetry. The eight sodium atoms of type 1 are all placed in definite positions at the centre of the six membered rings (Figs.1 and 2), but no precise positions can be assigned to the remaining four (per unit cell) sodium atoms of type 2. There is some X - ray evidence and substantial physical adsorption evidence[3] to show that these sodium ions are situated in the eight membered rings, i.e. two cell windows

have two sodium ions in each, while the other four have one each. This means that there is a large degree of randomness in the location of these ions, particularly so, since the optimum position for one ion is not in the centre of the large ring but off centre, half way between any two of the ring oxygen atoms. For computation purposes the average mean position was taken by assuming one and a quarter sodium ions at the centre of each large window.

With the above assumptions it was sufficient to compute the potentials within a tetrahedron whose apex was at (0,0,0) and whose triangular base lay in the plane X = 0.5 with corners at (Y,Z) = (0,0), (0.5,0), and (0.5,0.5). If a random arrangement of Na_2 atoms were assumed the potentials would have to be calculated throughout a whole unit cell whose volume is 48 times greater than that of the above tetrahedron.

To keep the number of points to a reasonable minimum a rectangular grid was used within the tetrahedron with $0.05a_o$ between the grid lines giving a total of 286 points.

At each selected grid point within the cell the interaction potential had to be calculated with respect to every structural atom within a certain radius from the grid. The simplest and smallest boundary that could be used is shown by the dotted line in Fig.1. This consists of taking a cube, representing an eighth of a unit cell, all around the cube

containing the grid. In this way, for every point within the positive quadrant, consideration is taken of every atom within at least $a_o/2$ from the quadrant.

The accuracy of this simplification can be estimated by taking more and more quadrants surrounding the positive central quadrant. Performing this calculation for the central point it was found that for the range shown in Fig. 1 an accuracy of about 20% can be expected in the dispersion and repulsion potentials. For preliminary calculations this is quite satisfactory in view of the uncertainity of the intermolecular potential constants.

Polarisation Contribution.

As shown earlier the total potential of an adsorbed nonpolar molecule is due to repulsion, dispersion and polarisation. The polarisation component decays as $1/r^4$ and it is the most difficult one to estimate. Firstly, because of the long ranging force a larger ring is required to estimate the contribution with sufficient accuracy. Secondly, the polarisation component is evaluated by determining the vector field at a point with respect to all the ions. Vector addition using a computer is much slower than scalar addition.

A Mercury Computer programme in CHLF3 Autocode for calculating the total potential including the polarisation component, has been written and partially tested. This programme has the facility for selecting any size ring around

the central quadrant so that the calculations can be performed to any required degree of accuracy. It was found that to make a full computation with this programme an excessive amount of computer time would be required which is not warranted for a preliminary investigation. Because of its length the programme is not included in this thesis but it is available in the department for future use.

Final Programme.

To eliminate the difficulties of determining the polarisation component, this component was completely neglected and a simpler programme was written for calculating the ordinary Lennard - Jones dispersion and repulsion potentials. The programme and the results are given in the appendix.

(d) Adsorption Equilibria

The Adsorption Partition Function.

At high temperatures, when quantum effects can be neglected, all the thermodynamic properties of adsorbed gases can be fully predicted from the gas - solid partition function[76,79,84]

$$Z = (2\pi mkT/h^2)^{3N/2} (1/N!) \int\int \ldots \int \exp(-\phi/kT) dr_1 \ldots dr_N$$

where N is the total number of adsorbed gas molecules, r the position vector, and the total potential is given by

$$\phi = \Sigma_i \phi_{gs}(r_i) + \tfrac{1}{2}\Sigma_i \Sigma_j \phi_{gg}(r_i, r_j)$$

consisting of gas - solid potential, ϕ_{gs}, and gas - gas potential ϕ_{gg}. The accuracy with which the properties can be predicted depends only on the accuracy of the potential and the ability to evaluate the multiple integral.

The partition function represents the interaction of all the adsorbed atoms and it is simplified by expanding it into two-, three-,... body interactions. We thus have for the adsorption equilibria[76]

$$n = \frac{pV_o}{RT} - \frac{p^2 V_o}{(RT)^2}\,(2B'-B) + O(p^3)$$

where n is the number of adsorbed gas atoms, B the second virial coefficient for bulk gas[79] and

$$V_o = \int \exp[-\phi_{gs}(r)/kT]dr$$

$$B' = -\frac{N}{2V_o}\iint\left\{\exp\left(-\frac{\phi gg(r_1 r_2)}{kT}\right) - 1\right\}\exp\left(-\frac{\phi gs(r_1)+\phi gs(r_2)}{kT}\right)dr_1\,dr_2$$

These equations are directly applicable to molecular sieves provided that no assumptions are made on the order of decrease of higher virial coefficients. In bulk gas systems at ordinary pressures and temperatures third and higher order interactions become extremely rare and most of the properties are determinable from two body interactions. This is true also to some extent for adsorption on reasonably uniform surfaces, eg. silica gel or charcoal, provided that we have monolayer adsorption. For adsorption on zeolites, however, as the cages fill up many body interactions become

prominent; moreover, the total potential may change sharply with the number adsorbed making any extrapolations very uncertain.

Equilibrium Isotherms at Zero Coverage.

The initial isotherm gradient can be determined by considering only one adsorbed atom per cage, in which case only V_o need be evaluated. This can be done as a first approximation, by direct summation of the computed exponentials, thus

$$V_o = \Sigma \exp(\phi/kT)\delta v$$

where the summation is carried out over the whole unit cell and δv is the volume element associated with each point.

The summation over the whole unit cell using the values computed for a tetrahedron must be done carefully so as to avoid reflecting points which are on the boundaries of the tetrahedron. The procedure for finding the sum for a large cage is shown in Table 11.

Table 11.

Point multiples for large cage summation.

For every point within			Multiply by	$\Sigma \exp(\phi/kT_2$
tetrahedron	-	-	48	507.77
triangle	a	Z=0	24	142.18
	b	Y=0.5	48	0
	c	Y=Z	24	120.06
	d	X=Y	24	140.91
line	ab	Z=0, X=0.5	24	0
	bc	Y=Z, X=0.5	24	0
	cd	X=Y=Z	8	5.91
	ad	Z=0, X=Y	12	31.52
	bd	X=Y=0.5	24	0
	ac	Z=Y=0	6	0.99
point	abc	X=0.5, Y=Z=0	6	0
	abd	X=Y=0.5, Z=0	12	0
	acd	X=Y=Z=0	1	0.00_3
	bcd	X=Y=Z=0.5	8	0
		Total for large cage		949.35×10^4

It was found similarly that the total exponential for a small cage is 1.43×10^9. Substituting these values into the above equations we find that the equilibrium adsorptions for large and small cages at 1/100 at. pressure are given by

$$q_{lc} = 0.0124 g CO_2/gM.S.$$

$$q_{sc} = 1.88 g CO_2/gM.S.$$

It is immediately apparent that the agreement between the theoretical and experimental gradients will depend on whether the small cages are accessible to carbon dioxide molecules. Unfortunately no accurate data is available at extremely low coverages. When the commercial curve, Fig.20, p.65, is plotted on a linear pressure scale the initial equilibrium gradient is found to be not less than 0.50g/g at 1/100 at. but the actual gradient cannot be determined because the curves do not go to sufficiently low coverages.

Chandrasekharan[26] has measured CO_2 adsorption on molecular sieve partially saturated with water, in which case it can be assumed that CO_2 would have no access to the small cages. He finds that the initial gradient is about 0.010 g/g at 1/100 at. which shows good agreement with the theoretical value.

Second Virial Coefficient B'.

Any isotherm which depends on adsorption in small cages will be influenced very significantly by the second and higher virial coefficients. This is because the small cages can hold only two or three atoms, and once the cages are filled up the partition exponential decreases by a factor of one hundred.

The second coefficient B', and possibly the third C', can be computed directly from the computed exponentials. Unfortunately time was not available to carry out this operation.

(e) Heats of Adsorption

The calculated adsorption potentials can be used directly to give the initial heats of adsorption since the difference in the potential of a free atom and an adsorbed atom is proportional to the heat of adsorption. The variation of heat of adsorption with coverage can be obtained by minimising the positions of the adsorbed atoms with respect to the potential. The minimising can be carried out using standard library computer programmes although the computation would become excessively long for more than, say, four atoms per cage. This is because further addition of atoms always shifts the minima of the earlier atoms, and for four atoms this amounts to minimising a problem in twelve independent variables.

3. CRYSTAL DIFFUSION

(a) Derivation of Equations

(i) Simple Probability Distribution.

For diffusion through zeolites consisting of one type of simply connected cages it can be shown easily that Fick's diffusion law applies, leading to the ordinary diffusion equation

$$D\nabla^2 q = \partial q/\partial t$$

where q is the concentration of the diffusing species.

Molecular sieves of Type A, however, consist of two types of cages, large and small (Fig.1, p.11), interconnected with two types of windows and it is not immediately apparent that the simple diffusion equation shown above should apply to the diffusion through this type of network.

To investigate this diffusion behaviour a stochastic approach was used to determine the probability distribution for finding a single diffusing atom placed in the centre of a molecular sieve crystal.

For simplicity a one dimensional case is considered. The physical arrangement of the aluminosilicate is such that through transition can occur only between large cages, the small cages being connected to the large cages but not to each other. In one dimension this is equivalent to the arrangement shown in Fig.30. Because the interconnecting windows are

different in size the probability of an adsorbed atom jumping from a large cage to a large cage, ρ, is different

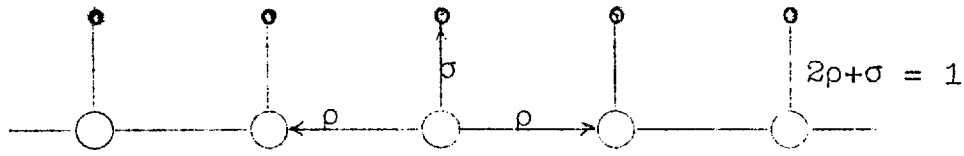

Simple Jump Probabilities. Fig.30

from the probability of the atom jumping from a large cage to a small one, σ.

Let s be the number of jumps made by the atom and m the position from the centre, then we have the following initial probability distribution as shown in Fig.31. Since we are considering the probability after a certain number of

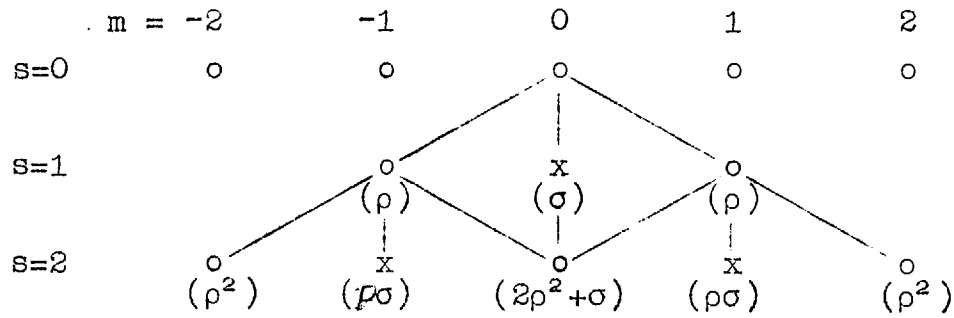

Initial Probability Distribution. Fig.31

jumps only alternate large cages have a chance of being filled, also if the atom is in a small cage then on its next jump it must enter a large cage with probability 1.

The above distribution can be written more conveniently in tabular form; thus for s=3 we have-

m	p	ρ^3	$\rho^2\sigma$	$\rho\sigma$	σ^2
-3	1	1			
-2	2		1		
-1	3	3		2	
0	4		2		1
1	5	3		2	
2	6		1		
3	7	1			
	Σ	8	4	4	1

where p is the position from the left and the body of the table contains the coefficients for ρ and σ. A check on the distribution can be made by summing all the probabilities, thus

$$\Sigma = 8\rho^3+4\rho^2\sigma+4\rho\sigma+\sigma^2$$
$$= 1.$$

By extrapolating this procedure a pattern soon becomes apparent and it can be shown that after s jumps the distribution in the large cages is given by the arrangement shown in Table 12.(Next page.)

We can therefore write that the probability of finding the atom in cage i (=s-2i+1 from the starting position) after s jumps is given by

$$R(i,s) = \sum_{j=1}^{i} \binom{s-j}{s-2j}\binom{s-2j}{i-j}\rho^{s-2j}\sigma^j$$

$$= \sum_{j=1}^{i} \binom{s-j}{j}\binom{s-2j}{i-j}\left(\frac{\sigma}{\rho^2}\right)^j.$$

Table 12.

Probability distribution in large cages after s jumps.

m	p	i	ρ^s	$\rho^{s-2}\sigma$	$\rho^{s-4}\sigma^2$	. .	$\rho^{s-2j}\sigma^j$	. .
-s	1	0	$1\binom{s}{0}$					
-(s-3)	3	1	$1\binom{s}{1}$	$\binom{s-1}{s-2}\binom{s-2}{0}$				
-(s-5)	5	2	$1\binom{s}{2}$	$\binom{s-1}{s-2}\binom{s-2}{1}$	$\binom{s-2}{s-4}\binom{s-4}{0}$			
. . . . .								
. . . . .								
s+2i+1	2i+1	i	$1\binom{s}{i}$	$\binom{s-1}{s-2}\binom{s-2}{i-1}$	$\binom{s-2}{s-4}\binom{s-4}{i-2}$	. . .	$\binom{s-j}{s-2j}\binom{s-2j}{i-j}$	. .
. . . . .								
. . . . .								
s	2s+1	s	$1\binom{s}{s}$					

A similar series can be written for the probability distribution in the small cages, but unfortunately neither of these series could be summed and an alternative approach was tried to obtain the sum indirectly.

Consider the more general case of one dimensional diffusion with a boundary condition. Suppose that the atom begins its random walk from the n^{th} large cage from the boundary and let R(m,s) denote the probability of finding the atom in the m^{th} large cage from the barrier after s jumps. We have then for m>2 the difference equation

$$R(m,s+1) = \rho R(m-1,s) + \rho R(m+1,s) + \sigma R(m,s-1).$$

If we assume the barrier to be a reflector, i.e. an impermeable wall, then for m = 1 and m = 0 we have

$$R(1,s+1) = 2\rho R(0,s) + \rho R(2,s) + \sigma R(1,s-1)$$

$$R(0,s+1) = \rho R(1,s) + \sigma R(0,s-1),$$

and for the initial conditions

$$R(m,1) = \rho\,(m,n-1) + \rho\,(m,n+1)$$

$$R(m,0) = \delta(m,n)$$

where δ is the Kronecker delta.

Let $\mathbf{r}_s$ be an infinite vector

$$\mathbf{r}_s = \begin{pmatrix} R(0,s) \\ R(1,s) \\ \vdots \\ R(m,s) \\ \vdots \end{pmatrix}$$

and **A** the infinite matrix

$$\mathbf{A} = \begin{pmatrix} 0 & \rho & 0 & 0 & 0 & . & . \\ 2\rho & 0 & \rho & 0 & 0 & . & . \\ 0 & \rho & 0 & \rho & 0 & . & . \\ 0 & 0 & \rho & 0 & \rho & . & . \\ 0 & 0 & 0 & \rho & 0 & . & . \\ & . & . & . & . & . & . \end{pmatrix}$$

then the above difference equations including the boundary conditions can be written simply as

$$\mathbf{r}_{s+1} = \mathbf{A}\mathbf{r}_s + \sigma\mathbf{r}_{s-1}$$

A similar matrix A could be written to represent a sink barrier or an infinite medium.

Suppose that the above equation can be reduced to the form

$$r_{s+1} = Br_s$$

then we can write immediately

$$r_s = B^s r_o \qquad \text{where} \quad r_o = \begin{pmatrix} 0 \\ 0 \\ \vdots \\ 1 \\ \cdot \end{pmatrix}$$

the 1 being in the n^{th} component. The procedure for evaluating B^s consists mainly of finding the eigen values of B. This is a standard procedure of Markoff chains and it could be carried out analogously to the method used by Kac[90] in treating brownian motion under gravity.

Unfortunately, matrix B could not be found because the matrix difference equation leads to a series which could not be summed. We have

$$r_1 = Ar_o$$

$$r_2 = Ar_1 + \sigma r_o$$

$$A^2 r_o + \sigma r_o$$

similarly $$r_3 = A^3 r_o + 2\sigma A r_o$$

and finally

$$r_s = \binom{s}{0} A^s + \binom{s-1}{1} \sigma A^{s-2} + \binom{s-2}{2} \sigma^2 A^{s-4} + \cdots$$

$$\cdots + \binom{s-s/2}{s/2} \sigma^{s/2} A^o \qquad s \text{ even}$$

$$\text{or} \cdots + \binom{s-(s-1)/2}{(s-1)/2} \sigma^{(s-1)/2} A \qquad s \text{ odd}$$

$$= r_o \sum_{i=0}^{s/2} \binom{s-i}{i} \left(\frac{\sigma}{A^2}\right)^i A^s \qquad \text{for } s \text{ even.}$$

There is an alternative difficulty with this simple approach. An attempt was made to find the probability distribution as a function of the number of jumps. In practice, however, we must have the distribution as a function of time, and there is no simple way of relating the time to the jumps. This will become more evident in the next section, when the probability will be expressed on a time basis.

(ii) Diffusion Equations.

Let 2ρ and σ be the probabilities of jumping from a large cage into a large and a small cage respectively, within a unit time interval, and let ν be the probability of not jumping in that time interval. Let τ be the probability of jumping back from the small cage and κ the probability of remaining in it during the time interval. We thus have

$$2\rho + \sigma + \nu = 1$$

$$\tau + \kappa = 1$$

As before we can write two difference equations

$$R(m,s+1) = \rho R(m-1,s) + \rho R(m+1,s) + \nu R(m,s) + \tau S(m,s)$$

$$S(m,s) = \rho R(m,s-1) + \kappa S(m,s-1)$$

where $R(m,s)$ and $S(m,s)$ are the probabilities of being in the m^{th} large and small cage respectively, after s jumps.

If we consider the distance between two large cages to be Δ and the time per jump θ then the difference equations can be written as

$$\frac{\Delta^2\rho}{\theta}\cdot\frac{[R(m+1,s) - 2R(m,s) + R(m-1,s)]}{\Delta^2}$$

$$= \frac{R(m,s+1) - R(m,s)}{\theta} + \frac{S(m,s+1) - S(m,s-1)}{\theta}$$

and $$\frac{S(m,s) - S(m,s-1)}{\theta} = \frac{\tau}{\theta}\left\{\frac{\sigma}{\tau} R(m,s-1) - S(m,s-1)\right\}.$$

In the limit as the interval Δ decreases to atomic dimensions as θ decreases we have

$$s\theta = t \ , \quad \Delta^2\rho/\theta = D \ , \quad \tau/\theta = k$$

and the difference equations reduce to

$$D\frac{\partial^2 R}{\partial x^2} = \frac{\partial R}{\partial t} + \frac{\partial S}{\partial t}$$

$$\frac{\partial s}{\partial t} = k\left(\frac{\sigma}{\tau} R - S\right).$$

Therefore, in three dimensions, we have

$$D\nabla^2 r = \frac{\partial r}{\partial t} + \frac{\partial s}{\partial t}$$

$$\frac{\partial s}{\partial t} = \lambda r - \mu s$$

where r and s are the concentrations in the large and small cages respectively, where λ and μ can be regarded as forward and reverse trapping rate constants, similar to those in diffusion with accompanying chemical reversible reaction.

The significance of λ and μ is that their ratio, $\lambda/\mu = \sigma/\tau$, can be determined from the potential barriers calculated from intermolecular forces. To determine the diffusion coefficient one has to calculate the jump frequency $\Gamma = 1/\theta$ and to multiply this by the transition probability ρ which would have to be determined also from the potential

transition barrier.

The above binary equation can be reduced, of course, to a simple diffusion equation by forbidding entry to the small cages, i.e. $\sigma = \tau = 0$. In this case the diffusion coefficient is simply $D = \Delta^2/(2\theta)$.

(b) Solution of Binary Diffusion Equations

It was shown earlier that the diffusion of small gas molecules through molecular sieve Type A can be represented by the simultaneous equations

$$D\left(\frac{\partial^2 r}{\partial x^2} + \frac{\partial^2 r}{\partial y^2} + \frac{\partial^2 r}{\partial z^2}\right) = \frac{\partial r}{\partial t} + \frac{\partial s}{\partial t}$$

$$\frac{\partial s}{\partial t} = \lambda r - \mu s \qquad (1)$$

where r amd s are the gas concentrations in the large and small cages respectively, and λ and μ are uptake and release constants for the small cages.

The above equations have to be solved so as to give the total quantity of gas desorbed from a single crystal of molecular sieve as a function of time. Examination of the crystals (Fig.3 p.12) shows that the boundary conditions of a cube would make the best approximation to reality.

The boundary conditions for eq.(1) can be written, therefore, as -

$$r + s = 1 \quad \text{and} \quad r = (\mu/\lambda)s \quad \text{at} \quad t \leq 0, \quad \text{all } x, y, z,$$

$$\text{and } r = 0 \text{ at } \begin{matrix} x = 0 & \text{and} & x = a \\ y = 0 & & y = a \\ z = 0 & & z = a. \end{matrix} \quad \text{all} \quad t > 0 \qquad (2)$$

These boundary conditions represent a cube, side a, initially at a uniform concentration 1 immersed into an infinite, well stirred fluid of concentration 0.

The solution of eq.(1) is simplified by the substitution

$$\begin{matrix} X = x\pi/a & & T = t\pi^2 D/a^2 \\ Y = y\pi/a & & L = \lambda\pi^2 D/a^2 \\ Z = z\pi/a & & M = \mu\pi^2 D/a^2 \end{matrix}$$

which changes equations (1) to

$$\nabla^2 r = \frac{\partial r}{\partial T} + \frac{\partial s}{\partial T}$$
$$\frac{\partial s}{\partial T} = Lr - Ms \qquad (3)$$

whose space variables X, Y, and Z have boundary conditions at 0 and π which makes it convenient for a direct fitting of a Fourier series with sine terms only.

It can be verified by direct differentiation that

$$\begin{aligned} r &= Ae^{-pT} \sin lX \sin mY \sin nZ \\ s &= Be^{-pT} \sin lX \sin mY \sin nZ \end{aligned} \qquad (4)$$

is a solution of eq.(3) provided that p is appropriately chosen. The constants A and B are then chosen so that the sum of all the possible solutions satisfies the boundary conditions.

Substituting (4) into eq.(3) we find that

$$(l^2+m^2+n^2)r = -pr - ps$$

and

$$-ps = Lr - Ms$$

and equating these with (4) the exponent is found to be the solution of

$$p^2 - (L+M+l^2+m^2+n^2)p + M(l^2+m^2+n^2) = 0 \qquad (5)$$

while A and B are related by

$$(l^2+m^2+n^2-p)A = pB. \qquad (6)$$

The solution of eq.(3) is the sum of all the possible solutions (4), viz.

$$r = \sum_{l=1}^{\infty}\sum_{m=1}^{\infty}\sum_{n=1}^{\infty}\left(A_1 e^{-p_1 T}+A_2 e^{-p_2 T}\right)\sin lX \sin mY \sin nZ$$

$$s = \sum_{l=1}^{\infty}\sum_{m=1}^{\infty}\sum_{n=1}^{\infty}\left(B_1 e^{-p_1 T}+B_2 e^{-p_2 T}\right)\sin lX \sin mY \sin nZ \qquad (7)$$

where p_1 and p_2 are the two roots of eq.(5) given by

$$p_1 = \frac{1}{2}\{L+M+l^2+m^2+n^2+[(L+M+l^2+m^2+n^2)^2-4M(l^2+m^2+n^2)]^{1/2}\}$$

$$p_2 = \frac{1}{2}\{L+M+l^2+m^2+n^2-[(L+M+l^2+m^2+n^2)^2-4M(l^2+m^2+n^2)]^{1/2}\}$$

and the Fourier coefficients A_1, A_2, B_1, and B_2 have to be determined to satisfy the boundary conditions.

The boundary conditions for $t > 0$ are satisfied directly by (7) because l,m,n are integers and X,Y,Z are 0 or π at the boundaries.

At $t = 0$ we have from (7), for the concentration in

the large cages

$$r = \Sigma_l \Sigma_m \Sigma_n \ (A_1 + A_2) \ \sin lX \ \sin mY \ \sin nZ = r_o \qquad (8)$$

where r_o is the initial concentration in the large cages given by

$$r_o = \mu/(\lambda+\mu) = M/(L+M).$$

The values of the coefficients $A_1 + A_2$ are found by multiplying both sides of (8) by $\sin iX$ terms, where i is an integer, and integrating from 0 to π, thus

$$\int_o^\pi \int_o^\pi \int_o^\pi \Sigma_l \Sigma_m \Sigma_n (A_1+A_2) \sin lX \sin iX \cdot \sin mY \sin jY \cdot \sin nZ \sin kZ \cdot dXdYdZ$$

$$= r_o \int_o^\pi \int_o^\pi \int_o^\pi \sin iX \sin jY \sin kZ \ dXdYdZ \qquad (9)$$

Performing this integration we find that identity (9) and hence identity (8) are satisfied when $A_1 + A_2$ assume the following values

$$A_1 + A_2 = \begin{cases} 0 & \text{for even } l,m,\text{or } n \\ \dfrac{64 r_o}{\pi^3} \cdot \dfrac{1}{lmn} & \text{for odd } l,m,\text{and } n. \end{cases}$$

Similarly, it can be shown that

$$B_1 + B_2 = \begin{cases} 0 & \text{for even } l,m,\text{or } n \\ \dfrac{64 s_o}{\pi^3} \cdot \dfrac{1}{lmn} & \text{for odd } l,m,\text{and } n \end{cases}$$

where $s_o = 1 - r_o$.

The coefficients A and B, and the indices p are all functions of the rate constants λ and μ and the integers l, m, and n. The concentration distribution curves for large

and small cages can be found now directly by summing the series in (7) over odd values of l,m,n.

For diffusion measurements it is more useful to have the total amount of gas diffusing from the cube. Adding the two solutions in (7) and utilising relationship (6) the total concentration within the crystal is given by

$q = r + s$

$$= \frac{64}{\pi^5} \Sigma_l \Sigma_m \Sigma_n \left(p_2 e^{-p_1 T} - p_1 e^{-p_2 T}\right) - \frac{u}{\lambda+u}(l^2+m^2+n^2)(e^{-p_1 T} - e^{-p_2 T}) \frac{\sin lX \sin mY \sin nZ}{lmn(p_2 - p_1)}$$

The total amount present in the cube is found by integrating over the whole cube, thus

$$Q = \int_0^{\pi}\int_0^{\pi}\int_0^{\pi} q\,dX\,dY\,dZ$$

$$= \frac{512}{\pi^5} \Sigma_l \Sigma_m \Sigma_n \frac{1}{lmn^2}(g_1 e^{-p_1 T} + g_2 e^{-p_2 T}) \qquad (10)$$

where $$g_1 = \frac{(l^2+m^2+n^2)u/(\lambda+u) - p_2}{p_1 - p_2}$$

and $$g_2 = \frac{p_1 - (l^2+m^2+n^2)u/(\lambda+u)}{p_1 - p_2}$$

One Dimensional Diffusion.

The solution of eq.(3) for the one dimensional case of diffusion in a wall of thickness a is

$$Q_{wall} = \frac{8}{\pi^2} \Sigma_l \frac{1}{l^2}(g_1 e^{-p_1 T} + g_2 e^{-p_2 T}) \qquad (11)$$

The same solution, expressed in a different form, has been found previously by Crank[87] for the one dimensional case using Laplace transforms. Crank gives also tables and curves for the fraction exchanged as a function of time for different values of λ and μ. A spot check of the series in (11) showed complete agreement with Crank's results.

(c) The Diffusion Coefficient

In deriving the binary diffusion equations for molecular sieves it was shown that the diffusion coefficient is given by

$$D = \Delta^2 \rho / \theta$$

where Δ is the distance between large cages, θ the jump time and ρ the large cage to large cage transition probability.

ρ Is proportional to the potential barrier height determined from the minimum cage adsorption potential and the minimum saddle point potential. This is easy to evaluate for open windows. For windows partially or fully blocked by sodium ions the saddle point has to be determined by minimising a function of two variables viz. the inter-molecular potential as a function of diffusing atom and sodium ion positions. The saddle point can be computed easily in principle (minimising a function of six independent variables) but practically the problem is very difficult because of the very long range of electrostatic ion - ion

interaction.

The jump frequency, $\Gamma = 1/\theta$, and hence the diffusion coefficient ($\Delta = 12.3\text{Å}$) can again be determined easily for open windows by applying Vineyard's theory for solid state diffusion.[94] We have

$$\Gamma = \left(\frac{kT}{2\pi}\right)^{1/2} \frac{\int_\sigma e^{-\phi/kT} d\sigma}{\int_A e^{-\phi/kT} dV}$$

where $\phi(y_1, y_2, \ldots y_n)$ is the total potential energy of the crystal, n degrees of freedom, A is the position around the minimum potential of the diffusing atom, in its configuration space, σ the hypersurface going through the saddle point such that it is perpendicular to the contours of constant potential energy.

For the diffusion of a single atom through open molecular sieve windows the Vineyard theory can be applied directly by assuming a rigid aluminosilicate structure. In this case the hypervolume and hypersurface of the configuration space reduce to volume and surface in three dimensional space, whence $\int_A$ is carried out over the volume of a large zeolite cage, and $\int_\sigma$ over the surface in the open window of the zeolite. The configuration integrals are thus reduced to the simple summation

$$\Gamma = \left(\frac{kT}{2\pi}\right)^{1/2} \frac{\Sigma_\sigma e^{-\phi/kT} \Delta\sigma}{\Sigma_V e^{-\phi/kT} \Delta V}$$

where the potentials have been computed at discreet points within the cage and in the plane of the window.

For the diffusion with two gas atoms in the cage the integrals are reduced analogously to

$$\Gamma = 2\left(\frac{kT}{2\pi}\right)^{1/2} \frac{\Sigma_V \Sigma_\sigma e^{-\phi/kT} \Delta V \Delta \sigma}{(\Sigma_i \Sigma_j)_V e^{-\phi/kT} \Delta V \Delta V}$$

where ϕ now represents gas - gas interaction as well as the gas - solid interaction. This summation can again be carried out quite simply on the computer by working with precalculated gas - solid interaction potentials. This method could be extended to three atoms in a cage, but above that the computation time would become prohibitively long.

Completely free windows occur only in molecular sieve 5A on which no experimental measurements or calculations were made. In molecular sieve 4A the large windows are partially blocked and the small windows are wholly blocked.

The large windows, with one sodium ion off centre could be treated as open windows with the sodium ion fixed. This, however, would be a very crude approximation not only because some atoms can diffuse through even the small windows but the coordinates of these ions are very uncertain. A better approximation would be to assume that the sodium ion can move only in the plane of the window, then, in keeping with the basic assumptions of the theory, we have for the diffusion of one atom

$$\Gamma = \left(\frac{kT}{2\pi}\right)^{1/2} \frac{\Sigma_\sigma \Sigma_\sigma e^{-\phi/kT}_{\Delta\sigma\Delta\sigma}}{\Sigma_V \Sigma_\sigma e^{-\phi/kT}_{\Delta V\Delta\sigma}}$$

where the potential ϕ consists of gas - solid, gas - ion, ion - solid interactions. Because of the long range forces involved for the ion - solid (ion) interaction, these calculations are difficult to perform.

Diffusion through the small windows is still more difficult to interpret because to allow the atom to diffuse the sodium ion must move completely out of the way. This means that the saddle point hypersurfaces cannot be determined easily and the theory cannot be applied directly.

4. DIFFUSION IN POWDER COMPACTS

(a) One Dimensional Powder Bed

(i) Solution Under Simplified Assumptions.

To explain selfdiffusion in a one dimensional packed powder bed an attempt was made to solve the composite equations under the simplest possible assumptions.

The bed was considered to be composed of uniform spherical particles with internal diffusion following the simple Fick's law rather than the actual diffusion equations derived earlier.

For convenience it is assumed that the bed is free of adsorbate and the diffusion commences from the outside of the bed. This formulation applies to selfdiffusion and to the diffusion of an adsorbate in the presence of an inert carrier gas in which the bed is initially immersed. Clearly, this formulation would not apply to intrinsic gas adsorption by a bed initially under vacuum when, besides interparticle diffusion through the pores, equations would have to be included for porous gas flow under pressure gradients.

We thus have to solve

$$\frac{\partial c}{\partial t} = D_p \frac{\partial^2 c}{\partial x^2} - \frac{1}{m} \frac{\partial Q}{\partial t} \qquad (12)$$

under the linear equilibrium assumption (no film resistance)

$$q_s = q(a,x,t) = Kc(x,t)$$

with the boundary conditions

$$c = c_o \quad \text{at} \quad x = \pm 1 \quad \text{for all } t$$

$$\text{and } c = 0 \quad \text{at} \quad t = 0 \quad \text{for } -1<x<1,$$

where $c = c(x,t)\text{mol/cm}^3$ - gas concentration in pores

c_o - gas concentration outside the bed

$q = q(r,x,t)\text{mol/cm}^3$ solid - gas concentration in solid

$q_s = q(a,x,t)$ - surface concentration on the solid

$Q = Q(x,t)$ - average concentration of solid particle

m - void volume/unit volume of adsorbent

K - equilibrium constant

x - distance from the centre of bed

r - distance from the centre of particle

a - particle radius

$2l$ - bed thickness

D_p - pore diffusion coefficient

The average particle concentration is a function of position and time and it can be obtained from the diffusion in a sphere under constant surface concentration by using Duhamel's theorem, thus

$$q(r,x,t)=2D\sum_{n=1}^{\infty}(-1)^{n-1}\sigma_n\frac{\sin(\sigma_n r)}{r}\int_o^t q_s(x,\lambda)e^{-D\sigma_n^2(t-\lambda)}d\lambda$$

where $\sigma_n = n\pi/a$ and D is the solid diffusion coefficient.

Now $$Q(x,t) = \frac{3}{a^3}\int_o^a qr^2\,dr \quad ,$$

therefore

$$\frac{\partial Q}{\partial t} = \frac{6D}{a^2} \sum_{1}^{\infty} \int_{o}^{t} \frac{\partial q_s(x,\lambda)}{\partial \lambda} \, e^{-D\sigma_n^2(t-\lambda)} d\lambda$$

and the equation to be solved is

$$\frac{\partial c}{\partial t} = D_p \frac{\partial^2 c}{\partial x^2} - 2\gamma \sum_{1}^{\infty} \int_{o}^{t} \frac{\partial c}{\partial \lambda} \, e^{-D\sigma_n^2(t-\lambda)} d\lambda \qquad (13)$$

where

$$\gamma = \frac{3DK}{ma^2} .$$

Taking Laplace transforms of eq.(13) with respect to time, in a method exactly analogous to Rosen's, the equation is transformed to

$$sC(x,s) = D_p \frac{\partial^2 C(x,s)}{\partial x^2} - 2\gamma \sum_{1}^{\infty} \frac{s}{s+D\sigma_n^2} C(x,s)$$

where $C(x,s)$ is the Laplace transform of $c(x,t)$. The transformed equation can be rewritten in the simplified form

$$D_p \frac{\partial^2 C(x,s)}{\partial x^2} = Y_D(s) + s\, C(x,s) \qquad (14)$$

where $$Y_D(s) = 2\gamma \Sigma \frac{s}{s+D\sigma_n^2} .$$

This equation is subject to the transformed boundary condition

$$C = c_o/s \quad \text{at} \quad x = \pm l \text{ for all } t.$$

Eq.(14) is of standard form[86] and its solution is

$$C = \frac{c_o \cosh(Y_E^{1/2} x)}{s \cosh(Y_E^{1/2} l)} \qquad (15)$$

where $$Y_E = [Y_D(s) + s]/D_p$$

To obtain the gas concentration as a function of position and time the inverse transform of C has to be obtained by performing the contour integral

$$c(x,t) = \frac{c_0}{2\pi i}\int_{\alpha-i\infty}^{\alpha+i\infty}(1/s)e^{st}\,\frac{\cosh(Y_E^{1/2}x)}{\cosh(Y_E^{1/2}l)}\,ds \qquad (16)$$

This integration can be performed by isolating all the singularities of the integrand. The singularities arise in three distinct ways:

(i) at $s = 0$,

(ii) when $\cosh(Y_E^{1/2}l)$ becomes zero,

(iii) when $\cosh(Y_E^{1/2}x)$ becomes infinite.

The pole at $s = 0$ is simple and need not be treated further.

The hyperbolic cosine term in the denominator will vanish when

$$Y_E^{1/2}(s)l = \pm(2k + 1)i\pi/2 \quad \text{for } k = 0,1,2,\ldots$$

i.e. $$Y_E(s) = -(2k + 1)^2\pi^2/(4l^2). \qquad (17)$$

$Y_E(s)$ is a function of $Y_D(s)$ and using the identity

$$2\sum_1^\infty \frac{-z^2}{n^2-z^2} = \pi z\cot(\pi z)-1 \quad \text{for } z \neq 0,\pm1,\pm2,\ldots$$

Y_E can be expressed as

$$Y_E(s) = \frac{\gamma(w\cot w - 1) - w^2D/a^2}{D_p} \qquad (18)$$

where $w = ia(s/D)^{1/2}$

Using this expression condition (17) is satisfied when $s = -\alpha_i$ where α_i are the roots of the equation

$$(2\alpha/\sigma)^{1/2}\cot(2\alpha/\sigma)^{1/2} - \alpha/\gamma = -\eta(2k+1)^2 + 1 \qquad (19)$$

where $\alpha = -s$

$\sigma = 2D/a^2$

$\eta = \pi^2 ma^2/(12l^2DK)$

By plotting the left hand side of eq.(19) as a function of α, and utilising the fact that for positive x

$$(-x)^{1/2}\cot(-x)^{1/2} = x^{1/2}\coth x^{1/2}$$

it can be shown that provided the right hand side of (19) is not greater than 1 all the roots α_i are real and positive. Because η is positive and k are positive integers this condition is satisfied and the poles due to the denominator lie all on the negative real axis of s.

Analysis of the left hand side of (19) shows too that infinity is reached by the numerator of (16) only for positive α also, and therefore the poles are confined again to the negative real axis of s.

The integrand of (16) is thus analytic in the real half-plane, except for the origin, and the contour integration can be performed by taking a small semicircle Γ of radius ϵ around the origin to give

$$c(x,t) = \frac{1}{2\pi i}\lim_{\epsilon\to 0}\left(\int_{-i\infty}^{-i\epsilon} + \int_{\Gamma} + \int_{i\epsilon}^{i\infty}\right)e^{st}C(s)ds.$$

By changing to polar coordinates and performing the integration around Γ, as ϵ approaches 0, then using the complex conjugate properties

$$C(x,\bar{s}) = \bar{C}(x,s)$$

$$C + \bar{C} = 2\mathcal{R}(C)$$

the above integral reduces to

$$c(x,t) = \frac{1}{2} + \frac{1}{\pi}\int_0^\infty \mathcal{R}[e^{i\beta t}C(x,i\beta)]d\beta \qquad (20)$$

where s has been transformed to $-i\beta$ and $i\beta$.[91]

Changing the variables of the integral by $\beta = \sigma\lambda^2$ and separating the real and imaginary parts with the help of the usual trigonometric and exponential complex transformations, it can be shown that (20) reduces to

$$c/c_o = \frac{1}{2} + \frac{2}{\pi}\int_o^\infty \left\{\cos(\lambda^2\sigma t)\left(\frac{FG-EH}{G^2+H^2}\right) + \sin(\lambda^2\sigma t)\left(\frac{EG+FH}{G^2+H^2}\right)\right\}\frac{d\lambda}{\lambda} \qquad (21)$$

where $E = \cosh(x\sqrt{\rho}\cos\theta/2)\cos(x\sqrt{\rho}\sin\theta/2)$

$F = \sinh(x\sqrt{\rho}\cos\theta/2)\sin(x\sqrt{\rho}\sin\theta/2)$

$G = \cosh(1\sqrt{\rho}\cos\theta/2)\cos(1\sqrt{\rho}\sin\theta/2)$

$H = \sinh(1\sqrt{\rho}\cos\theta/2)\sin(1\sqrt{\rho}\sin\theta/2)$

where $\rho = (\gamma/D_p)\{H_{D_1}^2(\lambda)+[H_{D_2}(\lambda)+\lambda^2\sigma]^2\}^{1/2}$

$\theta = \tan^{-1}\{H_{D_1}(\lambda)/[H_{D_2}(\lambda)+\lambda^2\sigma]\}$

where $H_{D_1}(\lambda) = \dfrac{(\sinh 2\lambda+\sin 2\lambda)}{(\cosh 2\lambda-\cos 2\lambda)-1}$

$H_{D_2}(\lambda) = \dfrac{\lambda(\sinh 2\lambda-\sin 2\lambda)}{(\cosh 2\lambda-\cos 2\lambda)}.$

It can be seen that although the integrand of (21) is complicated it is explicit in λ and it can be computed directly but not simply because of the oscillating trigonometric components. The H_{D_1} and H_{D_2} have been tabulated by Rosen[9.1] and these could be used in evaluating the integral.

The solution would have to be computed for selected values of $\sigma = 2D/a^2$, the bed length l, and the parameter $\gamma/D_p = 3DK/(ma^2D_p)$, the calculations being made for bed positions x and time t. It should be noted that it is impossible to separate $K/(mD_p)$. This is consistent with the earlier discussion on powder bed diffusion, neglecting the particle diffusion (p.101).

Alternatively, integral (20) could be solved directly on a computer programmed to evaluate complex trigonometric and hyperbolic functions. The Mercury computer, for example, can evaluate the square root and exponentials directly, and the other functions could be done by writing them as routines at the end of the programme.

The total gas taken up by the powder bed is given by

$$Q_{av}(t) = \int_o^t \left(\frac{\partial c}{\partial x}\right)_o dt$$

and the fraction exchanged, for predicting, say, the curve in Fig.29, p.99, is given by

$$\text{Fraction exchanged} = 1 - Q_{av}(t).$$

(ii) Approach To Real Conditions.

The first improvement to the previous solution would be to consider cubic particles while preserving the simple solid diffusion equations.

The solution for simple diffusion in a cube is known[86] and it consists of a triple cosine series with an exponential term of the form

$$e^{-k(l^2+m^2+n^2)}$$

where the summation is carried out over all odd values of l,m, and n. Using Duhamel's theorem and then applying Laplace transforms as before leads to the expression

$$\Sigma_l \Sigma_m \Sigma_n \frac{s}{s+k(l^2+m^2+n^2)}$$

which cannot be summed. This is not because of the odd terms, for which a sum exists, but because of the triple summation for which there is no known solution.

If the real molecular sieve diffusion equations (1) are used their solution contains an even more complicated exponential, cf. eq.(7), whose transform leads again to an insoluble form.

The best improvement to the previous powder bed solution, eq.(21), would probably result by considering an actual particle size distribution. This is evident from the derivation of (21) that an average or equivalent particle size cannot be substituted for the single size, which means

that the concentration distribution depends on the actual distribution. The same can be concluded from physical considerations when a wide range particle size would result in a rapid initial diffusion and a slow final diffusion.

A solution similar to (21) can be obtained, however, by performing the calculations for a definite and known particle size range. This can be done by confining the particle sizes to $Y_E(s)$ which now would consist of a finite sum of fractional $Y_D(s)$ representing the fraction at each selected particle size.

To show that such a solution can be obtained it is only necessary to show that all the poles still lie on the negative real axis. This can be seen by considering two particle sizes for which we can write the root determining equation, similar to eq. (19)

$$y_1 (2\alpha/\sigma_1)^{1/2} \cot(2\alpha/\sigma_1)^{1/2} - y_1\alpha + y_2 (2\alpha/\sigma_2)^{1/2} \cot(2\alpha/\sigma_2)^{1/2} - y_2\alpha = -(2k+1)^2\pi^2/(4l^2)$$

The value of the left hand side is a complicated function of α for positive α, because of the superimposition of cotangent curves. However, for negative values of α the left hand side is a monotonously increasing function, going from 1 at $\alpha = 0$ to infinity as $-\alpha$ goes to infinity. Clearly all the roots are positive and all the poles are on the negative real axis of s.

(b) Pellets

(i) Spherical Pellets.

Consider a spherical pellet, radius b, made up of spherical particles, radius a, then for the diffusion through the pores and particles we can write

$$D_p\left(\frac{\partial^2 c}{\partial x^2} + \frac{2}{x}\frac{\partial c}{\partial x}\right) = \frac{\partial c}{\partial t} + \frac{1}{m}\frac{\partial Q}{\partial t} \qquad (22)$$

where $Q(x,t)$ is the average concentration in the particles, as defined earlier.

Applying Duhamel's theorem eq.(22) reduces to the integro-differential equation

$$D_p\left(\frac{\partial^2 c}{\partial x^2} + \frac{2}{x}\frac{\partial c}{\partial x}\right) = \frac{\partial c}{\partial t} + 2\gamma\Sigma_n\int_o^t \frac{\partial c}{\partial \lambda} e^{-D\sigma_n^2(t-\lambda)}\,d\lambda$$

which can be transformed to

$$\frac{\partial^2 xC}{\partial x^2} = Y_E\, xC \qquad (23)$$

where $C(x,s)$ is the Laplace transform of $c(c,t)$, and γ and $Y_E(s)$ are the same as defined earlier.

The solution to eq.(23), satisfying the boundary conditions

$$c(x,t) = c_o \quad \text{at } x = b \quad \text{for all } t$$

and $$c(x,t) = 0 \quad \text{at } t = 0 \quad \text{for } x \leq 1$$

can be shown to be

$$C(x,s) = \frac{c_o b}{sx}\,\frac{\sinh(\sqrt{Y_E}x)}{\sinh(\sqrt{Y_E}b)} \qquad (24)$$

Applying the inversion theorem as for the powder bed, the concentration distribution inside a spherical pellet is given by

$$c(x,t) = \frac{1}{2} + \frac{1}{\pi}\int_0^\infty \mathcal{R}[e^{i\beta t}C(x,i\beta)]d\beta .$$

and the solution becomes almost identical to (21)

$$c/c_o = \frac{b}{x}\left\{\frac{1}{2} + \frac{2}{\pi}\int_o\left(\cos(\lambda^2\sigma t)\,\frac{FG-EH}{G^2+H^2} + \sin(\lambda^2\sigma t)\frac{EG+FH}{G^2+H^2}\right)\frac{d\lambda}{\lambda}\right\} \qquad (25)$$

where $E = \sinh(x\sqrt{\rho}\,\cos\theta/2)\cos(x\sqrt{\rho}\,\sin\theta/2)$

$F = \cosh(x\sqrt{\rho}\,\cos\theta/2)\sin(x\sqrt{\rho}\,\sin\theta/2)$

$G = \sinh(b\sqrt{\rho}\,\cos\theta/2)\cos(b\sqrt{\rho}\,\sin\theta/2)$

$H = \cosh(b\sqrt{\rho}\,\cos\theta/2)\sin(b\sqrt{\rho}\,\sin\theta/2)$

ans ρ and θ are the same as defined earlier.

(ii) Cylindrical Pellets.

For a short cylinder, radius b, length l, we can write

$$D_p\left(\frac{\partial^2 c}{\partial z^2} + \frac{\partial^2 c}{\partial x^2} + \frac{1}{x}\frac{\partial c}{\partial x}\right) = \frac{\partial c}{\partial t} + \frac{1}{m}\frac{\partial Q}{\partial t} \qquad (26)$$

and taking Laplace transforms with respect to time this reduces to

$$D_p\left(\frac{\partial^2 C}{\partial z^2} + \frac{\partial^2 C}{\partial x^2} + \frac{1}{x}\frac{\partial C}{\partial x}\right) = Y_E C$$

The solution of this equation can be obtained by assuming a product solution[86] $C(x,z,s)=C_1(x,s)\cdot C_2(z,s)$, but the locations of the singularities are not easily apparent and the evaluation of the inverse contour integral was not attempted.

VI CONCLUSIONS

The system of gas adsorption and diffusion through zeolites has been found to be very interesting experimentally and theoretically. The practical usefulness of synthetic zeolites makes the study of this system highly desirable.

Experimental Methods.

All the diffusion measurements were made using a simple radioactive isotope selfdiffusion technique. This has the unique advantage of allowing the diffusion measurements to be made under dynamic equilibrium conditions and an invariable adsorption equilibrium constant. Even under these conditions the mathematics has been found to be very difficult and a direct attempt to interpret adsorption or desorption under actual conditions of variable partial pressure, variable equilibrium constant (with respect to pressure and temperature) and variable temperature (due to high heat of adsorption) would have been unlikely to succeed.

The flow technique used has the advantages of easy modification and approach to real conditions by varying the carrier gas flow rate and thus introducing gas film resistance. The method was applied to the measurement of self-diffusion in molecular sieve pellets and powders, and it was also used to measure directly the pore diffusion coefficient. It can be further extended for diffusion

measurement in any desired arrangement, for example in highly compressed molecular sieve plugs or squat one dimensional beds to test mathematical solutions. So far measurements have been made only on molecular sieves but the method is clearly applicable to all other types of adsorbents and catalysts in pellet or powder form.

The accuracy of the diffusion measurements is determined mostly by the characteristics of the radiation detection tubes. Large capacity tubes have a large delay time but they are capable of detecting small traces of activity. Tubes with a small volume have little delay and give a good resolution for rapidly changing activity. For best resolution, particularly in measuring powder diffusion, it would be desirable to use a scintillation counter; measurements can be made on minute volumes of gas by passing the gas through a plastic scintillation tube (ca. 0.1 cm. dia) placed over the photocell of a scintillation counter.

There is an intrinsic limitation to the ability to measure selfdiffusion in very small particles, and the self-diffusion of carbon dioxide in molecular sieve 4A is at that limit. The difficulty arises because of the formation of a stagnant gas film around each particle making it difficult to achieve "zero" concentration conditions on the outside of the particle. This difficulty can be partially overcome by assuming packed column behaviour. Rosen's theory was applied

to interpret the measurements on solid diffusion in powder but only an estimate of the diffusion coefficient could be obtained, mainly because Rosen's theory applies only to a bed made up of a single particle size, whereas the powder has a size range (0.1 to 5 μ). However even if an accurate theory were available the measure of the diffusion coefficient would still be relatively inaccurate because the coefficient would depend on the precise shape of the breakthrough curve rather than on its position.

A more desirable approach consists of measuring the solid diffusion coefficient at a lower temperature. The activation energy for diffusion through molecular sieves is much higher than for bulk gas diffusion and by performing the measurements at a lower temperature the gas film resistance becomes less significant, moreover, the gas viscosity decreases and higher carrier gas flow rates can be used resulting in even lower gas film resistances. Low temperature measurements can then be extrapolated (log D v. 1/T) to higher temperatures. This approach should be used for all molecular sieve powder diffusion coefficient measurements, because the low temperature measurements can be used to test diffusion theories while high temperature extrapolations are sufficient for practical purposes since then pore diffusion will be the controlling factor and the solid diffusion a secondary effect.

Equipment has been designed to make the low temperature measurements, but unfortunately time was not available to do any experiments in that region.

Carbon Dioxide Diffusion in Pellets.

The original diffusion curve (Fig.5,p.17) has not yet been fully interpreted. The solid diffusion coefficient has been estimated by assuming an exponentially decaying crystal surface concentration and from Rosen's theory of packed beds.

The pore diffusion coefficient has been measured by using a special experimental arrangement in which solid diffusion could be neglected. The effective pore diffusion coefficient was reduced, in terms of equilibrium constant and porosity to the actual pore diffusion (p.101) which would have been measured in the absence of adsorption. This diffusion coefficient was found to be about 73% of bulk gas coefficient. A theoretical equation exists[97] for predicting this from porosity.

For selfdiffusion of carbon dioxide in a pellet it is found that pore diffusion and solid diffusion seem to be both significant and to interpret the experimental curve a solution is required for the pellet diffusion equation. This solution could not be found. A solution has been obtained for the diffusion in a spherical pellet and in a "one dimensional" pellet. It is also possible that a solution

could be written down for a cylindrical pellet. However, all these solutions are in the form of infinite integrals and the numerical results must be evaluated on a computer; even then, the computation will be very tedious because of the periodic nature of the functions. For practical purposes it would be desirable to find simpler approximate solutions although the accurate solution ought to be evaluated in order to test any approximate theory.

The Slow Diffusion Rate.

Plotting the percentage of carbon dioxide exchanged as a function of time it was found that in every case two distinct diffusion rates exist; a fast initial rate in which 90 to 98% is exchanged, and a final much slower rate.

Initial theoretical analysis showed that this could be due to the small cages which change the simple diffusion equation to a binary equation whose solution can show two distinct rates. However, a decrease of the kink point from 90% for pellets to 98% for powder suggests that another mechanism must be in action. A possible cause of this is agglomeration of crystals, particularly in the presence of binder. There may well be up to 10% of crystals fully encased by the binder thus decreasing the diffusion rate substantially. The same conclusion is suggested by the weight loss on heating (Fig.18,p.59). The much smaller quantity of low diffusion material in the powder may be due

to crystal aggregates also, or it could be due to the binary diffusion equations. It should be noted that the derived binary equations apply equally well to diffusion in the presence of small retaining pockets or agglomerates.

Intermolecular Potential Calculations.

Attempts to calculate the adsorption potentials have met with difficulty because of the slow convergence of polarisation contributions. A preliminary calculation was made neglecting the polarisation contributions (which should amount to some 20% of the total contribution) and these results were used to predict the initial adsorption equilibrium constant. Semiquantitative agreement was obtained with the limited experimental data, and it was possible to conclude that carbon dioxide has access to the small molecular sieve cages (this implies the binary diffusion process).

It is highly desirable to carry out improved calculations on a simpler system, such as argon on molecular sieve 5A. Since the statistical mechanical adsorption theory is now well established, comparison of the theoretical equilibrium constants with experimental ones would lead to a better estimate of the intermolecular forces, or alternatively it could be used to study the extent of ionisation of the aluminosilicate atoms.

There are no specific theories for diffusion in

molecular sieves. The Vineyard theory for solid state diffusion (vacancy mechanism) was simplified so that it can be easily applied to predict the diffusion coefficients for open and partially blocked molecular sieve windows. This is probably the most useful field for further work, because the ability to predict the solid diffusion coefficient, combined with the known way of estimating the pore diffusion coefficient, would give a complete insight into the whole problem of dynamics of adsorption on molecular sieves.

Extension to Intrinsic Adsorption and Desorption.

The two most serious problems in dealing with intrinsic adsorption are the heat generation and the variable equilibrium constant. Heat generation could be treated in principle using simultaneous equations for heat and mass transfer but the solutions would probably be too complicated to be of practical use. Theoretical treatment of variable equilibrium constant is at the present impossible because this is equivalent to diffusion with a variable diffusion coefficient for which the mathematical solutions are restricted to a few special cases.

The most practical approach is to solve the diffusion equations numerically on a computer. This can be done explicitly if all the diffusion coefficients and constants are known. Alternatively, experimental break-through curves could be used to work back and find the missing coefficients. For

systems in which the pore diffusion is controlling (e.g. adsorption of carbon dioxide at room temperature and above) the pore diffusion coefficient can be written down directly for any simple gas, and using published adsorption equilibrium results, there is no reason why a standard programme could not be written for predicting accurately the break-through curves under any desired conditions.

The effective pellet pore diffusion coefficients are obtainable directly from the gas diffusion coefficient, equilibrium constant, porosity, and pore diffusion factor[97] as outlined on p.101, thus for example, pellet diffusion coefficients obtained from packed column measurements[26] can be interpreted in terms of gas diffusion or pore diffusion coefficients. Applying Rosen's solutions to an adsorption column packed with molecular sieve 4A pellets Chandrasekharan[26] found that the pellet diffusion coefficient varied between 2×10^{-5} for short beds to 2×10^{-6} for long beds when adsorbing 6% carbon dioxide from air. Taking $m = 0.50$, $k = 812$ (6% CO_2) we find that the effective diffusion coefficient should be 5×10^{-5} assuming the same gas diffusion coefficient for the pellet as for the one dimensional powder bed ($m = 2.5$). However during the initial adsorption CO_2 concentration in the pores is lower resulting in an equilibrium constant up to ten times higher than at 6% concentration (cf. Fig.20,p.65). This shows that the effective pellet diffusion coefficient can be expected to vary from .

5×10^{-5} to 5×10^{-6} which shows fair agreement with the packed column results.

These conclusions show that we are at a stage where, at least for some simpler systems, it should be possible to predict numerically the complete behaviour of packed adsorption columns.

- o -

APPENDIX

Computer Programme and Results

The following programme has been arranged to calculate the adsorption potential ϕ and the partition function $\exp(\phi/kt)$ for the adsorption of carbon dioxide on molecular sieve 4A.

Calculations were made with respect to 366 atoms enclosed by the dotted line in Fig.1, as explained in Section V 2.(c), to give the potentials (dispersion and repulsion) in a rectangular mesh within the tetrahedron defined by (cf. Fig.1)

$$x = 0(0.05)0.5$$

$$y = 0(0.05)x$$

$$z = 0(0.05)y$$

Data Input.

The data consists of the coordinates of alumino-silicate atoms (a_o units) and potential constants.

The programme uses the positions (a_i, b_i, c_i) of all the atoms within and on the edges of the positive quadrant of a unit cell, as shown in Fig.1, the other positions being derived by reflections. The coordinates are given in the order O(0 to 11), Si,Al(12 to 17), Na_1(18), and Na_2(19 to 21).

The potential constants (π_i) have been obtained from Table 9 by converting them to units of $a_o(=\pi_o)$. We thus have,

for example, for oxygen

$$\phi = V = -\pi_1/r^6 + \pi_2(\pi_1/r^6)^2$$

where r is in units of a_o and potential ϕ is given in units of 10^{-10} erg/molecule. The following pairs π_3 and π_4 etc. refer similarly to SA (average silicon aluminium atom), Na_1, and Na_2. As explained in Section V, 2.(c) Na_2 is considered to represent $1\frac{1}{4}$ sodium atoms and hence its potential constants are $1\frac{1}{4}$ times those for Na_1.

The final three constants π_9, π_{10}, and π_{11} are used in calculating the partition exponential, thus

$$\pi_9 = 10^{-10}/kt_1$$

where k is the Boltzman constant (1.38×10^{-16} erg/deg), t_1 is the absolute temperature 198°K (-75°C), and 10^{-10} is the factor arising from the units of ϕ. π_{10} And π_{11} refer similarly to temperatures of 25 and 150°C respectively.

Programme Notes.

The first three cycles

k = 0(1)10

l = 0(1)k

m = 0(1)l

are used to select the coordinates(x,y,z) for which the potential is calculated.

The next cycle

i = 0(1)21

selects an atom (a_i,b_i,c_i) from the data table. The next set of operations followed by the three cycles at 9) performs successive reflections on the coordinates (a_i,b_i,c_i) to give values (u_p,u_q,u_r) which represent in turn the corresponding positions of (a_i,b_i,c_i) in all the quadrants being considered.

(a,b,c) Are the coordinates of (u_p,u_q,u_r) with respect to the previously selected (x,y,z) and d is the square of the distance for which the potential interaction is calculated.

The appropriate potential constants are used by selecting them according to the atom (a_i,b_i,c_i) being considered as shown in jumps 11, 12, and 13.

Programme Output.

The potential ϕ (10^{-10} erg/molecule) and the three exponentials $\exp(\phi/kT)$ for -75,25, and 150°C have been printed in floating decimal point for the values of x,y, and z shown above.

```
title
t.c.dworjanyn, chemical engineering department, amit.
title
carbon dioxide potentials in molecular sieve ca
title
production programme no.1/1
chapter a
a=21
b=21
c=21
d=3
u=6
w=3
n=11
z=3.5e
i=o(1)21
read(ai)
read(bi)
read(ci)
repeat
i=o(1)11
read(ni)
repeat
t=o
w1=o
w2=o
w3=o
k=o(1)1o
x=o.o5k
newline
caption
x =
print(x)1,2
l=o(1)k
y=o.o5l
newline
caption
y =
print(y)1,2
m=o(1)l2
z=o.o5m
newline
space
space
print(z)8,2
space
v=o
```

```
   l=o(1)=1
   u0=a1
   u1=-a1
   u2=1-a1
   check(a1,0,0.01,1)
   check(a1,0.5,0.01,2)
   in=0
   jn=2
   jump3
1)in=1
   jn=2
   jump3
2)in=0
   jn=1
3)u3=b1
   u4=-b1
   u5=1-b1
   check(b1,0,0.01,4)
   check(b1,0.5,0.01,5)
   kn=3
   ln=5
   jump6
4)kn=4
   ln=5
   jump6
5)kn=3
   ln=4
6)u6=c1
   u7=-c1
   u8=1-c1
   check(c1,0,0.01,7)
   check(c1,0.5,0.01,8)
   mn=6
   nn=28
   jump9
7)mn=7
   nn=8
   jump9
8)mn=6
   nn=7
9)p=in(1)jn
   a=up-x
   an=aa
   q=kn(1)ln
   b=uq-y
   bn=bb
   r=mn(1)nn
   c=ur-z
```

```
      d=cc+qll+bm
      jump10,d>0.01
      v=1000
      e1=0
      e2=0
      e3=0
      jump15
10)e=1/d
      jump11,i>12
      g=π1000
      h=π99g-g
      jump14
11)jump12,i>18
      g=π3000
      h=π49g-g
      jump14
12)jump13,i>15
      g=π5000
      h=π69g-g
      jump14
13)g=π7000
      h=π89g-g
14)v=v+h
      repeat
      repeat
      repeat
      repeat
      e1=βexp(-vπ9)
      w1=π1+e1
      e2=βexp(-vπ10)
      w2=w2+e2
      t=t+1
      zt=e2
      e3=βexp(-vπ11)
      w3=w3+e3
15)print(v)o,3
      print(e1)o,3
      print(e2)o,3
      print(e3)o,3
      repeat
      repeat
      repeat
```

```
newline
caption
 total =
print(t/3,0
print(w1/0,4
print(w2)0,4
print(w3)0,4
1=r(r)t
newline
print(zr)0,4
repeat
*
end
$exp
psa
close
0          0.2773     0.5
0          0.5        0.2771
0.2771     0          0.5
0.2771     0.5        0
0.5        0          0.2771
0.5        0.2771     0
0.2063     0.2063     0.5
0.2063     0.5        0.2063
0.5        0.2063     0.2063
0.1593     0.3883     0.3883
0.3883     0.1593     0.3883
0.3883     0.3883     0.1593
0.1287     0.3178     0.5
0.1287     0.5        0.3178
0.3178     0.1283     0.5
0.3178     0.5        0.1287
0.5        0.1287     0.3178
0.5        0.3178     0.1287
0.2918     0.2918     0.2918
0          0          0.5
0          0.5        0
0.5        0          0
12.30
5.57,-7
620
2.63,-8
2320
6.62,-8
2520
8.28,-8
3150
3660
2430
1710
&&&&&&&&&&&&&&&&&&&&&&&&
```

l.o.dworjanyn, chemical engineering department, iest.

carbon dioxide potentials in molecular sieve 4a

production programme no.1/1

o ago 638 pa0

x = 0.00								
y = 0.00								
0.00	-1.341,	-3	1.354,	2	2.602,	1	9.907,	0
x = 0.05								
y = 0.00								
0.00	-1.404,	-3	1.707,	2	3.034,	1	1.104,	1
y = 0.05								
0.00	-1.471,	-3	2.176,	2	3.565,	1	1.537,	1
0.05	-1.540,	-3	2.807,	2	4.232,	1	1.393,	1
x = 0.10								
y = 0.00								
0.00	-1.574,	-3	3.171,	2	4.577,	1	1.474,	1
y = 0.05								
0.00	-1.649,	-3	4.181,	2	5.500,	1	1.670,	1
0.05	-1.728,	-3	5.579,	2	6.661,	1	1.920,	1
y = 0.10								
0.00	-1.855,	-3	8.897,	2	9.080,	1	2.307,	1
0.05	-1.944,	-3	1.229,	3	1.125,	2	2.775,	1
0.10	-2.168,	-3	3.003,	3	2.056,	2	4.214,	1
x = 0.15								
y = 0.00								
0.00	-1.877,	-3	9.641,	2	9.576,	1	2.479,	1
y = 0.05								
0.00	-1.970,	-3	1.354,	3	1.200,	2	3.905,	1
0.05	-2.066,	-3	1.934,	3	1.515,	2	3.423,	1
y = 0.10								
0.00	-2.239,	-3	3.403,	3	2.347,	2	4.517,	1
0.05	-2.334,	-3	5.121,	3	2.903,	2	5.406,	1
0.10	-2.628,	-3	1.502,	4	5.039,	2	8.348,	1
y = 0.15								
0.00	-2.693,	-3	1.906,	4	6.946,	2	9.994,	1
0.05	-2.813,	-3	2.960,	4	9.304,	2	1.228,	2
0.10	-3.143,	-3	9.911,	4	3.075,	3	2.159,	2
0.15	-3.652,	-3	6.381,	5	7.146,	3	5.154,	2

x = 0.20											
y = 0.30											
	0.00	−2.354,	−3	5.593,	3	3.070,	2	5.536,	1		
y = 0.05											
	0.00	−3.480,	−3	2.750,	3	4.142,	3	6.946,	1		
	0.05	−3.605,	−3	1.381,	4	5.[illegible],	2	0.[illegible],	1		
y = 0.10											
	0.00	−2.931,	−3	3.943,	4	9.487,	2	1.345,	3		
	0.05	−3.258,	−3	4.934,	4	1.[illegible],	3	1.550,	3		
	0.10	−3.318,	−3	1.641,	5	3.130,	3	2.[illegible],	2		
y = 0.15											
	0.00	−3.405,	−3	2.592,	5	3.310,	3	3.377,	2		
	0.05	−3.536,	−3	4.292,	5	5.415,	3	4.240,	2		
	0.10	−3.860,	−3	1.398,	6	1.203,	4	7.434,	2		
	0.15	−4.017,	−3	2.431,	6	1.737,	4	9.638,	2		
y = 0.20											
	0.00	−4.171,	−3	4.319,	6	2.544,	4	1.259,	3		
	0.05	−4.234,	−3	5.376,	6	2.044,	4	1.395,	3		
	0.10	−4.186,	−3	4.502,	6	2.515,	4	1.284,	3		
	0.15	−1.461,	−3	2.103,	2	3.485,	1	1.217,	1		
	0.20	3.362,	−3	1.700,	−54	2.050,	−36	7.717,	−26		
x = 0.25											
y = 0.00											
	0.00	−2.910,	−3	4.324,	4	1.178,	3	1.449,	2		
y = 0.05											
	0.00	−3.113,	−3	6.862,	4	1.927,	3	2.049,	2		
	0.05	−3.308,	−3	1.771,	5	3.[illegible],	3	2.[illegible],	2		
y = 0.10											
	0.00	−3.585,	−3	5.073,	5	6.137,	3	4.639,	2		
	0.05	−3.753,	−3	9.231,	5	9.[illegible],	3	6.124,	2		
	0.10	−4.114,	−3	3.459,	7	2.[illegible],	4	1.135,	1		
y = 0.15											
	0.00	−4.115,	−3	3.477,	6	2.203,	4	1.138,	3		
	0.05	−4.236,	−3	5.495,	6	2.953,	4	1.398,	3		
	0.10	−4.296,	−3	6.776,	6	3.[illegible],	4	1.554,	2		
	0.15	−2.657,	−3	3.477,	4	1.[illegible],	3	1.823,	2		
y = 0.20											
	0.00	−4.099,	−3	3.868,	6	2.[illegible],	4	1.106,	3		
	0.05	−3.738,	−3	6.728,	5	6.[illegible],	3	5.966,	2		
	0.10	−1.073,	−3	4.567,	2	2.[illegible],	1	1.748,	1		
	0.15	1.168,	−2	1.606,	−19	3.328,	−13	1.657,	−9		
	0.20	2.588,	−1	0.000,	0	0.000,	0	0.000,	0		
y = 0.25											
	0.00	−4.947,	−4	6.115,	0	3.328,	0	2.330,	0		
	0.05	4.449,	−3	8.468,	−3	2.[illegible],	−3	4.[illegible],	−4		
	0.10	2.595,	−2	5.598,	−43	4.[illegible],	−28	5.[illegible],	−20		
	0.15	1.056,	−1	0.000,	0	0.000,	0	0.000,	0		
	0.20	3.646,	0	0.000,	0	0.000,	0	0.000,	0		
	0.25	1.000,	3	0.000,	0	0.000,	0	0.000,	0		

		exp(S/kt1)	exp(S/kt2)	exp(S/kt3)
x = 0.30				
y = 0.00				
0.00	2.033, -4	4.764, -1	6.116, -1	7.073, -1
y = 0.05				
0.00	-1.340, -3	1.343, 3	2.526, 1	5.691, 0
0.05	-2.361, -3	5.663, 3	3.103, 2	5.886, 1
y = 0.10				
0.00	-3.179, -3	1.119, 5	2.303, 3	2.335, 2
0.05	-3.436, -3	3.603, 5	4.389, 3	3.946, 2
0.10	-3.986, -3	6.034, 4	1.605, 3	1.957, 2
y = 0.15				
0.00	-1.844, -3	9.507, 1	2.037, 1	8.398, 0
0.05	-1.609, -3	3.607, 2	4.986, 1	1.566, 1
0.10	7.941, -4	5.467, -2	1.452, -1	2.372, -1
0.15	1.852, -3	4.143, -21	2.933, -14	2.999, -10
y = 0.20				
0.00	1.103, -3	2.940, -18	2.291, -12	6.441, -9
0.05	1.000, -2	1.351, -16	2.765, -11	3.716, -8
0.10	1.684, -3	1.150, -30	1.126, -20	1.026, -14
0.15	5.873, -2	0.000, 0	1.083, -62	2.442, -44
0.20	5.345, -1	0.000, 0	0.000, 0	0.000, 0
y = 0.25				
0.00	4.171, -2	4.997, -67	9.556, -45	1.955, -31
0.05	6.596, -2	0.000, 0	2.449, -73	1.031, -49
0.10	2.317, -1	0.000, 0	0.000, 0	0.000, 0
0.15	5.737, -1	0.000, 0	0.000, 0	0.000, 0
0.20	9.866, 0	0.000, 0	0.000, 0	0.000, 0
0.25	1.000, 1	0.000, 0	0.000, 0	0.000, 0
y = 0.30				
0.00	1.396, -1	0.000, 0	0.000, 0	0.000, 0
0.05	4.586, -1	0.000, 0	0.000, 0	0.000, 0
0.10	3.886, 0	0.000, 0	0.000, 0	0.000, 0
0.15	1.596, 1	0.000, 0	0.000, 0	0.000, 0
0.20	1.000, 1	0.000, 0	0.000, 0	0.000, 0
0.25	1.000, 1	0.000, 0	0.000, 0	0.000, 0
0.30	1.000, 1	0.000, 0	0.000, 0	0.000, 0
x = 0.35				
y = 0.00				
0.00	1.545, -1	0.000, 0	0.000, 0	0.000, 0
y = 0.05				
0.00	7.876, -2	0.000, 0	0.000, 0	3.240, -59
0.05	4.195, -2	2.082, -67	5.344, -45	7.007, -32
y = 0.10				
0.00	1.616, -3	2.064, -26	8.243, -18	9.982, -13
0.05	1.064, -3	5.814, -18	3.604, -12	6.858, -9
0.10	1.705, -3	8.047, -28	1.036, -18	2.194, -13
y = 0.15				
0.00	4.533, -3	3.334, -74	1.245, -49	4.044, -35
0.05	3.648, -3	1.051, -58	3.207, -39	6.100, -30
0.10	7.155, -2	0.000, 0	3.306, -75	7.855, -54
0.15	3.153, -1	0.000, 0	0.000, 0	0.000, 0

	P	exp(P/kT1)	exp(P/kT2)	exp(P/kT3)
x = 0.35				
y = 0.00				
0.00	5.396, -1	0.000, 0	0.000, 0	0.000, 0
0.05	2.178, -1	0.000, 0	0.000, 0	0.000, 0
0.10	1.350, -1	0.000, 0	0.000, 0	0.000, 0
0.15	7.102, -1	0.000, 0	0.000, 0	0.000, 0
0.20	3.649, 0	0.000, 0	0.000, 0	0.000, 0
y = 0.05				
0.00	1.209, 0	0.000, 0	0.000, 0	0.000, 0
0.05	7.312, -1	0.000, 0	0.000, 0	0.000, 0
0.10	1.146, 0	0.000, 0	0.000, 0	0.000, 0
0.15	2.659, 0	0.000, 0	0.000, 0	0.000, 0
0.20	4.159, 0	0.000, 0	0.000, 0	0.000, 0
0.25	1.000, 3	0.000, 0	0.000, 0	0.000, 0
y = 0.10				
0.00	1.453, 0	0.000, 0	0.000, 0	0.000, 0
0.05	2.733, 0	0.000, 0	0.000, 0	0.000, 0
0.10	4.404, 1	0.000, 0	0.000, 0	0.000, 0
0.15	1.000, 3	0.000, 0	0.000, 0	0.000, 0
0.20	1.171, 3	0.000, 0	0.000, 0	0.000, 0
0.25	1.000, 3	0.000, 0	0.000, 0	0.000, 0
0.30	1.000, 3	0.000, 0	0.000, 0	0.000, 0
y = 0.15				
0.00	1.478, 0	0.000, 0	0.000, 0	0.000, 0
0.05	1.802, 1	0.000, 0	0.000, 0	0.000, 0
0.10	1.000, 3	0.000, 0	0.000, 0	0.000, 0
0.15	1.000, 3	0.000, 0	0.000, 0	0.000, 0
0.20	1.000, 3	0.000, 0	0.000, 0	0.000, 0
0.25	1.000, 3	0.000, 0	0.000, 0	0.000, 0
0.30	1.000, 3	0.000, 0	0.000, 0	0.000, 0
0.35	1.003, 1	0.000, 0	0.000, 0	0.000, 0
x = 0.40				
y = 0.00				
0.00	1.000, 3	0.000, 0	0.000, 0	0.000, 0
y = 0.05				
0.00	5.616, 0	0.000, 0	0.000, 0	0.000, 0
0.05	1.871, 0	0.000, 0	0.000, 0	0.000, 0
y = 0.10				
0.00	3.551, -1	0.000, 0	0.000, 0	0.000, 0
0.05	1.908, -1	0.000, 0	0.000, 0	0.000, 0
0.10	1.794, -1	0.000, 0	0.000, 0	0.000, 0
y = 0.15				
0.00	5.883, -1	0.000, 0	0.000, 0	0.000, 0
0.05	3.873, -1	0.000, 0	0.000, 0	0.000, 0
0.10	3.354, -1	0.000, 0	0.000, 0	0.000, 0
0.15	1.000, 1	0.000, 0	0.000, 0	0.000, 0
y = 0.20				
0.00	1.156, 1	0.000, 0	0.000, 0	0.000, 0
0.05	4.997, 0	0.000, 0	0.000, 0	0.000, 0
0.10	3.624, 0	0.000, 0	0.000, 0	0.000, 0
0.15	3.619, 1	0.000, 0	0.000, 0	0.000, 0
0.20	1.630, 3	0.000, 0	0.000, 0	0.000, 0

	β	$\exp(-\beta/kT_1)$	$\exp(-\beta/kT_2)$	$\exp(-\beta/kT_3)$
$x = 0.40$				
$y = 0.25$				
0.00	$1.253_{\,}$ 3	$0.000_{\,}$ 0	$0.000_{\,}$ 0	$0.000_{\,}$ 0
0.05	$3.587_{\,}$ 1	$0.000_{\,}$ 0	$0.000_{\,}$ 0	$0.000_{\,}$ 0
0.10	$4.920_{\,}$ 0	$0.000_{\,}$ 0	$0.000_{\,}$ 0	$0.000_{\,}$ 0
0.15	$2.005_{\,}$ 1	$0.000_{\,}$ 0	$0.000_{\,}$ 0	$0.000_{\,}$ 0
0.20	$6.682_{\,}$ 1	$0.000_{\,}$ 0	$0.000_{\,}$ 0	$0.000_{\,}$ 0
0.25	$2.013_{\,}$ 1	$0.000_{\,}$ 0	$0.000_{\,}$ 0	$0.000_{\,}$ 0
$y = 0.30$				
0.00	$1.473_{\,}$ 2	$0.000_{\,}$ 0	$0.000_{\,}$ 0	$0.000_{\,}$ 0
0.05	$4.830_{\,}$ 1	$0.000_{\,}$ 0	$0.000_{\,}$ 0	$0.000_{\,}$ 0
0.10	$8.055_{\,}$ 1	$0.000_{\,}$ 0	$0.000_{\,}$ 0	$0.000_{\,}$ 0
0.15	$1.000_{\,}$ 3	$0.000_{\,}$ 0	$0.000_{\,}$ 0	$0.000_{\,}$ 0
0.20	$1.000_{\,}$ 3	$0.000_{\,}$ 0	$0.000_{\,}$ 0	$0.000_{\,}$ 0
0.25	$1.408_{\,}$ 1	$0.000_{\,}$ 0	$0.000_{\,}$ 0	$0.000_{\,}$ 0
0.30	$5.187_{\,}$ 0	$0.000_{\,}$ 0	$0.000_{\,}$ 0	$0.000_{\,}$ 0
$y = 0.35$				
0.00	$1.575_{\,}$ 1	$0.000_{\,}$ 0	$0.000_{\,}$ 0	$0.000_{\,}$ 0
0.05	$3.668_{\,}$ 1	$0.000_{\,}$ 0	$0.000_{\,}$ 0	$0.000_{\,}$ 0
0.10	$1.000_{\,}$ 3	$0.000_{\,}$ 0	$0.000_{\,}$ 0	$0.000_{\,}$ 0
0.15	$1.000_{\,}$ 3	$0.000_{\,}$ 0	$0.000_{\,}$ 0	$0.000_{\,}$ 0
0.20	$1.000_{\,}$ 3	$0.000_{\,}$ 0	$0.000_{\,}$ 0	$0.000_{\,}$ 0
0.25	$1.000_{\,}$ 3	$0.000_{\,}$ 0	$0.000_{\,}$ 0	$0.000_{\,}$ 0
0.30	$2.718_{\,}$ 0	$0.000_{\,}$ 0	$0.000_{\,}$ 0	$0.000_{\,}$ 0
0.35	$3.763_{\,}$ -1	$0.000_{\,}$ 0	$0.000_{\,}$ 0	$0.000_{\,}$ 0
$y = 0.40$				
0.00	$3.765_{\,}$ 0	$0.000_{\,}$ 0	$0.000_{\,}$ 0	$0.000_{\,}$ 0
0.05	$5.493_{\,}$ 1	$0.000_{\,}$ 0	$0.000_{\,}$ 0	$0.000_{\,}$ 0
0.10	$1.000_{\,}$ 3	$0.000_{\,}$ 0	$0.000_{\,}$ 0	$0.000_{\,}$ 0
0.15	$1.000_{\,}$ 3	$0.000_{\,}$ 0	$0.000_{\,}$ 0	$0.000_{\,}$ 0
0.20	$1.000_{\,}$ 3	$0.000_{\,}$ 0	$0.000_{\,}$ 0	$0.000_{\,}$ 0
0.25	$1.000_{\,}$ 3	$0.000_{\,}$ 0	$0.000_{\,}$ 0	$0.000_{\,}$ 0
0.30	$2.938_{\,}$ 0	$0.000_{\,}$ 0	$0.000_{\,}$ 0	$0.000_{\,}$ 0
0.35	$9.999_{\,}$ -1	$0.000_{\,}$ 0	$0.000_{\,}$ 0	$8.686_{\,}$ -72
0.40	$4.540_{\,}$ -3	$6.975_{\,}$ -6	$1.617_{\,}$ -5	$4.850_{\,}$ -4
$x = 0.45$				
$y = 0.00$				
0.00	$1.000_{\,}$ 3	$0.000_{\,}$ 0	$0.000_{\,}$ 0	$0.000_{\,}$ 0
$y = 0.05$				
0.00	$1.000_{\,}$ 3	$0.000_{\,}$ 0	$0.000_{\,}$ 0	$0.000_{\,}$ 0
0.05	$1.000_{\,}$ 3	$0.000_{\,}$ 0	$0.000_{\,}$ 0	$0.000_{\,}$ 0
$y = 0.10$				
0.00	$5.734_{\,}$ 0	$0.000_{\,}$ 0	$0.000_{\,}$ 0	$0.000_{\,}$ 0
0.05	$1.992_{\,}$ 0	$0.000_{\,}$ 0	$0.000_{\,}$ 0	$0.000_{\,}$ 0
0.10	$9.297_{\,}$ -1	$0.000_{\,}$ 0	$0.000_{\,}$ 0	$0.000_{\,}$ 0
$y = 0.15$				
0.00	$4.576_{\,}$ 0	$0.000_{\,}$ 0	$0.000_{\,}$ 0	$0.000_{\,}$ 0
0.05	$8.368_{\,}$ 0	$0.000_{\,}$ 0	$0.000_{\,}$ 0	$0.000_{\,}$ 0
0.10	$6.876_{\,}$ 0	$0.000_{\,}$ 0	$0.000_{\,}$ 0	$0.000_{\,}$ 0
0.15	$1.000_{\,}$ 3	$0.000_{\,}$ 0	$0.000_{\,}$ 0	$0.000_{\,}$ 0

$x = 0.45$	ϕ	$\exp(\phi/kt_1)$	$\exp(\phi/kt_2)$	$\exp(\phi/kt_3)$
$y = 0.20$				
0.00	1.000, 3	0.000, 0	0.000, 0	0.000, 0
0.05	1.129, 2	0.000, 0	0.000, 0	0.000, 0
0.10	3.504, 1	0.000, 0	0.000, 0	0.000, 0
0.15	1.000, 3	0.000, 0	0.000, 0	0.000, 0
0.20	1.000, 3	0.000, 0	0.000, 0	0.000, 0
$y = 0.25$				
0.00	1.000, 3	0.000, 0	0.000, 0	0.000, 0
0.05	1.000, 3	0.000, 0	0.000, 0	0.000, 0
0.10	1.000, 3	0.000, 0	0.000, 0	0.000, 0
0.15	1.000, 3	0.000, 0	0.000, 0	0.000, 0
0.20	1.000, 3	0.000, 0	0.000, 0	0.000, 0
0.25	1.000, 3	0.000, 0	0.000, 0	0.000, 0
$y = 0.30$				
0.00	1.000, 3	0.000, 0	0.000, 0	0.000, 0
0.05	1.000, 3	0.000, 0	0.000, 0	0.000, 0
0.10	1.000, 3	0.000, 0	0.000, 0	0.000, 0
0.15	1.000, 3	0.000, 0	0.000, 0	0.000, 0
0.20	1.000, 3	0.000, 0	0.000, 0	0.000, 0
0.25	3.951, 1	0.000, 0	0.000, 0	0.000, 0
0.30	3.994, 0	0.000, 0	0.000, 0	0.000, 0
$y = 0.35$				
0.00	1.000, 3	0.000, 0	0.000, 0	0.000, 0
0.05	1.000, 3	0.000, 0	0.000, 0	0.000, 0
0.10	1.000, 3	0.000, 0	0.000, 0	0.000, 0
0.15	1.000, 3	0.000, 0	0.000, 0	0.000, 0
0.20	1.000, 3	0.000, 0	0.000, 0	0.000, 0
0.25	3.241, 1	0.000, 0	0.000, 0	0.000, 0
0.30	9.334, -1	0.000, 0	0.000, 0	0.000, 0
0.35	8.371, -2	0.000, 0	0.000, 0	6.804, -63
$y = 0.40$				
0.00	6.975, 0	0.000, 0	0.000, 0	0.000, 0
0.05	1.495, 1	0.000, 0	0.000, 0	0.000, 0
0.10	1.000, 3	0.000, 0	0.000, 0	0.000, 0
0.15	1.000, 3	0.000, 0	0.000, 0	0.000, 0
0.20	1.000, 3	0.000, 0	0.000, 0	0.000, 0
0.25	5.903, 1	0.000, 0	0.000, 0	0.000, 0
0.30	1.055, 0	0.000, 0	0.000, 0	0.000, 0
0.35	3.536, -2	5.611, -57	4.80+, -38	5.520, -37
0.40	-3.930, -3	1.833, 6	1.434, 4	0.415, 2
$y = 0.45$				
0.00	5.773, -1	0.000, 0	0.000, 0	0.000, 0
0.05	3.616, 0	0.000, 0	0.000, 0	0.000, 0
0.10	1.011, 2	0.000, 0	0.000, 0	0.000, 0
0.15	1.000, 3	0.000, 0	0.000, 0	0.000, 0
0.20	1.000, 3	0.000, 0	0.000, 0	0.000, 0
0.25	1.214, 1	0.000, 0	0.000, 0	0.000, 0
0.30	4.373, -1	0.000, 0	0.000, 0	0.000, 0
0.35	1.473, -2	3.906, -[illegible]	2.900, -1[illegible]	1.165, -11
0.40	-6.321, -3	2.316, 10	7.61[illegible], 6	6.[illegible], 4
0.45	-7.164, -3	3.440, 11	3.655, 7	3.0[illegible], 5

x = 0.50	Φ		$\exp(\Phi/kt_1)$		$\exp(\Phi/kt_2)$		$\exp(\Phi/kt_3)$	
y = 0.00								
0.00	1.000,	3	0.000,	0	0.000,	0	0.000,	0
y = 0.05								
0.00	1.000,	3	0.000,	0	0.000,	0	0.000,	0
0.05	1.000,	3	0.000,	0	0.000,	0	0.000,	0
y = 0.10								
0.00	1.000,	3	0.000,	0	0.000,	0	0.000,	0
0.05	5.000,	0	0.000,	0	0.000,	0	0.000,	0
0.10	1.000,	0	0.000,	0	0.000,	0	0.000,	0
y = 0.15								
0.00	1.000,	1	0.000,	0	0.000,	0	0.000,	0
0.05	9.000,	0	0.000,	0	0.000,	0	0.000,	0
0.10	3.000,	1	0.000,	0	0.000,	0	0.000,	0
0.15	1.000,	3	0.000,	0	0.000,	0	0.000,	0
y = 0.20								
0.00	1.000,	3	0.000,	0	0.000,	0	0.000,	0
0.05	1.000,	3	0.000,	0	0.000,	0	0.000,	0
0.10	1.000,	3	0.000,	0	0.000,	0	0.000,	0
0.15	1.000,	3	0.000,	0	0.000,	0	0.000,	0
0.20	1.000,	3	0.000,	0	0.000,	0	0.000,	0
0.25	1.000,	3	0.000,	0	0.000,	0	0.000,	0
y = 0.30								
0.00	1.000,	3	0.000,	0	0.000,	0	0.000,	0
0.05	1.000,	3	0.000,	0	0.000,	0	0.000,	0
0.10	1.000,	3	0.000,	0	0.000,	0	0.000,	0
0.15	1.000,	3	0.000,	0	0.000,	0	0.000,	0
0.20	1.000,	3	0.000,	0	0.000,	0	0.000,	0
0.25	1.000,	3	0.000,	0	0.000,	0	0.000,	0
0.30	6.616,	0	0.000,	0	0.000,	0	0.000,	0
y = 0.35								
0.00	1.000,	3	0.000,	0	0.000,	0	0.000,	0
0.05	1.000,	3	0.000,	0	0.000,	0	0.000,	0
0.10	1.000,	3	0.000,	0	0.000,	0	0.000,	0
0.15	1.000,	3	0.000,	0	0.000,	0	0.000,	0
0.20	1.000,	3	0.000,	0	0.000,	0	0.000,	0
0.25	4.643,	0	0.000,	0	0.000,	0	0.000,	0
0.30	5.065,	-1	0.000,	0	0.000,	0	0.000,	0
0.35	5.614,	-2	0.000,	0	5.717,	-50	2.045,	-43

x = 0.30	0	exp(W/kTx)	exp(P/kTa)	exp(-/kT$_j$)
y = 0.40				
0.00	1.627, 1	0.000, 0	0.000, 0	0.000, 0
0.05	5.371, 0	0.000, 0	0.000, 0	0.000, 0
0.10	1.000, 0	0.000, 0	0.000, 0	0.000, 0
0.15	1.000, 0	0.000, 0	0.000, 0	0.000, 0
0.20	4.580, 1	0.000, 0	0.000, 0	0.000, 0
0.25	4.634, 0	0.000, 0	0.000, 0	0.000, 0
0.30	3.078, -1	0.000, 0	0.000, 0	0.000, 0
0.35	1.502, -3	1.633, -14	1.181, -10	6.107, -12
0.40	-5.565, -3	7.010, 8	7.469, 5	1.358, 4
y = 0.45				
0.00	3.761, -1	0.000, 0	0.000, 0	0.000, 0
0.05	6.884, -1	0.000, 0	0.000, 0	0.000, 0
0.10	6.369, 0	0.000, 0	0.000, 0	0.000, 0
0.15	1.964, 1	0.000, 0	0.000, 0	0.000, 0
0.20	1.143, 1	0.000, 0	0.000, 0	0.000, 0
0.25	1.721, 0	0.000, 0	0.000, 0	0.000, 0
0.30	1.494, -1	0.000, 0	0.000, 0	0.000, 0
0.35	4.260, -3	1.695, -7	3.197, -5	6.265, -4
0.40	-6.696, -3	9.144, 10	1.894, 7	1.322, 5
0.45	-6.965, -3	1.178, 11	2.243, 7	1.488, 5
y = 0.50				
0.00	6.917, -2	0.000, 0	0.000, 0	6.023, -67
0.05	2.803, -1	0.000, 0	0.000, 0	0.000, 0
0.10	1.352, 0	0.000, 0	0.000, 0	0.000, 0
0.15	2.970, 0	0.000, 0	0.000, 0	0.000, 0
0.20	2.745, 0	0.000, 0	0.000, 0	0.000, 0
0.25	5.995, -1	0.000, 0	0.000, 0	0.000, 0
0.30	6.504, -1	0.000, 0	3.311, -69	5.017, -49
0.35	-8.326, -4	2.083, 1	7.300, 0	4.132, 0
0.40	-7.[illegible], -3	1.347, 11	2.659, 7	1.584, 5
0.45	-6.702, -3	4.467, 11	1.284, 7	9.478, 4
0.50	-6.396, -3	1.485, 10	5.647, 6	3.619, 4
total = 2.00		6.7141, 11	1.3532, 8	9.0104, 5

REFERENCES

Molecular sieve properties and preparations:

1. Barrer R.M. and Baynham J.W., J.Chem.Soc.1956,2892.
2. Bering B.P., Dubinin M.M., Zhukovskaya E.G. and Serpinskii V.V., Doklady Akad. Nauk SSSR 131,865(1960).
3. Breck D.W., Eversole W.G., Milton R.M., Reed T.B. and Thomas T.L., J.Am.Chem.Soc.78,5963(1956).
4. Breck D.W. and Smith J.V., Scientific American p.1, Jan.1959.
5. Broussard L. and Shoemaker D.P., J.Am.Chem.Soc.82, 1041(1960).
6. Flanigen E.M. and Breck D.W., Abstract 137, Meeting A.C.S., April 1960, Cleveland, Ohio.
7. Galich P.N. et al., Dokl.Akad.Nauk SSSR 144,147(1962).
8. Kratky Z., Czech.Pat.87,636; C.A.54,14506h(1960).
9. Labine R.A., Chem.Eng.66,No.16,104(1959).
10. Meditsch J.de O., Eng.e quim (Rio de Janeiro)12,No.3, 4(1960).
11. Mirskii Ya.V. and Mitro Janov M.G., Intern.Chem.Eng. 2,207(1962).
12. Mitchell W.J. and Moore W.E., Ger.Pat.1,040,005; C.A.54,23125g(1960).
13. Piguzova L.I., Intern.Chem.Eng.2,189(1962).
14. Reed T.B. and Breck D.W., J.Am.Chem.Soc.78,5972(1956).
15. Torcheshnikov et al., Zhur.Vsesoyuz.Khim.Obshch.im. D.I.Mendeleeva 5,710(1960).

Molecular sieve isotherms and heats of adsorption:

16. Ackley R.D. and Browning W.E., Oak Ridge National Laboratory, Central Files No.61-2-32, Feb.1961.

17. Barrer R.M. and Bratt G.C., J.Phys.Chem.Solids 12, 130(1960).

18. Barrer R.M. and Stuart W.I., Proc.Roy.Soc.243A,172(1957), 249A,464(1959).

19. Basmadjian D., Canad.J.Chem.38,141(1960).

20. Breck D.W., Eversole W.G., Milton R.M., Reed T.B. and Thomas T.L., J.Am.Chem.Soc.78,5963(1956).

21. Eberley P.E., J.Phys.Chem.65,68(1961); 66,812(1962).

22. Linde Company, Adsorption Equilibria Data Sheets, New York(1959).

23. Redlich O. and Peterson D.L., J.Phys.Chem.63,1024(1959).

24. Turuizumi A., Nippon Kagaku Zasshi (J.Chem.Soc.Japan) 80,221(March 1959); Chem.Zentralblatt 131,2778.

Molecular sieve diffusion measurements:

25. Barrer R.M. and Fender B.E.F., J.Phys.Chem.Solids 21, 1(1961).

26. Chandrasekharan K., Ph.D. Dissertation, Imperial College University of London (1962).

27. Eberley P.E. and Spencer E.H., Trans.Faraday Soc.57, 289(1961).

28. Freeman D.C. and Stamires D.M., J.Chem.Phys.35,799(1961).

29. Habgood H.W., Can.J.Chem.36,1384(1958).

Natural zeolites:

30. Barrer R.M., Proc.Roy.Soc.167A,392(1938).

31. Barrer R.M., Trans.Faraday Soc.45,358(1949).

32. Barrer R.M. and Rees L.V.C., Trans.Faraday Soc.56, 709(1960).

33. Hey M.H., Mineralog.Mag.24,99(1935).

34. Kingston G.L. and Macleod A.C., Trans.Faraday Soc.55, 1799(1959).

35. Strunz H., Neues Jahrb.Mineral., Monatsch.11,250(1956).

36. Tiselius A. and Brohult S., Zeit.Phys.Chem.168A,248, 169A,425(1934);174A,401(1935); Nature 133, 212(1934).

General physical adsorption:

37. Barrer R.M. and Rideal E.K., Proc.Roy.Soc.149A,231(1935)

38. Boer J.H.de, Dynamics of Adsorption, Clarendon Press (1953).

39. Burnette R.D., Graham W.W. and Morse D.C., Second Nuclear Reactor Chemistry Conference, Gatlinburg, Tennessee, Oct.1961.

40. Hill T.L., "Statistacal Mechanics", McGraw Hill (1956).

41. Kisalev A.V., Quarterly Rev.15,99(1961).

42. Maggs F.A.P, Schwabe D.H. and Williams J.H., Nature 186,956(1960).

43. Pierce C., J.Phys.Chem.63,1076(1959).

44. Waller J.G., Nature 186,429(1960).

Solid state diffusion:

45. Allen R.L. and Moore W.J., J.Phys.Chem.63,223(1959).

46. Barrer R.M., Diffusion in and through Solids, University Press, Cambridge (1951).

47. Hauffe K., Reaktionen in und an festen Stoffen, Springer Verlag (1955).

48. Haul R. et al., Reactivity of Solids, 4th International Symposium, Ed. J.H. de Boer (1960).

49. Jost W., Diffusion in Solids, Liquids, Gases, Academic Press, New York, (1952).

50. Linder Van R. and Metzke H., Z. Naturforschung 14a, 582(1959).

Experimental methods:

51. Anderson J.E., Rev.Sci.Instr.6,66(1935).

52. Banks T.E. et al., Biochem.J.64,408(1956).

53. Bradley J.E.S. et al., Biochem.J.57,192(1954).

54. Emmett P.H. and Brunauer S., J.Am.Chem.Soc.56,35(1934).

55. Joy A.S., Vacuum 3,254(1953).

56. Jura G. and Horkius W.D., J.Am.Chem.Soc.66,1356(1944).

57. Orr C. and Dallavalle J.M., Fine Particle Measurement, Macmillan, New York, (1959).

Radiation measurement: :

58. Banks T.E. et al., Biochem.J.64,408,411,(1956).

59. Bernstein W. and Ballentine R., Rev.Sci.Instr.21, 158(1950).

60. Bradley J.E.S. et al., Biochem.J.57,192(1954).

61. Brown S.C. and Miller W.W., Rev.Sci.Instr.18,496(1947).

62. Buchanan D.L. and Nakao A., J.Am.Chem.Soc.74,2389(1952).

63. Cuddock B.D. and Davies P.L., Nature 184,2011(1959).

64. Cameron J.F., Nature 176,1264(1955).

65. Eidinoff M.L. and Knoll J.E., Science 112,250(1950).

66. Feldstein O. and Broda E., Nature 168,599(1951).

67. Francis G.E., Mulligan W. and Wormall A., Isotopic Tracers, Athlone Press (1959).

68. Gillespie A.B., Signal, Noise and Resolution, McGraw-Hill (1953).

69. Glascock R.F., Isotopic Gas Analysis for Biochemists, Academic Press (1954).

70. Hayes F.N. and Gould R.G., Science 117,480(1953).

71. Nilsson G. and Aniansson G., Nucleonics 13,No.2,35,(1955).

72. Tykva R., Coll. of Chek.Chem.Comm.25,1874(1960).

73. Van Slyke D.D. et al., J.Bial.Chem.192,769(1951).

74. Wing J. and Johnson W.H., Science 121,674(1955).

75. Zlotowski I. and Wincel H., Nature 192,550(1961).

Potential calculations:

76. Barker J.A. and Everett D.H., Trans.Faraday Soc.58, 1608(1962).

77. Girifalco L.A. and Streetman J.R., J.Phys.Chem.Solids 4,182(1958).

78. Gluekauf E., Trans.Faraday Soc.49,1066(1953).

79. Hirschfelder J.O., Curtiss C.F., and Bird R.B., Molecular Theory of Gases and Liquids, John Wiley, New York (1954).

80. Howlett K.E., Science Prog.48,270(1960).

81. Mortenson E.M. and Eyring H., J.Phys.Chem.64,433(1960).

82. Orr W.J.C., Trans.Faraday Soc.35,1247(1939).

83. Sams J.R., Constabaris G. and Halsey G.D., J.Phys. Chem.64,1689(1960); J.Chem.Phys.36,1334 (1962).

84. Steele W.A. and Ross M., J.Chem.Phys.35,850(1961).

Mathematics of diffusion:

85. Amudson N.R., Ind.Eng.Chem.48,26(1956).

86. Carslow H.S. and Jaeger J.C., Conduction of Heat in Solids, Clarendon Press(1959).

87. Crank J., The Mathematics of Diffusion, Clarendon Press, Oxford(1956).

88. Girifalco L.A. and Grimes H.H., Phys.Rev.121,982(1961).

89. Girsanov I.V., Doklady Akad.Nauk SSSR 136,761(1961).

90. Kac M., Selected Papers on Noise and Stochastic Processes, Ed.Wax N., Dover Publications, New York(1951).

91. Rosen J.B., J.Chem.Phys.20,387(1952).

92. Tien Chi, Canad.J.Chem.Eng.38,25(Feb.1960); Am.Inst. Chem.Eng.J.7,410(Sept.1961).

93. Vermeulen T., Advances in Chemical Engineering, Vol.II, Ed.Drew T.B. and Hooper J.W., Academic Press, New York(1958).

94. Vineyard G.H., J.Phys.Chem.Solids,3,121(1957).

General:

95. Taylor H.S. and Glasstone S., A Treatise on Physical Chemistry, Vol.II, States of Matter, Van Nostrad, New York(1951).

96. Welch J.H., J.Sc.Inst.31,458(1954).

97. Scott D.S. and Dullien F.A.L., Am.Inst.Eng.J.8, 113(1962).

98. Landolt - Börnstein Tables, 6th Edition, Ed.Euken A., Springer Verlag, Berlin(1950).